THE DURABILITY OF AIRFIELD CONCRETE EXPOSED TO AIRCRAFT DE-ICERS

by

Irene Antonia Wijoyo

A thesis

presented to the University of Waterloo

in fulfillment of the

thesis requirement for the degree of

Master of Applied Science

In

Mechanical Engineering

Waterloo, Ontario, Canada, 2007

AUTHOR'S DECLARATION

I hereby declare that I am the sole author of this thesis. This is a true copy of the thesis, including any required final revisions, as accepted by my examiners.

I understand that my thesis may be made electronically available to the public.

ABSTRACT

A large portion of an airport property is occupied by runways and taxiways, which must be kept in excellent condition to ensure the safety of the airplanes, and the people on board. Any free objects on the airfield can cause damage to aircraft and are a possible danger to both the airplanes and the passengers. However, deterioration of the concrete airfield can be a major hazard and the presence of de-icing and anti-icing fluids may accelerate degradation.

The focus of this project was the evaluation and assessment of aircraft de-icing and anti-icing fluids on the deterioration of airfield concrete. These fluids are used to remove and prevent snow and ice formation on aircraft by lowering the freezing temperature of water. The primary component in both fluids is ethylene glycol, while additives, which are proprietary and unknown, are mixed in to control various properties. Very little research has been done regarding the effect of the de-icer and anti-icers on the concrete deterioration. The aim of this study was to gain a better understanding of its influence on the deterioration of airfield concrete through a series of mechanical and electro-chemical tests, as well as microscopic and elemental analysis.

Based on the comparative experiments and analyses performed using water, ethylene glycol, de-icer, and anti-icer, it appears that de-icing fluids do not prematurely cause concrete deterioration. In addition, experimental procedures in this study utilized the de-icing fluids as a concentrate, which are unrealistic conditions on an airfield, where dilution occurs from the addition of water and the presence of snow and ice. There was precipitate formation in all cases of cement paste exposure to de-icing fluid, however, which indicates that reactions are occurring and should be investigated further to determine the long term effects on concrete. With respect to the scope of this study, it was determined that the use of de-icers and anti-icers cause no significant detrimental effects on concrete mechanical properties and durability.

ACKNOWLEDGEMENTS

TABLE OF CONTENTS

LIST OF FIGURES

LIST OF TABLES

CHAPTER 1 - INTRODUCTION

1.1 The Airfield

Aircraft play a major role as a part of the global transportation infrastructure, transporting hundreds of thousands of people everyday worldwide. Each year, over 30 million passengers travel through Toronto's Lester B. Pearson International Airport alone [GTAA, 2006]. With such a high volume of people and a great domestic and international impact, maintenance at the airport is a critical and continuous process.

A large portion of an airport's land is occupied by runways and taxiways, which allow the airplanes to move around, take off and land. The airfield must be kept in excellent condition to ensure the safety of the airplanes, as well as the people on board, at all times. When the airplane engines are running, the jet engine area will easily intake any loose objects in its path, which could subsequently cause significant damage, as seen in Figure 1.1. Considering the size of the airfield at major international airports, maintenance is no small feat and inspection is required numerous times a day. Any free objects on the airfield could cause problems and would be a possible threat to airplanes and its passengers. These unwanted loose objects are formally referred to as foreign object debris (FOD) and are dealt with very seriously at all airports [FODNews].

(a)   (b)

Figure 1.1 (a) Jet engine turbine blade damages [FODNews]; (b) Example of a cargo box being a large FOD hazard [Unusual Aviation Pictures].

FOD can range in size from nuts and bolts to large luggage carts. The term even includes wildlife and people on the airfield. Anything that is out of place on an airfield and can cause damage to the engine or flight control mechanisms is considered FOD. In addition to the passenger injuries and plane damage, potentially caused by FOD, a great deal of money can be lost in terms of flight delays, minor repairs, and lost productivity. An estimated 4 billion dollars is spent annually because of FOD, with the majority of it spent on engine repairs [FODNews].

The best prevention for FOD-related problems is by addressing the sources and minimizing, or eliminating, the cause of debris on airfields. In the case of litter and tools, the maintenance crews should be educated in recognizing the importance of identifying and removing potential hazards when working on the field. For wildlife control, several airports employ predatory birds, dogs, or visual and auditory deterrents to discourage wild animals from approaching the airfield. There is another source of FOD, however, that is present as a potential hazard over the entire airfield and is much more difficult to predict and control. It is the airfield itself, which can be a major contributor if it deteriorates and yields loose pieces of concrete.

1.2 Airfield Structural Defects

Airfields are typically constructed of asphaltic concrete, portland cement concrete (PCC), or a combination of both [Transport Canada Civil Aviation]. The type of pavement used determines the type of deterioration that will typically be found. Deterioration of the concrete can be a major source of the FOD found on runways and taxiways. As seen in Figure 1.2, there are several structural defects that can plague PCC airfields.
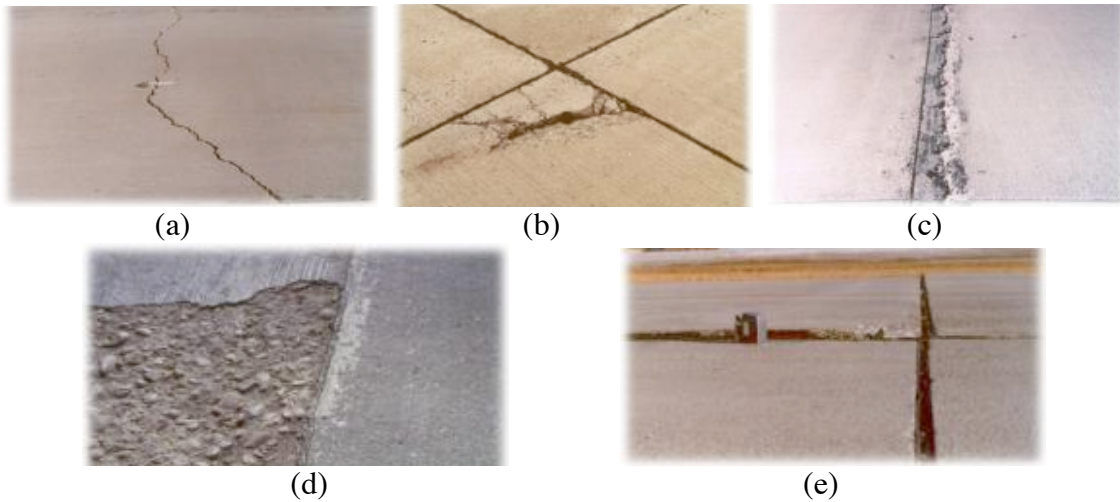
Figure 1.2 Common structural defects found in PCC airfields: (a) slab cracking, (b) corner cracking, (c) edge cracking (d) scaling/spalling, and (e) stepping [Transport Canada Civil Aviation].

All these defects can eventually result in loose pieces of concrete and popouts, which can pose a danger to the aircraft. In addition to the physical impact and load caused by the immense weight of the airplanes when at rest and upon landing, they could also be caused by a variety of chemical reasons. For example, the use of large amounts of de-icing and anti-icing chemicals used at airports located in cold regions may play a part in accelerating the deterioration of the airfield.

1.3 Lester B. Pearson International Airport

Lester B. Pearson International Airport is situated in Toronto, Ontario, Canada and is one of the top 30 busiest international airports. Pearson International Airport saw thirty-one million passengers travel through in 2006, a number that is steadily growing each year. It is currently operated by the Greater Toronto Airports Authority (GTAA), which oversees the operations, management, and development for improving services to meet the growing needs of the region. Sustainability and the environment are important factors, however, and the GTAA has been able to keep them in consideration throughout the growth of Pearson Airport [GTAA, 2006].

A key example of the GTAA's progress in environmental consciousness is the construction of the Central De-icing Facility (CDF), which was built to reduce the environmental impact of aircraft de-icing operations at the airport. There have been numerous studies that have examined the harmful impact of glycol-based aircraft de-icing fluids on the environment, particularly on aquatic life and vegetation in the vicinity of airports. The purpose of the CDF is to minimize the negative effects on the surrounding environment by containing as much of the aircraft de-icing fluids as possible. This is achieved by building the entire facility on a special liner, which limits the spread of de-icing fluids through the soil system, and running a vast collection system under the entire de-icing pad, which is capable of storing over 12 million litres of spent de-icing fluid. The CDF was in place and ready for its first de-icing season during the 1997/1998 winter season. There was one operational bay, which could accommodate 2 small planes or 1 large plane. It was further expanded over the next two years with the addition of five bays, allowing for simultaneous de-icing of 12 small planes or 6 large planes. More recently, for the 2006/2007 season, an on-site recovery facility was launched to recycle the collected de-icing fluid waste for processing into a product that could be sold to a secondary market, such as the auto industry [GTAA, 2003; GTAA Winter Operations, 2007].

1.4 CDF De-icing Operations

The de-icing season at the GTAA Pearson International Airport runs from October to April. During these months, de-icing operations commence when it is deemed necessary, based on up-to-the-minute weather conditions. Canadian Federal government regulations state that aircraft must be de-iced when the probability of ice formation is high because they are not allowed to take-off with ice on their wings [City of Toronto, 2002]. Consequently, de-icing operations play an extremely critical role in ensuring passenger safety for the airport industry in cold climates.

There are currently 24 de-icing trucks and 4 glycol recovery vehicles, some of which can be seen in Figure 1.3 below. One de-icing truck is positioned on each side of the airplane

and the controller applies the de-icing fluids, which will remove any snow and ice accumulated on the airplane surface.

<div align="center">(a)   (b)</div>
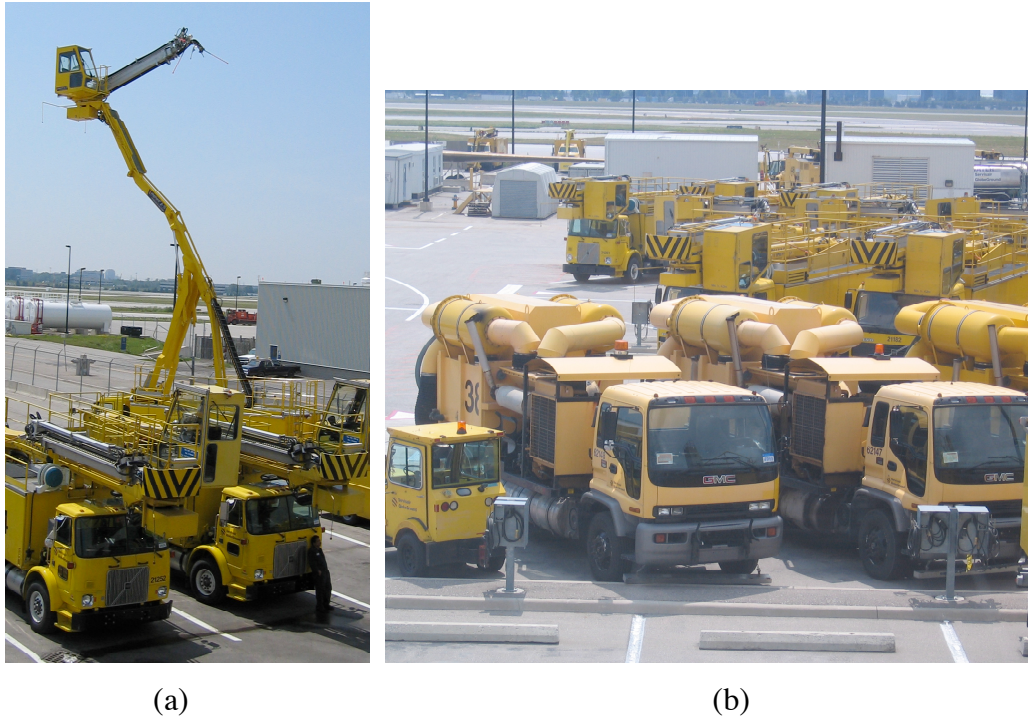
Figure 1.3 a) A de-icing truck with its de-icing arm fully extended and b) a glycol recovery truck.

At Toronto's Pearson International Airport alone, a large amount of de-icing fluid is spent to treat aircraft each winter. In order to give an indication of just how much fluid could be spent each year, 2004-2005 de-icing statistics were obtained. With 14,229 airplanes de-iced during that season, 5.729 million litres of Type I de-icing fluid and 1.472 million litres of Type IV anti-icing fluid were used.   This amounted to a total of 7.201 million litres of fluid used at the Toronto Pearson Airport alone. It is clear that, globally, extraordinary amounts of de-icing fluids are used each year [Forbes].

Much of the de-icing fluid falls onto the concrete pad beneath the airplane; therefore, glycol recovery trucks are sent out to collect any of the waste fluid. Depending on de-icing demands put upon the CDF, glycol recovery trucks may have to wait several turns before getting a chance to collect fluid on the ground. Ideally, a recovery truck would be sent out immediately after every airplane de-icing operation because the collected fluid

would be less contaminated. In reality, however, this is not possible, as up to 500 airplanes could require de-icing in one day, limiting the time available for recovery trucks to collect the spent fluid. Thus, as a result of de-icing operations, the concrete pad at the CDF is exposed to a great deal of de-icing fluid every winter.

1.5 Objectives

Deterioration of airfield concrete can be a hidden FOD hazard since concrete is present over the entire airfield, making it hard to recognize as a risk. In addition, literature searches have uncovered many studies regarding the adverse impact of aircraft de-icing fluids on the environment, but very little regarding the effects of aircraft de-icers on concrete. Therefore, as a preventative measure, the aim of this research project was to determine whether aircraft de-icers are potentially accelerating concrete degradation. This was accomplished by conducting a series of mechanical tests followed by microscopic and elemental analyses.

CHAPTER 2 - LITERATURE REVIEW

2.1 Ordinary Portland Cement

Ordinary Portland Cement (OPC) is produced in a rotating kiln by combining limestone, which yields calcium oxide, and clays, which yield silicon oxide, aluminum oxide, and iron oxide. Various compounds form as the temperature rises from 50°C to 1450°C and the raw materials begin to react with each other. The resulting clinker is composed of four major components, which, in order of formation, are dicalcium silicate (C_2S)[1], tricalcium aluminate (C_3A), tetracalcium aluminoferrite (C_4AF), and tricalcium silicate (C_3S). Gypsum $(CaSO_4 \cdot 2H_2O)$ is then added to the clinker and the mixture is ground to produce OPC.

The four components in OPC have several different functions during hydration, each affecting the cement properties in various ways. C_2S and C_3S both hydrate, according to Equation 2.1 and 2.2, to form calcium hydroxide (CH) and calcium silicate hydrate (C-S-H), which gives good strength and bonding properties.

$$2\ C_3S + 6\ H \rightarrow 3\ C\text{-}S\text{-}H + 3\ CH \qquad (2.1)$$
$$2\ C_2S + 4\ H \rightarrow C\text{-}S\text{-}H + CH \qquad (2.2)$$

The C_3S hydrates rapidly, giving early strength within the first week, while the C_2S hydrates at a steady slow rate over a much longer period of time, on the order of months. The heat of hydration of C_3S is also double that of C_2S, at 500J/g versus 250J/g. However, both components contribute equally to the overall long-term strength of the cement paste [Bogue and Lerch, 1934].

The CH component comprises 18% of the C_2S and 40% of the C_3S total hydration product and buffers the pH of the cement to approximately 12.5 as it saturates the liquid present. This is generally desireable because many concrete structures will incorporate

---

[1] This particular shorthand notation is very commonly used in the cement and concrete industry, where C represents CaO, S represents SiO_2, A represents Al_2O_3, F represents Fe_2O_3, $\bar{S}$ represents SO_4, and H represents H_2O.

embedded steel reinforcing bars. A high pH, like that found in concrete, provides a passive protective environment against corrosion. The C-S-H component is often referred to as a rigid gel because of its porosity, poor crystallinity, and undefined structure. Initial set refers to the start of rapid C_3S hydration that occurs after CH and C-S-H begin to crystallize. As hydration proceeds, C-S-H forms around cement particles and progressively fills in the spaces in between adjacent particles. The hydrated cement product occupies more than double the volume of the original cement particles before hydration, although less volume than that of the separate anhydrous cement and the water components. Stiffening of the cement paste occurs as C-S-H coats cement particles and contacts C-S-H forming on adjacent particles. Final set refers to the peak of C_3S hydration before the reaction starts to slow down. Gel pores, which are interstitial spaces formed between C-S-H particles, and capillary pores, which are formed from areas of residual unused water, are present throughout the C-S-H gel structure. Consequently, the water-to-cement ratio and the degree of hydration have a large effect on the resulting concrete microstructure.

C_3A hydrates rapidly upon contact with water to produce calcium aluminate hydrate (C-A-H), which contributes to rapid setting conditions, known as flash set. This results in the consumption of water, producing a stiff cement paste with very little strength, and is also accompanied by high heat evolution. C_3A is, generally, an undesirable by-product of clinker production. Gypsum is added to cement to control the hydration and avoid flash set by reacting to produce ettringite ($C_6A\overline{S}_3H_{32}$), which coats the C_3A particles and retards further hydration. Although ettringite formation is expansive, it is harmless if it occurs while concrete is still plastic. Any unconsumed C_3A remaining after gypsum consumption will react with present ettringite and water to revert to a stable monosulphoaluminate ($C_3A \cdot CaSO_4 \cdot H_{12}$), which is normal. The formation of ettringite and monosulphoaluminate contribute slightly to early stiffening, but play insignificant roles in overall long-term strength of the cement paste. If there is future exposure to sulphates during the cement paste's lifetime, monosulphoaluminate will revert back to ettringite, which can then cause detrimental expansion in already hardened cement paste and is referred to as sulphate attack. On the other hand, too much gypsum addition can

also be detrimental by extending the formation time of ettringite past the final set time of the cement paste, resulting in cracking of hardened paste.

C_4AF is another by-product of clinker formation and reacts in a similar manner to C_3A, but at a slower rate and with lower heat evolution. It does not contribute a great deal to cement paste strength.

2.2 Aircraft De-icing and Anti-icing Fluids

The two main fluids that are typically used at the airport for aircraft de-icing operations are designated Type I aircraft deicing fluid (ADF/de-icer) and Type IV aircraft anti-icing fluid (AAF/anti-icer). The de-icer is always applied during de-icing operations and is used to remove any snow, or ice, that has already collected on the aircraft surface. On site, the as-received de-icer concentrate is diluted with water to 38% or 48% concentration, based on weather conditions, before application. The anti-icer is subsequently used on aircraft, when necessary, to prevent ice from forming on the surfaces again. It is applied at full concentration and its application depends on the temperature, weather conditions, and the estimated time delay between the deicing operation and take-off.

The de-icer and anti-icer used for all experiments were supplied by the Greater Toronto Airports Authority (GTAA) Central Deicing Facility (CDF). Both of the fluids are currently purchased from The DOW Chemical Company as concentrates and the de-icer is diluted, on site, to appropriate concentrations.

The primary constituents, ethylene glycol and water, are present in different quantities within de-icer and anti-icer fluids. Proprietary additives are also present in small amounts, but no information could be obtained regarding composition. A breakdown of the constituents in both fluids can be found in Table 2.1, according to information sheets provided [The Dow Chemical Company, 2002].

Table 2.1 Dow Chemical Company de-icer and anti-icer composition breakdown.

Type	Ethylene Glycol	Water	Additives
De-icer Type I	92%	7.5%	0.5%
Anti-icer Type IV	64%	35%	≤ 1%

2.2.1 Ethylene Glycol

Ethylene glycol, $C_2O_2H_6$, is an organic chemical belonging to the glycol family and is characterized by two hydroxyl groups. It is a colourless, odourless, and viscous liquid with a density of 1.1132 g/cm^3 and is commonly used as a freezing point depressant, such as an anti-freeze in automobile cooling systems. The freezing point of ethylene glycol is –12.9^{o}C, but it forms a eutectic mixture with water, resulting in lower freezing points at various concentrations.   A phase diagram of water and ethylene glycol, shown in Figure 2.1, shows that the eutectic occurs at approximately 57% ethylene glycol and 43% water, corresponding with the lowest stable freezing temperature of approximately -50°C. The dashed line portion of the curve represents the meta-stable freezing curve of the system at those locations. Above the solid line curve, there will be a liquid mixture of water and ethylene glycol, while at temperatures below the eutectic, there will be a solid mixture of water and ethylene glycol. The regions in between these two yield varying ratios of the two constituents in a solid-liquid state.

Ethylene glycol is readily miscible in water because hydrogen bonding that naturally occurs between ethylene glycol molecules is similar to those formed between water molecules, as shown in Figure 2.2. Consequently, ethylene glycol molecules and water molecules bond easily when mixed together and ethylene glycol has been found to absorb up to 200% its weight in water when placed in 100% relative humidity conditions [Health Canada, 2000].
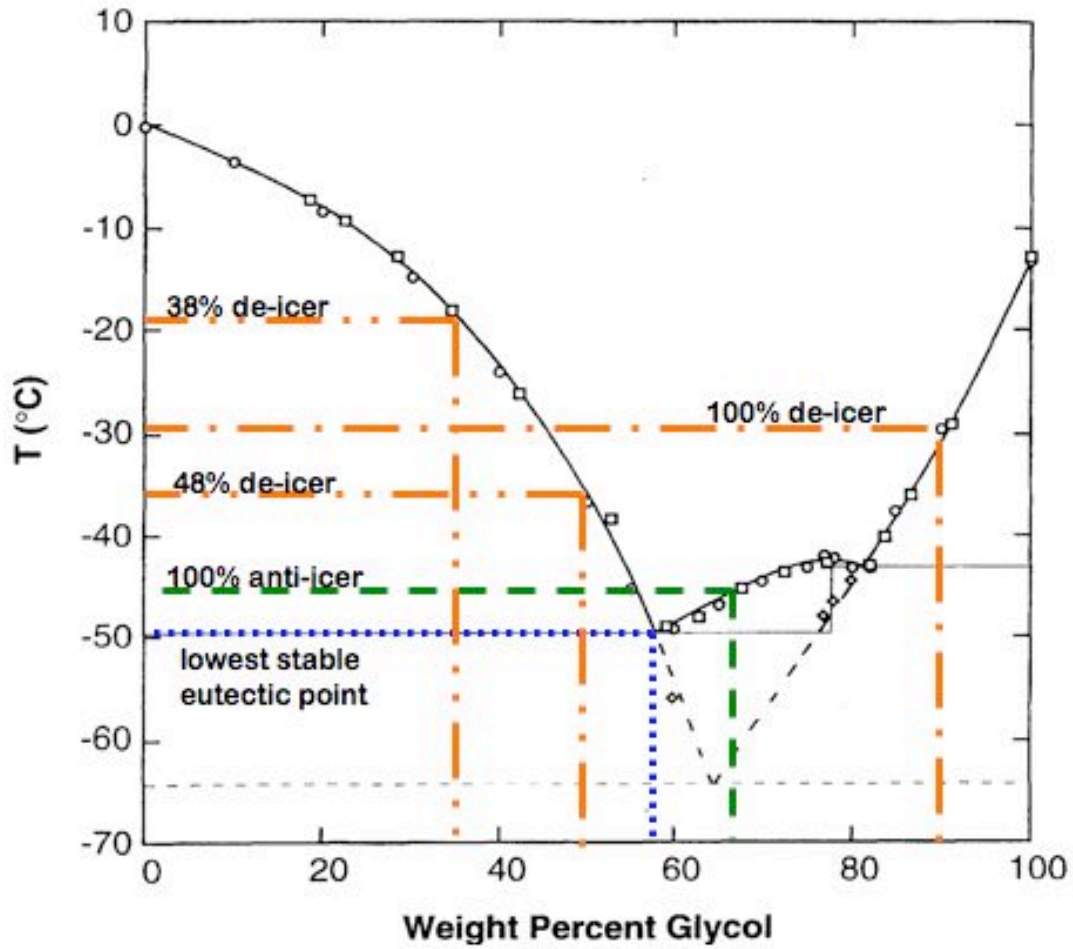
Figure 2.1 Ethylene glycol and water phase diagram [Cordray, 1996].
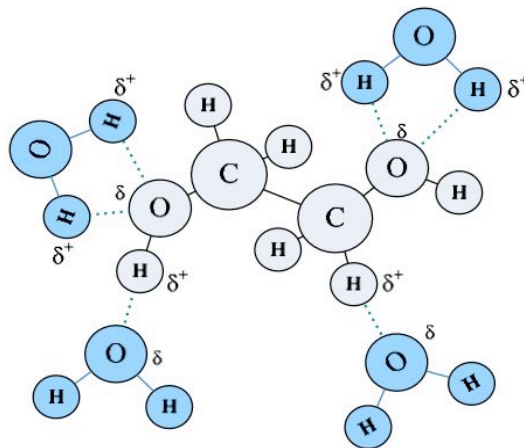
Figure 2.2 Ethylene glycol molecules interacting with water molecules [Kao, 2005].

The toxicity of ethylene glycol has made de-icing practices at airports a major concern, since much of the de-icer and anti-icer falls on the airfield and could eventually drain into stormwater sewers. Health Canada studies have found that the highest release of ethylene glycol to the land environment comes from de-icing operations at airports [Health Canada, 2000]. Many, including Toronto's Lester B. Pearson International Airport, have responded by constructing dedicated de-icing pads, which are areas used specifically for de-icing purposes and, often, have built-in recovery systems to contain as much of the excess de-icing fluid as possible. It is illegal to re-use the recovered de-icing fluid to de-ice aircraft; however it can be sold to industries for use in less critical applications such as the production of automobile anti-icing fluid.

2.2.2 Additives

The additives in de-icer and anti-icer are part of a package, referred to in the industry as an Ad-Pack. These are used to control various chemical and mechanical properties of the product being manufactured. There are various Ad-Packs available for different applications, but the one needed for aircraft deicers has been found to contain surfactants, corrosion inhibitors, pH modifiers, fire retardants, and dyes [Corsi, 2006; EPA, 2000]. The dye is used as a visual indicator to easily distinguish between the two types of fluids. DOW Chemical Company identifies its products by using orange for Type I deicer and green for Type IV anti-icer [The Dow Chemical Company, 2002]. A thickener is also added to the anti-icer formulation to increase holdover time, which is the length of time that the fluid will be effective for preventing ice formation. De-icer typically has a holdover time of approximately 15 minutes, while anti-icer has a holdover time of 30 to 80 minutes. There is a large variability in the anti-icer holdover time because it is greatly affected by the weather conditions at the time of application. The chemicals used in the Ad-Pack are proprietary. Formulations were not released by DOW Chemical Company for this research project [MacKinnon, 2005].

Very few studies have been conducted regarding the effects of these de-icing and anti-icing fluids on concrete, although many studies have investigated their effects on the

environment and, in particular, aquatic life in airport vicinities [Corsi, 2006; EPA, 2000; Gray, 2002]. The components that have been repeatedly identified in many of the different studies are likely to be present in the fluids used at the GTAA De-icing Facility as well. These include tolyltrizaoles as corrosion inhibitors, nonylphenol ethoxylates as surfactants, and polymer-based emulsions or carrageenan for thickeners.

In one study [Van Dam, 2006], the effects of aircraft de-icers on concrete at nine airports throughout North America that have dedicated de-icing facilities, such as the one at the GTAA, were studied. Visual inspections were done on-site and concrete cores were taken from each de-icing pad for petrographic analyses. He concluded that microbial and chemical concrete deterioration could not be directly attributed to the use of aircraft de-icers. The predominant causes of distress found in the concrete cores were related to workmanship regarding consolidation, finishing, and curing performance at the time of concrete placement. Inconsistencies in air void systems, resulting in inadequacies in certain regions, also contributed to concrete deterioration.

In another study [Rogers, Sullivan, Bremnar, 1999], the performance of two concrete pavement joint sealants was examined. In particular, the effects of temperature and the effects of water and ethylene glycol immersion were evaluated. It was concluded that ethylene glycol, in fact, decreased the glass transition temperature of the tested joint sealants, which is, in fact, desirable for low-temperature applications such as an airport de-icing facility during the de-icing season.

2.3 Freeze-Thaw Damage

2.3.1 General

Freeze-thaw damage is a major concrete durability problem in climates where the temperature fluctuates about freezing conditions. According to Environment Canada statistics, Pearson International Airport experienced an average of 75.3 freezing and thawing cycles between 1960 and 1989 [Ho, 2005]. Damage primarily appears as pop-outs, which are conical fragments of surface concrete, scaling, internal cracking, and D-

cracking, which is a type of cracking commonly found near expansion joints and edges. Expansion of surface aggregates or fracture within aggregates result in pop-outs, while expansion of cement paste near the surface results in scaling or spalling. Excessive tensile forces within the concrete microstructure will cause internal cracking, while D-cracking originates at the bottom of concrete slabs, where aggregates can easily become saturated from water accumulation and undergo expansion upon freezing and thawing. Due to greater moisture availability and an un-restrained concrete boundary condition, this type of cracking appears parallel to expansion joints and edges.

At cold climate airports, repeated freezing and thawing is a major concern due to the application of de-icing fluids, which depress the freezing point of water, causing freeze-thaw conditions for the concrete in, what otherwise would have been, constant freezing conditions. The presence of de-icers also increases moisture availability at the concrete surface, resulting in greater saturation. Thus, the use of de-icers may physically enhance concrete damage by increasing the number of freeze-thaw cycles that an area experiences, which is more detrimental than having a condition where the concrete remains frozen [West, 2005].

2.3.2 Internal Cracking

The dilation mechanism leading to freeze-thaw damage has been a long debated topic with many proposed theories [Powers and Helmuth, 1953; Powers, 1955]. Three main internal freeze-thaw mechanisms that have been proposed are hydraulic pressure, ice accretion, and osmotic pressure. In all cases, however, damage occurs when pressure exerted within the microstructure is great enough to exceed the tensile strength of the cement paste.

The most commonly accepted freeze-thaw damage model is that of hydraulic pressure. Initially, water is present in gel pores and capillary pores of the cement paste microstructure but, as water freezes into ice, it expands 9% in volume. In theory, the critical saturation level of the cement paste is 91.7% [Powers, 1955], since the volume increase can be accommodated by unfilled pore space. Realistically, pore water is not

distributed evenly within concrete, causing critical saturation to occur locally and decreasing the overall critical saturation level. As ice forms within capillary pores, any unfrozen water must redistribute itself to adjacent pores or air voids to accommodate the volume expansion. Otherwise, pressure within the pore cavity may exceed the tensile strength of the cement paste and cause cracking [Powers and Helmuth, 1953].

Osmotic pressure is another proposed cause of internal pressure generation [Powers, 1955]. As pore water freezes, the concentration of metal hydroxides in the surrounding unfrozen water increases because ice can only form from nearly pure water. This causes osmotic pressure because there is an increase in metal hydroxides near the ice-liquid interface and the resulting concentration gradient causes more water to be drawn into the pore in order to restore equilibrium. As the liquid surrounding the ice becomes diluted, more ice forms and the cycle continues [Powers, 1955].

Ice formation within the concrete pore structure can also occur due to ice accretion, which is also referred to as capillary ice growth. As ice begins to form within a cavity, there is a change in energy equilibrium between the ice inside the cavity and the liquid in the surrounding paste. Air voids are rarely filled to capacity, while capillaries can be, thus capillary ice is likely to experience greater pressure during the expansion of freezing ice. Consequently, the free energy of capillary ice is greater than that of air void ice [Powers and Helmuth, 1953]. Likewise, the free energy of gel pore water is greater than that of capillary ice, thus, gel pore water cannot freeze until it relocates to a capillary pore or air void. At the same temperature, the free energy of gel pore water is greater than that of ice in the capillaries and air voids because gel pores offer a much smaller space. As a result, the water in gel pores has a tendency to move towards cavities in order to reduce its energy potential, contributing to the growth of ice crystals [Powers and Helmuth, 1953].

For the osmotic pressure and ice accretion theories, the cause of cracking is not due to physical growth of ice crystals, but, rather, the movement of water into spaces surrounding ice crystals. Consequently, a swelling effect occurs on the cavity wall, placing it under pressures that could be great enough to cause damage.

In all cases, when gel pore water tries to redistribute to other locations, such as capillary pores or air voids, its movement through the cement paste generates pressures that may cause cracking. The presence of an adequate air-entrainment system, however, has a great impact on the behaviour of concrete under freeze-thaw conditions by providing convenient spaces for excess water.

It is likely that a combination of various freeze-thaw mechanisms leads to frost damage, as not one single theory can account for the behaviour of concrete under different freezing conditions [Pigeon, 1994; Powers, 1955].

Freezing and thawing is particularly damaging when air voids are not given sufficient drying time after thawing to empty themselves. Realistically, there will always be residual water within air voids and, if water is present to saturate the concrete, less space would be available to accommodate the ice upon freezing as the air void gradually accumulates more water [West, 2005].

2.3.3 Scaling

Scaling is the gradual removal of cement paste near the concrete surface and can range from "light severity", in which there is no exposure of coarse aggregates, to "very severe", in which there is loss of aggregates and mortar to a depth greater than 22 mm [ACI 201.2R-01]. When depth loss is greater than the maximum aggregate size, it can be classified as spalling [Transport Canada Civil Aviation, 2005].

Various sources found that scaling occurs only in the presence of road de-icers [Korhonen, 2002; Valenza and Scherer, 2006] and there is a pessimum concentration, after which the scaling effect decreases with increasing concentration. For example, the scaling versus sodium chloride solution concentration, shown in Figure 2.3, indicates that the pessimum concentration occurs at approximately 3%. It was found that, regardless of the solute, the pessimum concentration occurs at approximately 3 % because of the effect

of the solute on the strength of ice formed at varying concentrations [Valenza and Scherer, 2006].
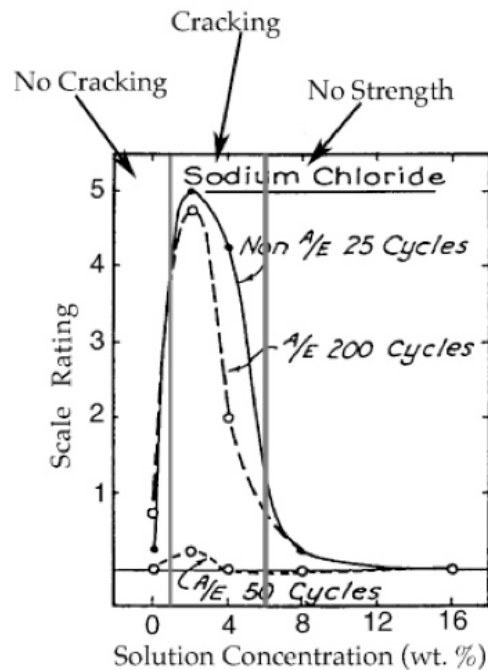
Figure 2.3 Effect of varying NaCl solution concentration on concrete scaling [Verbeck and Klieger, 1957].

2.3.4 Air Entrainment and Air-Entraining Admixtures

The most important chemical admixture for freeze-thaw durability of concrete is air-entraining admixture (AEA), which functions to stabilize air voids that form within the paste during mixing. Since it is mixing action that creates air voids throughout the paste, adequate mixing time is an important function of the effectiveness of an air void system.

AEA molecules, which are often hydrocarbon-based are hydrophobic at one end and hydrophilic at the other end. Because of the molecule's polarity, the hydrocarbon chains will arrange themselves into a low-energy configuration, which reduces the surface tension within the paste, as shown in Figure 2.4. Air voids also become well-distributed within the paste due to the repulsive forces between the polarized admixture molecules, providing space to accommodate for extra water during freezing conditions.

17

(a)   (b)
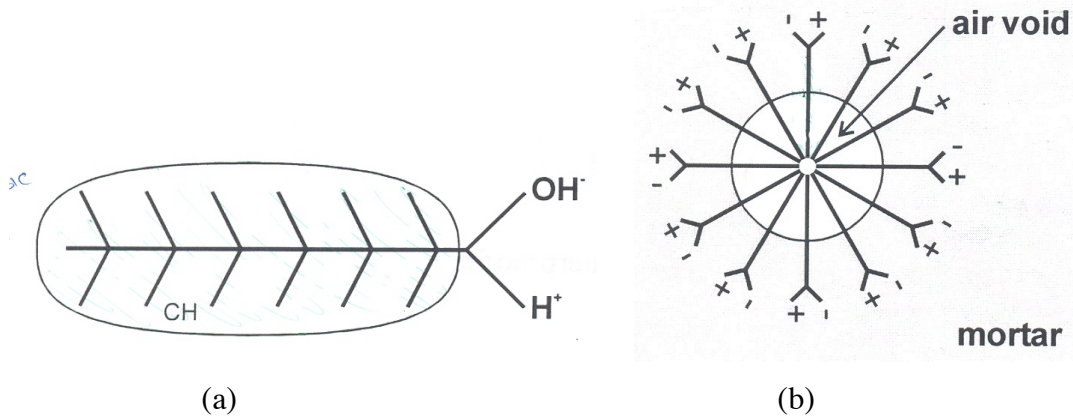
Figure 2.4 (a) typical hydro-carbon AEA molecule; (b) low energy AEA configuration of AEA molecules.[West, 2006]

Experimental studies have shown that many factors can influence the behaviour of cement paste upon exposure to freezing temperatures. However, the entrained air content of the paste has, by far, the greatest impact on the durability of concrete exposed to freeze-thaw action [Powers, 1955; Pigeon, 1994]. In fact, properly air-entrained concrete should not experience any internal cracking due to freeze-thaw damage [Pigeon, 1994]. The air void system should allow protection by providing space into which water can diffuse as ice forms and expands within capillary pores.

In addition to the existence of a good air-entrainment system, the air void spacing and rate of freezing are important parameters that affect concrete freeze-thaw behaviour [Powers, 1955]. Concrete with a total air content composed of primarily several large air voids would not provide the same frost resistance as concrete with numerous small air voids. This is because the distance that water would have to travel in order to reach the air void, referred to as the void spacing factor.   Pressure on the paste increases approximately in proportion to the square of the distance to the void, so the spacing factor greatly influences the effectiveness of the air void system in controlling expansion within the concrete microstructure. There is a certain distance away from an air void at which the pressure equals the tensile strength of the paste. The area bounded by this distance can be visualized as a protective shell within which the pressure can never be great enough to cause damage. Thus, if air voids are sufficiently close together to have

18

overlapping protective shells, the likelihood of damage by hydraulic pressure generation can be eliminated [Powers and Helmuth, 1953].

Air void spacing also greatly affects the pressures generated by diffusion of water through the cement microstructure. As the temperature decreases, the free energy of water within the system increases within the gel pores and, to a lesser extent, the capillary pores. Thus, gel pore water tries to diffuse to the nearest air voids and capillary pores to restore equilibrium. Unless an air void is completely full of ice, its free energy will remain constant, even when gel pore water diffuses into it. On the other hand, the free energy level of capillary pore ice will increase when gel water diffuses to it because it is likely near capacity and will experience increasing pressure as the ice crystal grows larger. The distance of the gel pore to the nearest air void affects the pressure experienced by capillary pores because during the time it takes for gel water to diffuse to an air void, thus decreasing the free energy in the gel water, the capillary pore ice will be receiving freezable gel water. This will occur as long as the free energy level of the gel water is greater than that of the capillary ice, causing increasing pressure within the capillary pore. Thus, if the distance between the gel pore and an air void is small, the amount of freezable water received by the capillary pore will be minor and unlikely to cause critical expansion [Powers and Helmuth, 1955].

The rate at which freezing occurs is an important variable because there are opposing forces acting within the cement paste as the temperature decreases and water freezes: contraction and expansion. Contraction occurs as water escapes from gel pores, whether from diffusion to air voids and capillary pores or from evaporation. Expansion occurs because of hydraulic pressure generation and capillary ice growth. The freezing rate influences the rate at which both of these processes occur since it affects the driving force behind them. Diffusion occurs gradually, as temperature decreases, and can still occur when temperature is held constant because it is a slow process that lags the driving temperature potential. On the other hand, expansion occurs rapidly when hydraulic pressure or capillary ice growth is present. These two opposing forces are present as the concrete experiences freeze-thaw cycling and place the paste under strains that may eventually lead to damage [Powers and Helmuth, 1955]. No studies have been found

regarding the effect of ethylene glycol on these particular processes. As a result, the present work aims to investigate and address this gap in information.

2.4 Alkali-Aggregate Reaction

Alkali-aggregate reaction (AAR) is a chemical attack that can result in the development of distress cracks on concrete surfaces [Rogers et al, 2000]. There are two types of reactions: alkali-silica reaction (ASR) and alkali-carbonate reaction (ACR). Both involve interactions between metal hydroxides and reactive aggregates, leading to the formation of expansive reaction products that, consequently, put pressure on the surrounding paste and cause cracking and deterioration.

Although no studies have been found concerning the effect of aircraft de-icing agents on the occurrence of AAR or the AAR mechanism, studies have been done regarding the effect of road de-icers on AAR [Diamond et al., 2006]. Potassium acetate, which is commonly used as an airfield de-icer, was found to instigate ASR by causing the concrete pH to jump from pH 11 to pH 15. This highly alkaline environment appeared to induce ASR in ASR-susceptible aggregates during laboratory testing.

Since crack formation due to AAR would result in greater ingress of substances into the de-icing pad and likely lead to FOD concerns, it was concluded that the effect of de-icing fluids on AAR should also be investigated in the present study.

2.4.1 Alkali-Silica Reactions

There are two requirements that must be satisfied for ASR to occur in concrete. First of all, the reactants must be present. One reactant is the alkali, which comes in the form of sodium or potassium hydroxides, which form during the hydration of portland cement. The second reactant is reactive silica, present in the aggregates. The other requirement is the presence of moisture, providing a relative humidity greater than 85% in the concrete structure [Sarkar, 2004]. The water is usually already present due to the concrete pore solution. When the reactants and ideal condition are met, the ASR process can take

place. As with most chemical reactions, it will continue until either one, or all, of the reactants is depleted [Tobin, 1995].

The deterioration mechanism caused by ASR can be divided into two steps. The first step is the formation of the ASR gel, which is an alkali-silica reaction product, at the aggregate-cement interface. The second step is the absorption of water by the ASR gel, causing it to swell and put expansive forces in the structure. The presence of ASR gel within the concrete structure is, in fact, normal and acceptable. It is detrimental only when it is generated in large quantities and causes expansive forces great enough to disrupt the concrete. The expansion often results in macro-cracking at the concrete surface, which can lead to FOD concerns at airports.

The type of aggregate present in the concrete is a significant factor in determining whether ASR will occur or not. If reactive silica is not present in the aggregate, then ASR will not occur. Aggregates can be classified into one of three types: crystalline, crypto-crystalline, and amorphous. Crystalline silica (quartz) is non-reactive because it is well-ordered, while amorphous silica is highly reactive because of its disorganized structure, allowing easy infiltration by the alkali ions, as shown in Figure 2.5. The crypto-crystalline silica, which is very finely crystalline, has also been found to be reactive as well, but to a lesser degree because it is crystalline with a more open structure [Sarkar, 2004; Bazant, 2000].
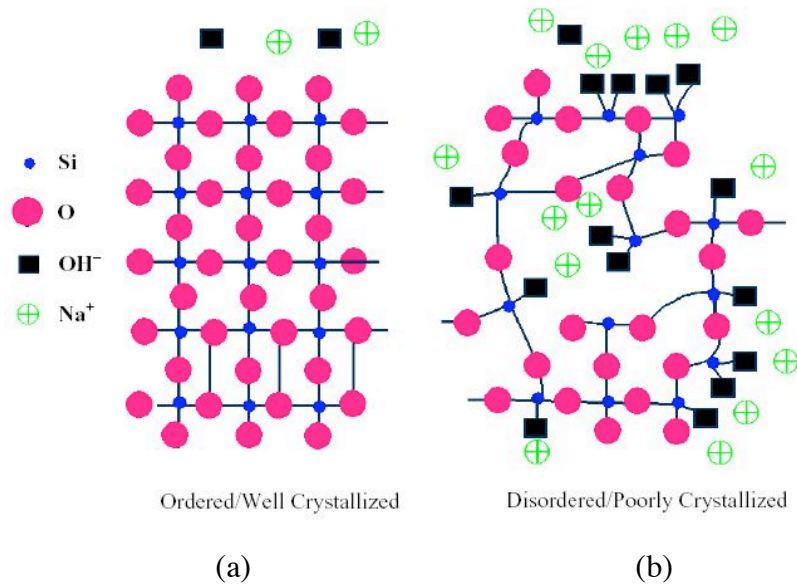
Figure 2.5 (a) crystalline structure (b) amorphous structure [Sarkar, 2004].

2.4.1.1 ASR Gel Formation

The formation of the silica gel is dependent on the diffusion of hydroxyl ions to the aggregates, causing the dissolution of silica. There is usually a thin layer of dissolved silica around the aggregate present, but further hydroxylation will occur if reactive aggregates are present. With the case of crystalline silica, the process is so slow that it is negligible, but the reaction with amorphous or crypto-crystalline silica occurs at a much faster rate [Bazant, 2000]. The dissolution of silica is, therefore, the controlling factor for latency time, which is the response time between initial exposure to the reactants and the first appearance of an effect [Ulm, 2000].

The presence of alkalis in the concrete is primarily due to the cement hydration process. Potassium and sodium are initially found in unhydrated phases in the cement paste as potassium oxide, K_2O, and sodium oxide, Na_2O. During cement hydration, the oxides dissolve to yield K^+, Na^+, and OH^- ions in the pore solution. Calcium hydroxide, $Ca(OH)_2$, is also present after cement hydration and dissolves to yield Ca^+ and OH^- ions, but at lower concentrations because of its limited solubility [Bazant, 2000].

The water molecule enters the silica structure and modifies it according to the following chemical reaction [Bazant, 2000]:

$$Si\text{-}O\text{-}Si + H_2O \rightarrow Si\text{-}OH + OH\text{-}Si \qquad (2.3)$$

The resulting structure is composed of silanol bonds, which further react with hydroxyl ions [Bazant, 2000]:

$$Si\text{-}OH + OH^- \rightarrow SiO^- + H_2O \qquad (2.4)$$

A gel substance forms around the aggregate as this process continues. The ASR gel is a weakly-bonded cross-linked alkali-silica network with interstitial water molecules dispersed throughout it[Jones, 1988]. In order to attain equilibrium, the negatively charged gel attracts positive ions, which include alkalis in the pore solution such as Na^+, K^+, and Ca^{2+}. The Ca^{2+} will be absorbed preferentially if it is in high concentration within the pore solution. The reaction will result in the formation of preferred C-S-H, which is a rigid and non-reactive constituent. However, if the pore solution has a low concentration of Ca^{2+} ions, which is more likely to be the case because of its poor solubility, the Na^+ and K^+ ions are absorbed, which produce a more viscous gel that will absorb more water [Bazant, 2000].

As mentioned before, the main source of the alkalis for the ASR reaction to occur comes from the cement itself. The total alkali content, given as a sodium oxide equivelent, is given by [Tobin, 1995]:

$$\text{Total alkali content} = (\% \ Na_2O) + 0.658 \ (\% \ K_2O) \qquad (2.5)$$

The total alkali content is normally below 1% of the cement weight and a limit of 0.6% is generally used as a maximum alkali content for ASR damage prevention. However, using this limit will not guarantee that ASR damage will not occur since other factors must be considered such as the size of the cementing materials and the admixtures used.[Tobin, 1995]

Furthermore, there are external sources that may contribute to higher alkali concentrations. Some pozzolanic materials, such as fly ash, contain alkalis although they

are used quite often as a replacement cementing material. Therefore, the total amount of alkalis in the concrete should include all alkali sources.

The temperature of the concrete is a major factor in the formation of ASR gel. As the temperature increases, the reaction rate increases, which is the case for most reactions. This leads to greater amounts of ASR gel produced around the aggregates. The temperature also has an effect on the equilibrium between the silica in the aggregates and the alkali in the pore solution, thus affecting the amount, but also the composition of the gel produced [Jones, 1988].

The permeability and dimensions of the aggregate are major factors in ASR gel formation. The surface area of the aggregate is the dominating factor when its permeability is low. This is because the reaction will mainly occur on the outer surface of the aggregate. Therefore, as the size of the aggregate increases, the surface area decreases and less gel will be produced. On the other hand, if its permeability is high, the reaction will be able to occur within the aggregate, as well as on the surface. This implies that the aggregate's volume would be a dominating factor in this case [Jones, 1988].

2.4.1.2 ASR Gel Expansion

The expansion of ASR gel can be broken down into two steps: hydration of the gel causing swelling and diffusion of the gel from the reaction site. The rate at which these processes occur determines the likelihood of the gel causing distress to the concrete. The expansion of the gel gives the characteristic time of the process, that is the time it takes for the system to undergo a critical change [Ulm, 2000].

As the gel absorbs water, it swells and occupies a greater volume. The gel has been found to absorb between 200 to 400% its weight in water in saturated atmosphere. The gel will initially occupy empty space provided by the interconnecting pore structure within the cement paste. Pressure will gradually be exerted on the surrounding paste as the available pores fill up with the gel. The aggregate size and surrounding cement

porosity has a direct effect on the amount of gel that will fill interfacial pores, which will not cause expansion, and the rate of gel diffusion into the cement paste, causing concrete expansion [Suwito et al., 2002]. Cracking occurs as a result of the gel pressure while crack propagation acts to decrease the gel pressure within the concrete [Moranville-Regourd, 1997].

Hydration is a function of the amount of water present at the reaction site. If there is sufficient water, the hydration process will be carried out relatively easily. However, if there is little water present, it implies that there would be a higher concentration of Na^+, K^+, and OH^- in the solution, causing the formation of the gel products to increase in production [Jones, 1988]. It can be seen that the water plays a considerable role in both the formation and expansion processes. It is the transport mechanism for reaction products and it is necessary for silica dissolution to occur in the first place [Ulm, 2000].

The gel structure plays an important part in the amount of swelling that occurs. As previously mentioned, temperature is a variable that can change the composition of the gel. The gel structure, in turn, affects the amount of water it attracts, controlling the amount of swelling and, thus, the pressure generated [Jones, 1988].

2.4.1.3 Crack Formation

Courtier [Courtier, 1990] suggests the concept of dividing the concrete depth into three zones to discuss the mechanics of surface crack formation due to ASR. The zones are classified as zone three for the concrete far enough from the surface that it is not influenced by surface conditions, while zone one refers to the topmost layer up to a depth of approximately 20 mm. Figure 2.6 shows the expansion and cracking mechanisms affecting each zone.
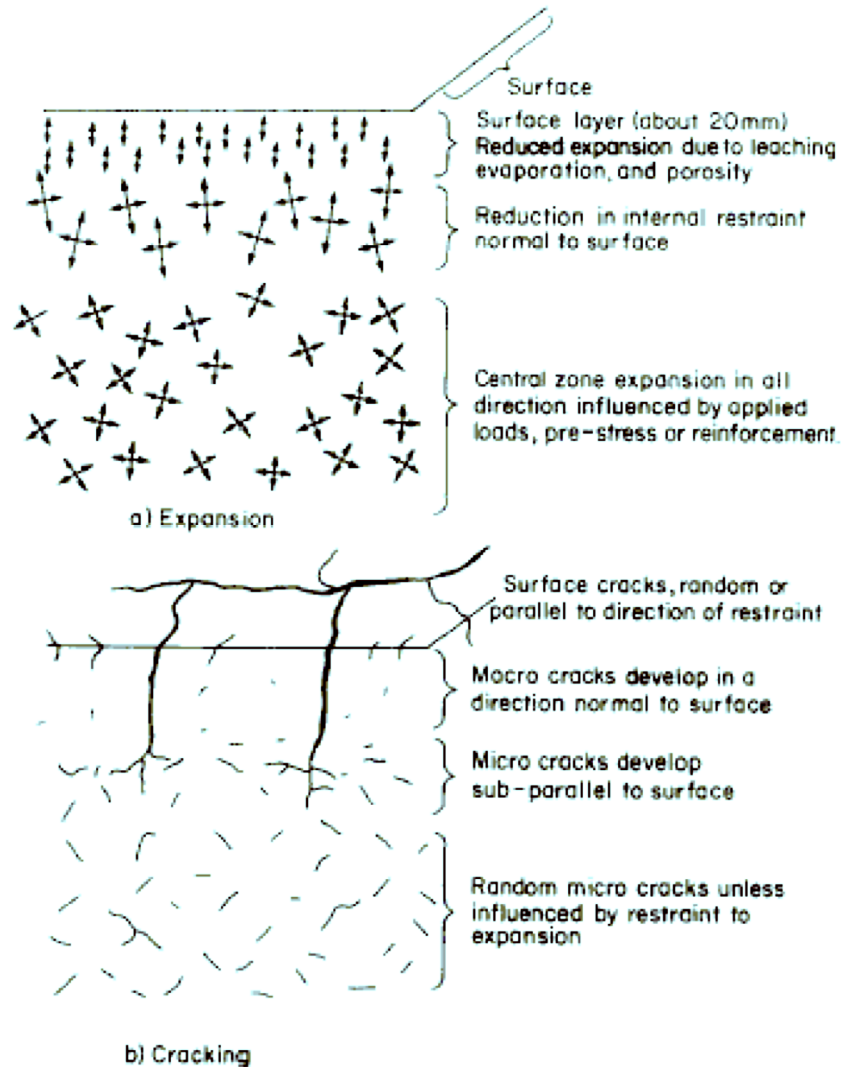
Figure 2.6 ASR crack zones: (a) expansion mechanism; (b) cracking mechanism [Courtier, 1990].

Reactions occurring in zone three, also known as the central zone, will be dependent upon the amount of reactants, including water, present at those locations. When the ASR gel expands, micro-cracks will form in the weakest directions, which are presumed to exist randomly because of the heterogeneity of concrete. Reaction processes will initiate easily with existing water, but will eventually slow down since transport of the necessary reactants, such as water, will be limited somewhat by the distance away from the surface.

Reactions in zone two will proceed at a faster rate than in zone three because of its proximity to the surface and, thus, greater availability of water. In terms of cracking

initiation and propagation, micro-cracks are more likely to form perpendicular to the concrete surface because there is less constraint in that direction.

Zone one experiences very different conditions since it is at the concrete surface. It is greatly affected by exterior conditions as well as variations due to the curing process. For horizontal surfaces, the concrete near the surface is usually more porous than the interior concrete due to bleeding during the curing process. This allows for easier transport of the reactants to reactive aggregates. As curing continues, the concrete may also experience drying shrinkage, which is caused by loss of moisture. Drying progresses inward from the concrete surface, creating non-uniform drying conditions. The expansion caused by ASR will cause the concrete to expand upward, normal to the surface, because of the lack of restraint. The porosity will accommodate the ASR gel to a greater extent than in the previous zones, thus relieving the expansive forces, but porosity also decreases the strength of the structure and increases the availability of reactants, as mentioned before.

The combination of these different reactions and crack mechanisms in the different zones creates a strain gradient over the depth of the concrete. Zone three experiences greater cracking, and thus expansion, in the longitudinal and transverse directions. Zone one experiences drying shrinkage and expansion, primarily in the direction normal to the surface. The differential expansion throughout the concrete is largely the cause of macro-crack formation on the concrete surface.

2.4.2 Alkali-Carbonate Reactions

Alkali-carbonate reactions refer to those that occur when dolomitic limestone aggregates are exposed to alkali solutions. The hydroxides may come from external sources, but often originate from the cement as dissolved ions within the cement pore solution.

Dolomite is calcium magnesium carbonate, $CaMg(CO_3)_2$, and can be found in rocks in certain regions. It is originally deposited as calcium carbonate (calcite) or aragonite, which is a different form of calcite, but turns into dolomite through exposure to magnesium sources, such as magnesium-rich ground water or warm ocean environments.

This process is known as dolomitization, but, through ACR attack, the reverse process of dedolomitization can occur, reverting dolomite back into calcium carbonate.

In Canada, dolomitic limestone can be found at the Pittsburg quarry near Kingston, Ontario. This particular aggregate is composed of large dolomite crystals within a fine-grained calcite and clay matrix [Hadley, 1961; Rogers et al., 2000]. There are also small amounts of silica within the aggregates, but its role in causing deleterious expansion has been dismissed in one report [Hadley, 1961] and acknowledged in another [Katayama, 2004].

The dedolomitization reaction of ACR-reactive aggregates occurs according to:

$$CaMg(CO_3)_2 + 2\ MOH \rightarrow CaCO_3 + MCO_3 + Mg(OH)_2 \qquad (2.6)$$
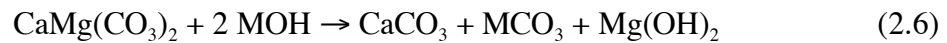
where MOH is a metal hydroxide, most often NaOH or KOH, which is readily available in pore solution. The reaction between dolomite in aggregates and a metal hydroxide results in the formation of calcium carbonate, metal carbonate, and brucite $(Mg(OH)_2)$.

The metal carbonates produced will further react with $Ca(OH)_2$ in a secondary process:

$$M_2CO_3 + Ca(OH)_2 \rightarrow 2\ MOH + CaCO_3 \qquad (2.7)$$
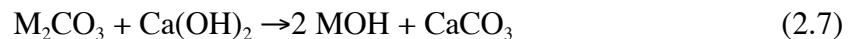
This reaction regenerates the MOH in the solution, providing more alkali for dedolomitization to occur. Thus, it is a self-sustaining process that continues until either one of the dedolomitization reactants is expended.

There are differences of opinion regarding the expansion mechanisms of ACR that result in concrete deterioration. However, the greatest amount of expansion appears to occur when there are approximately equal amounts of calcite and dolomite content in the aggregate, as shown in Figure 2.7 [Hadley, 1961; Rogers et al., 2000].
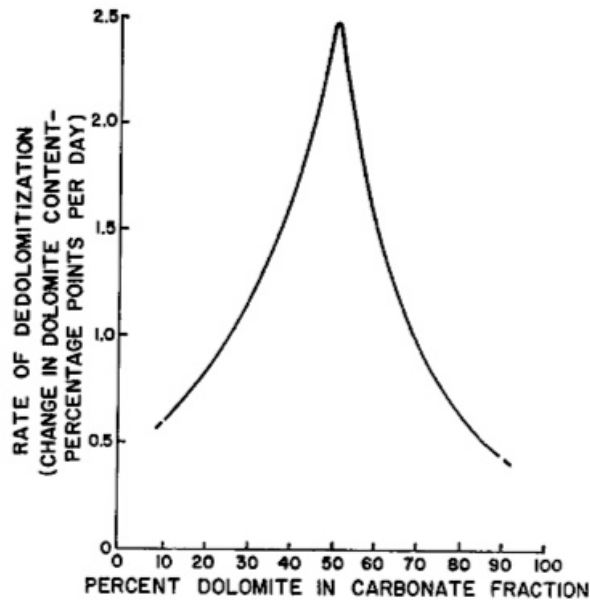
Figure 2.7 Rate of dedolomitization versus percent dolomite in carbonate fraction [Hadley, 1961].

One theory [Hadley, 1961] states that crystallization of brucite causes expansion. In addition, dedolomitization exposes clay surfaces that absorb water and swell, causing expansive pressure on the surrounding paste.

Another theory [Katayama, 2004] states that the dedolomitization process causes insignificant expansion itself, but leads to the exposure of crypto-crystalline silica within the aggregate. Upon exposure to alkalis, the silica reacts in the same manner as ASR-reactive aggregates, producing ASR gel, which subsequently absorbs water, swells, and causes expansive pressure on its surroundings. Thus, cracking is due to ASR reactions following the initial ACR reactions, although it is a combination of dedolomitization and ASR that produces expansion within concrete [Katayama, 2004]. This theory has been corroborated by others [Lopez, 2006; Lu et al., 2006] who found ASR expansion occurring in alkali-carbonate reactive aggregates as well. Lopez investigated the effect of various aggregates on ACR, while Lu investigated the effect of various type of metal alkali solutions. The presence of clay and chert were found to be related to ASR activity of the carbonate aggregates and aggregate porosity was potentially found to increase expansion activity, if any ACR or ASR was to occur, although it does not cause reactivity

29

on its own [Lopez, 2006]. In comparing metal alkali solutions involved in ACR reactions, NaOH was found to cause more severe reactions than KOH, but both solutions resulted in the formation of ASR gel product. An LiOH solution, which was also tested, was found to cause a very weak attack on ACR aggregates and did not produce ASR gel as with the other two solutions.

CHAPTER 3 - EXPERIMENTAL PROCEDURE

3.1 General

A series of experiments was conducted in order to investigate the effects of aircraft de-icing fluids on airfield concrete. The following mechanical and chemical tests were used to examine the different ways that de-icing fluids could interact with, and possibly affect, the integrity of the concrete.

1. Steel reinforcing bar corrosion test to determine the corrosivity of de-icing fluids.
2. Submerged cement paste test to examine the possible reactions between cement paste and de-icing fluids.
3. Rapid freeze-thaw test to expose concrete prisms to freeze-thaw conditions under the additional constant exposure to the de-icing fluids.
4. Four point bending test to observe the combined effects of freeze-thaw cycling and simultaneous exposure to de-icing fluids on the rupture strength of the concrete prisms.
5. Cylinder compression test to examine the effects of constant de-icing fluid exposure on compressive strength.
6. Accelerated mortar bar expansion test to investigate the behaviour of carbonate-reactive aggregates in concrete when under constant exposure to de-icing fluids.
7. Copper and steel plate exposure tests to study the reactivity of the two metals with de-icing fluids when uncontaminated, as well as when contaminated with cement paste.
8. Raman spectroscopy and environmental scanning electron microscopy (ESEM), combined with energy dispersive x-ray spectroscopy (EDS), to obtain micrographs and elemental analysis of various cement and concrete surfaces, as well as precipitates formed in the fluids.
9. Thermo-gravimetric analysis (TGA) of precipitates to observe differences between various fluid and specimen reaction products.
10. X-ray diffraction (XRD) to determine the chemical compounds of crystalline substances in the precipitates.

3.2 Concrete and Cement Paste Mixture Designs

Unless otherwise stated, concrete specimens for the following experiments were created using a mix design formulated to meet the GTAA airfield concrete specifications:

Table 3.1 GTAA airfield concrete specifications.

Cement Type	Portland cement type 10
Cement Content	300 to 328 kg/m^3 of concrete mix
Minimum 28-day Compressive Strength	35 MPa
Air Content	4 to 6 % immediately after discharge
Maximum water to cement ratio	0.45 by mass
Chemical Admixture Use	Only when workability cannot be achieved by proportioning of cement, water, aggregates, and air-entraining admixture

3.3 Steel Reinforcing Bar Corrosion Test

Objective :

The purpose of this test is to determine whether aircraft de-icer and anti-icer are corrosive to steel reinforcing bars, which may be present near, or around, the de-icing pad. An example of this would be dowels used at slab joints.

Specimens:

As-received carbon steel reinforcing bars (rebars) were used for this test without any prior cleaning or pickling techniques, in order to provide a good representation of rebar conditions in the field. Twelve 10M (metric designation for ribbed bar with a 100 mm^2 cross-sectional area) rebar specimens were cut to lengths of approximately 180 mm. A wire was attached to one end of the bar by drilling a hole into one end of each rebar and then soldering the wire in place. The two ends of the rebar, flanking an 80 mm length in the centre, were epoxy-coated to create a known exposure area on the rebar. This area was used to calculate a corrosion current density, based upon a measured corrosion

current and the exposed surface area. Layers of masking tape were used to protect the exposure area, while three coats of epoxy, applied at one-day intervals, were applied to ensure complete coverage. These rebars served as the working electrode of the corrosion cell. Graphite bars were also outfitted with one wire each to serve as a counter electrode for the corrosion cell.

Test Setup:

Three rebars were tested for each of the following test fluids: type I de-icer, type IV anti-icer, ethylene glycol, and water as a control. Thus, each corrosion cell container consisted of three steel rebars, as the working electrodes, one graphite bar, as a counter electrode, and a saturated calomel electrode (SCE) was used as a reference electrode.

All three working electrodes were inserted into the container through holes drilled through the plastic container lid. They were subsequently hot glued to the lid to hold them in place and prevent them from shifting around and touching the bottom of the container. The layout of the corrosion cell positioned the three reinforcement bars at equal distances away from the centre of the lid, which was the location of the reference electrode during measurement testing. The counter electrode was placed away from the working electrodes, but at an equal distance away from the reference electrode. The corrosion cell setup can be seen in Figure 3.1.
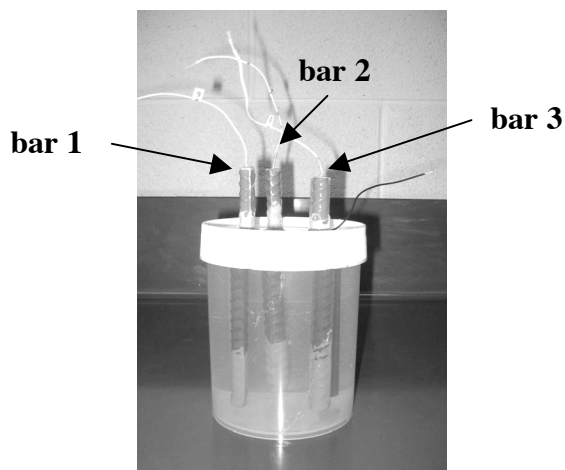
Figure 3.1 Water corrosion cell with white-wired working electrodes and a black-wired counter electrode.

A potentiostatic linear polarization resistance technique (LPR) was used to examine the corrosion activity of each of the reinforcement bars. Measurements were taken upon initial submersion into the test fluids and subsequent measurements were taken at random intervals. The corrosion cells were monitored until nearly steady state behaviour was observed, which resulted in four measurements.

Measurement Technique:

Determination of the linear polarization resistance is used to determine the corrosion activity of a system based on the linear region of a polarization curve between ±20 mV away from a material's open circuit potential. Within this region, corrosion current can be related to polarization resistance through the Stern Geary equation [Stern and Geary, 1957], as follows:

$$R_p = \frac{B}{i_{corr}} = \frac{(\Delta E)}{(\Delta i)}_{\Delta E \to 0} \tag{3.1}$$

where R_p is the polarization resistance, B is a proportionality constant, i_{corr} is the corrosion current, ΔE is the applied voltage range, and Δi is the corresponding response current range.

The polarisation resistance, R_p, can be determined if ΔE and Δi are known. The ΔE value used for this experiment was 0.04 V, representing an applied square wave voltage of -20 mV and +20 mV. The corresponding Δi value is determined by monitoring the steady state current response to the applied voltage. This yields a R_p value, which can then be used to determine i_{corr}, assuming a B value for the particular system. For corrosion of black steel in a concrete environment, appropriate B values for active and passive systems were found to be 0.026 V and 0.052 V, respectively [Andrade and Gonzales, 1978]. The states of the systems in this experiment were unknown, therefore, a B value of 0.052 V was taken to assume passivity. The major aim of this test was to make a distinction between passive and active corrosion, thus absolute values were not a necessity.

This corrosion monitoring technique is based on several system assumptions in order to determine corrosion current. One major assumption is that of general corrosion behaviour, where corrosion is uniform over a given surface area. Another is negligible solution resistance, since a high solution resistance would alter any measurements. Lastly, the B value for the given working electrode material must be known or reasonably estimated.

These assumptions were assumed to be valid for this experiment for several reasons. General corrosion behaviour was expected to occur because exposure of the black steel to the fluid was uniform over the entire exposed area. In addition, if the corrosion were found to be localized, rather than uniform, the actual corroded area could be reasonably estimated through visual inspection and used to calculate a more accurate corrosion density. The solution resistance was assumed to be negligible for these four fluids and the accuracy of the B value used for this experiment was assumed to be fairly inconsequential, since the results were evaluated relative to one another in this comparison test.

3.4 Submerged Cement Paste Test

Objective:

The purpose of the test was to observe the possible interactions occurring between cement paste and de-icing fluids.

Specimens:

Cement paste cylinders, batched with Type 10 cement and a water to cement ratio of 0.45, had been cast in 1998 and kept continuously moist in a humidity room. These 50mm Ø x 200 mm cylinders were cut perpendicular to the axes to yield three cylindrical disks of approximate equal size. The curved sides were epoxy-coated to create a 1-D flow condition through the disk, while the flat sides were ground to create a relatively even penetration surface.

Test Setup:

The cement paste specimens were placed in separate small plastic containers with the ground side facing the bottom of the container, as shown in Figure 3.2. Nylon tubing was used to support the specimens and provide access to the bottom surface of the specimen, allowing free fluid movement beneath the disks. Five different fluids were tested: 100% ethylene glycol, 38% ethylene glycol mixed with water, 48% ethylene glycol mixed with water, de-icing fluid, and anti-icing fluid. The fluids were used to half-fill two containers each, in order to fully submerge one ground end of the specimen while leaving the opposite ground end exposed to air.

Figure 3.2. Setup of a 50mm Ø x 200 mm cement paste specimen in a container for the submersion test.

Analysis Technique:

The specimens were periodically visually inspected to note any changes in the appearance of the fluid or cement paste specimens. Photographs were taken to record any changes and precipitates from any reactions were collected for further testing. The cement paste surfaces and cross-sectional profiles were examined by environmental scanning electron microscopy (ESEM) and elemental analysis using energy dispersive x-ray spectrometry (EDS). Thermal gravimetric analysis (TGA) was used, along with ESEM and EDS, on dried precipitates that were collected from the containers.

3.5 Rapid Freeze-Thaw Test

Objective:

The objective of this test was to determine if exposure to the de-icing fluids had any impact on the ability of concrete to withstand repeated freezing and thawing. The test equipment simulates freeze-thaw cycling that concrete may experience during its service life. Cycling was conducted at an accelerated rate in order to subject the specimens to a large number of cycles in a relatively short period of time.

Standards:

The Test for Resistance of Concrete to Rapid Freezing and Thawing [ASTM C 666] was used as a guideline for setup conditions and test requirements. Changes were made to accommodate the use of several test fluids, rather than just water. The ASTM test is normally used to assess and compare the behaviour of various concrete types under freeze-thaw conditions, with water as the freeze-thaw fluid. In this modified test, the concrete type was kept as a control while the freeze-thaw fluid surrounding the concrete prisms was varied.

The Test for Fundamental Transverse, Longitudinal, and Torsional Resonant Frequencies of Concrete Specimens [ASTM C 215] was used to obtain a resonant frequency for each specimen at regular intervals throughout the ASTM C 666 test duration.

Specimens:

The concrete prisms for the freeze-thaw test were prepared in two batches, designated as A and B. This was due to the size of the in-house concrete mixer, which was large enough to batch concrete for approximately 10 specimens and additional test cylinders. The concrete mixture designs used for the prisms can be found in Table 3.2.

Table 3.2. Concrete mixture designs for the freeze-thaw prisms.

Component	Amount	
	Batch A	Batch B
Cement	320 kg/m^3	
Coarse Aggregate (20mm maximum)	902 kg/m^3	
Fine Aggregate (sand)	602 kg/m^3	
Water	139 kg/m^3	
Air Entraining Agent	130 ml/m^3	260 ml/m^3

With two batches, the aim was to keep all parameters the same in order to produce concrete prisms of consistent composition. However, the air entraining agent was doubled for batch B because air content readings from batch A, at 3.2%, fell short of the concrete specifications given by the GTAA for airfield concrete, shown in Table 3.1, which was 4% to 6%. Doubling of the air-entraining agent yielded an air content of 5% for batch B.

Curing of the prisms followed the regime stated in ASTM C 666. For this regime, the prisms were de-moulded one day after casting and stored in a saturated Ca(OH)$_2$ bath at room temperature for two weeks. They were then moved quickly from the bath to individual containers within the freeze-thaw chamber, which was set at a thaw temperature between -1°C and 2°C. Water was poured into the containers during this initial period, in order to bring the temperature of all the specimens to the same thawing temperature for initial resonant frequency testing.

When the pilot specimen (described below) reached thawing temperature, the prisms were removed from the freeze-thaw cabinet, one at a time, to obtain initial resonant frequency values. These values were used to represent the prism in its preliminary condition, before any freeze-thaw action or fluid effects had occurred. The prisms were also weighed using a scale with a resolution of 0.1 g before being returned to the freeze-thaw cabinet, in order to keep track of any mass loss related to freeze-thaw damage. Immediately after these measurements, the prisms were returned to their individual stainless steel containers for placement within the freeze-thaw chamber for cycle commencement.

Test Setup:

The freeze-thaw equipment used for this test, manufactured by Humboldt Mfg. Ltd, can hold seventeen test specimens and one pilot specimen, as shown in Figure 3.3. The pilot specimen is required by the equipment to control the temperature cycling and to obtain continuous temperature readings.
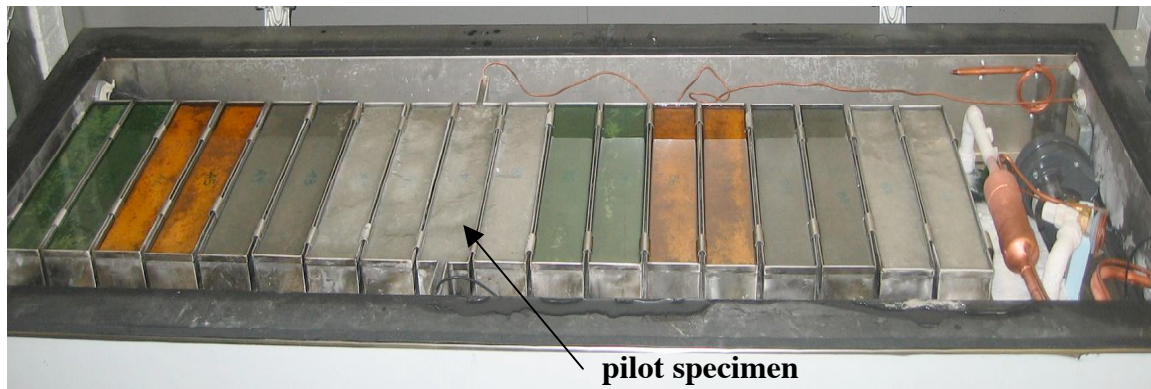
Figure 3.3 Interior of the freeze-thaw chamber, with specimens and test fluids in place.

The specimens were placed within individual stainless steel containers that ensured between 1mm and 3mm of fluid on all sides when the prism was placed correctly within the container. In addition, a clearance was achieved at the bottom surface of the container by resting the prism on top of a brass shims placed in the container. This was also done to prevent the heat-exchange media, such as the heating elements and the refrigeration plate, from transferring energy directly to the specimen surface through the steel containers, thus subjecting the specimens to significantly non-uniform temperature conditions.

The temperature was cycled between $+4^{\circ}$C and -18°C, which is the stated temperature range in ASTM C 666. It was noted that, as seen in Figure 2.1, the four test fluids freeze at different temperatures. Water would undergo freezing and thawing over the temperature range and ethylene glycol would undergo freezing and thawing with a freezing temperature of -12.9°C. On the other hand, the de-icer and anti-icer would not undergo any freezing within the cycle temperature range since their freezing temperatures of –approximately 29°C and -45°C, respectively, are well below -18°C. All specimens

would experience some degree of freeze-thaw damage, however, because all prisms were saturated in lime water upon placement in the freeze-thaw chamber.

Each cycle had to be completed within 2 to 5 hours to meet the ASTM standard requirements. This was regulated by the pilot specimen, which housed a thermometer bulb and a temperature cycle bulb, as seen in Figure 3.4. The temperature cycle bulb is used to measure the temperature within the freeze-thaw machine, which then feeds into a temperature controller that turns the heating and refrigeration elements on and off. The thermometer bulb was connected to a temperature recorder, which plotted the real-time temperature readings on a graph. The pilot specimen was constructed with the same dimensions as the test prisms, however it was cast in a mould with specially-designed stainless steel rods, which resulted in cavities at both ends of the prism. The two bulbs were placed in the cavities and then sealed with putty to prevent any fluid from entering the cavity.

(a)   (b)
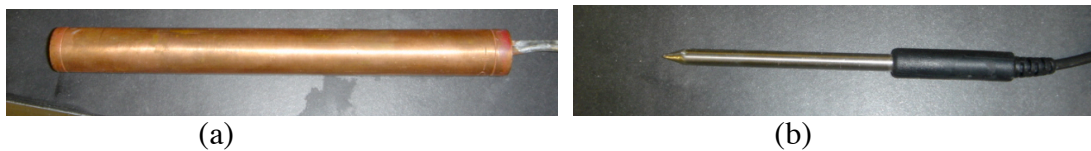
Figure 3.4 (a) 7"×3/4" Ø cycle control bulb and (b) 3"×1/4" Ø temperature bulb.

Determination of the test fluid to be placed within the pilot specimen container was conducted using a dummy specimen. The cycling operation was conducted with each the four fluids used, in turn, as the working fluid in the pilot container. The temperature plots for the four fluids were compared to see which fluid produced the slowest cycle time. In this case, the specimen in water took the longest time to complete one cycle, thus water was chosen to be the pilot container medium to ensure that all test prisms had sufficient time to reach the two extreme temperature requirements.

The specimens were placed in a random order within the freeze-thaw machine, which was changed after every non-destructive testing period. This eliminated any bias caused by temperature gradients within the equipment that were uncontrollable. According to ASTM standards, prisms must be measured at intervals of no more than 36 cycles, thus

prisms were measured at 30 cycle intervals for this test. This included weight measurements, to gauge mass loss, and resonant frequency measurements, to determine a durability factor for the prism.

Freeze-thaw cycling always started and ended at the thawing temperature measurement for consistency, which is especially important for the highly temperature-dependent resonant frequency testing. The specimens were maintained within that temperature range by keeping them in the freeze-thaw chamber. Specimens were removed from the chamber, one by one, just prior to being tested. Upon removal from the stainless steel container, the prism was quickly rinsed under cold water to wipe away any fluid residue or spalled concrete.

The resonant frequency testing was always performed first to try to minimize the effects of any temperature change upon removal from the chamber. The weight measurement was taken immediately after resonant frequency testing was completed for each specimen.

Analysis Technique:

The fundamental frequency was obtained for each concrete prism using the standard Test for Fundamental Transverse Resonant Frequency of Concrete Specimens [ASTM C 215]. There are two methods listed in the standard that can be used: impact resonance method and forced resonance method. The equipment used in the lab is the Erudite MKIV by CNS Farnell Limited, which uses the forced resonance method, as shown in Figure 3.5. The driving force is created by an electromechanical input device, which can be controlled to oscillate at a set frequency or sweep through a range of frequencies. The driver is placed at the centre of the prism to cause resonance in its transverse mode. The output frequency is then acquired through a sensor that is placed at either end of the prism. It is lightweight so it does not interfere with the oscillation of the prism.
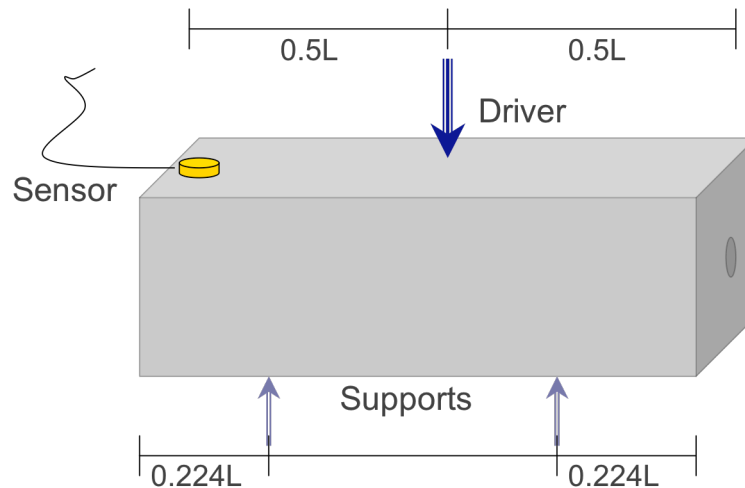
Figure 3.5 Transverse mode resonant frequency setup.

The Erudite MKIV was programmed to sweep through a range of frequencies in order to pinpoint the fundamental frequency. The range of the frequency sweep is very important in determining the correct fundamental frequency. When a prism is set in motion by an electromechanical driver, it will have one major peak and several lesser peaks at other frequencies. The frequency sweep must pass through the major peak in order to locate the true fundamental frequency, otherwise it may identify a lesser peak as the fundamental frequency. There are guidelines that suggest frequency ranges for prisms of certain dimensions. However, in this case, the correct frequency range was verified using an oscilloscope to monitor the Lissajous curve produced by the input and output frequency [Kramarczyk et al., 1999].

The Lissajous curve uses the known input frequency of the driver as the x-axis value and the measured output frequency from the sensor as the y-axis value. The pattern produced by the combination of the two values allows a distinction to be made whether the resonant frequency peak was located or whether a lesser peak was found.

When the concrete prism resonates at its resonant frequency, the output frequency detected by the sensor is equivalent to the input frequency supplied by the driver. Graphically, the Lissajous curve for this particular situation appears as a circle. Therefore, if the correct frequency range is selected for the equipment, a circle will appear on the display at the moment it sweeps through the resonant frequency of the

prism. Otherwise, if the frequency range selected only sweeps through a lesser peak, a distinct Lissajous curve will be produced, but not a circle.

The ASTM standard recommends that resonant frequency testing ceases for a particular prism when its relative dynamic modulus value falls below 60% of its initial modulus. Otherwise, testing is continued for 300 cycles. Resonant frequency measurements were used to calculate a relative dynamic modulus, P_c, for each prism [ASTM C 666]:

$$P_c = \frac{n_c^2}{n_0^2} \times 100 \qquad (3.2)$$

where n_c is the resonant frequency after c cycles and n_0 is the resonant frequency at 0 cycles. A durability factor, DF, is then calculated to account for the number of freeze-thaw cycles that a prism is exposed to relative to the total number of freeze-thaw cycles at test termination:

$$DF = \frac{P_N \cdot N}{M} \qquad (3.3)$$

where P_N is the relative dynamic modulus at N cycles, N is the number of cycles at which freeze-thaw exposure is discontinued, and M is the number of cycles at which the test is terminated.

3.6 Four Point Bending Test

Objective:

The purpose of this test was to determine any influence of the simultaneous exposure to de-icing fluids and 300 freezing and thawing cycles on the rupture strength of concrete. A four-point bending test, following ASTM C 78, was used because it is particularly influenced by surface conditions, which would be affected the greatest by the given exposure conditions.

Specimens:

The tests were conducted on the same prisms that were previously used in the rapid freeze-thaw test and experienced 300 freeze-thaw cycles. Of the four specimens for each

43

fluid, two were taken for the four-point bending test: one from batch A and one from batch B. This was done to obtain a representative sample set of the test specimens available and, possibly, examine the effects of air content on mechanical strength.

In total, eight specimens were removed from the freeze-thaw chamber for the four-point bending test. In addition, two control specimens were tested in order to give a comparative standard. The control specimens were extra concrete prisms that were cast at the same time as batch B for the freeze-thaw specimens, cured in the same $Ca(OH)_2$ solution bath as the prisms from the freeze-thaw test, but remained in the bath at room temperature for a total period of five months. Afterwards, they were removed from the bath and left to cure in air for an additional five months.

Test Setup:

An upper and lower fixture was attached to a MTS 810 Universal Testing Machine to create a four-point bending condition. The lower fixture has two supports for the specimen to rest on while the upper fixture is used to apply the load at two central loading points. It can be used to determine the rupture strength of a concrete prism. This setup can be seen in Figure 3.6. The loading rate used was 7 kN/min and loading was applied until failure.
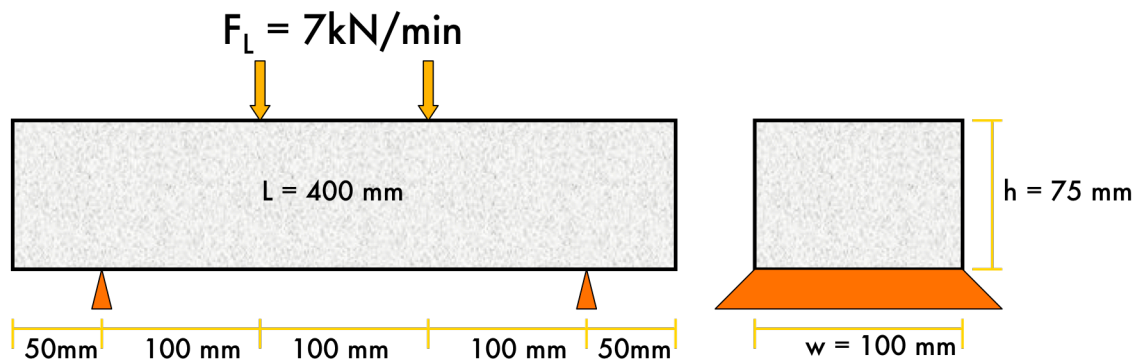
Figure 3.6 Four-point bending test setup.

The prism should fracture in the mid-section between the two upper loading points, between which the bending moment is a maximum and remains constant. If a prism

fractures at a location greater than 5% of the length outside of the mid-section, results from that test should be discarded [ASTM C 78].

Bending stress for each prism was calculated using the flexural formula:

$$\sigma = \frac{3FL}{4wh^2}$$

(3.4)

where σ is the bending stress experienced by the prism, F is the applied load, L is the length of the prism, w is the width of the prism, and h is the height of the prism.

In this study, L was 400 mm, w was 100 mm, and h was 75 mm. The maximum bending stress, σ_{max}, on the prism occurs on the top and bottom surface of the prism in the loading setup shown in Figure 3.6. The prism will fail due to the maximum tensile bending stress, which occurs on the bottom surface and is responsible for causing fracture. Thus, in order to calculate the rupture strengths, F was taken to be the maximum load at fracture measured for each prism.

3.7 Compression Test

Objective:

The objective of this test was to determine the effect of the de-icing agents on the early strength development of concrete. Standard concrete cylinders were subject to a compression test to gauge the strength.

Specimens:

Twenty-four concrete cylinders were batched using the same mix design as that of batch B from the rapid freeze-thaw test, shown in Table 3.2. The cylinders were 10 mm Ø by 200 mm in length.

The cylinders were wet-cured by placing damp burlap on top of the specimens. A plastic tarp was placed on top of the burlap to delay water evaporation, and the burlap was kept wet for three days. The cylinders were then de-moulded and placed in the humidity room

for an extra three days of curing. Afterwards, they were removed from the humidity room and placed in ambient air to dry for twelve days. This was done to encourage absorption upon being submerged in the test fluids.

Test Setup:

On the eighteenth day after casting, the cylinders were submerged in the test fluids: water, ethylene glycol, de-icer, and anti-icer. Eight 10 L containers were used to hold three specimens each, for a total of 6 specimens in each test fluid. The cylinders remained submerged for ten days.

Twenty-eight days after casting, the cylinders were prepared for compression testing. They were removed from the fluid containers and both ends were leveled using an end grinder to obtain flat, parallel surfaces. They were tested in a Forney compression machine to determine the maximum compressive forces required to cause fracture.

3.8 Accelerated Expansion Test of Concrete Prisms

Objective:

The objective of the Accelerated Expansion Test was to determine the effects of different fluids on the expansion of Pittsburg aggregate, which is known to be highly alkali-carbonate reactive. The procedure followed is the LS-626 from Ministry of Transportation of Ontario (MTO) for the Detection of Alkali-Reactive Coarse Aggregate by Accelerated Expansion of Concrete Prisms [MTO LS 626], which is based on the ASTM C 1260 test for Alkali Reactivity of Aggregates and an ACR Accelerated Test Method.

Specimens:

The concrete prisms required for this test were made using a specific mixture design and procedure, as follows, to yield four expansion prisms, which were 40 mm x 40 mm x 285 mm:

- 2 kg of cement paste mixed according to ASTM C 305 [ASTM C 305]
- 2 kg of coarse aggregate added afterwards and mixed by hand until well coated, allowed to sit for 30 seconds, and then mixed for an additional 10 seconds

Pittsburg aggregate was sieved to obtain coarse aggregates, ranging in size from 4.75 mm to 9.5 mm maximum diameter. They were then submerged in a water bath for one day to prepare them for the required aggregate condition. On casting day, the aggregates were removed from the water bath and spread evenly to obtain saturated surface dry conditions. The concrete specimens prepared for this test consisted of only cement paste and coarse aggregate, in order to eliminate any effects from other variables such as sand or replacement cementitious material. The cement paste, with a water to cement ratio of 0.3, was prepared according to ASTM C 305 standards, which are as follows:

- place all mixing water in bowl

- add cement to bowl and let sit for 30 seconds

- turn on mixer on slow speed for 30 seconds

- stop mixing for 15 seconds and scrape any side residue into bowl

- turn on mixer on medium speed for 1 minute

This was followed by the addition of coarse aggregate, which was mixed in by hand using a large spatula. The concrete was immediately cast into moulds, as shown in Figure 3.7(a), which are specially designed to place gauge studs on both ends of the prism, as required. The gauge studs are used for taking length measurements of the prisms using a CT-384D digital length comparator by ELE International, shown in Figure 3.7(b), which can measure 254 mm length prisms accurate to 0.002 mm.

Figure 3.7. Equipment used during the expansion test: (a)two-gang expansion test concrete mould with embedded gauge studs and (b) digital length comparator.

The concrete prisms were placed in a humidity room for 24±2 hours to cure before being removed from the moulds. They were then put into pre-heated lidded containers of tap water at 80°C and placed in an oven for an extra 24 hours to cure.

After the two-day curing period in the humidity room and the oven, the concrete prisms were placed in their respective test fluids to initiate the experiment. The fluids used for this test were ethylene glycol, de-icer, anti-icer, and a 1M NaOH solution, as a control set by the test standard. The presence of control specimens ensures that the experimental method is correct and that the aggregates are indeed expansive. The fluids in all the containers were pre-heated to 80°C in order to minimize the temperature change experienced by the prisms when being moved from the water to the test fluid.

Due to the availability of only two two-gang expansion test specimen moulds, the eight specimens needed for the expansion test were batched and cast on two consecutive days. The second set of four prisms was batched and cast on the same day that the first set was removed from the humidity room and de-moulded. In order to account for any changes in batching operation between the two sets, the four prisms per set were distributed

evenly across all containers. Thus, each fluid container held a specimen from set one and a specimen from set two. Consequently, any procedures outlined for this test were performed for set one and set two, but one day apart.

Test Setup:

Tight temperature tolerances were required for the oven because a change in temperature could cause significant differences in the behaviour of the concrete specimens. Thus, the oven had to be able to maintain a temperature of 80°C with no more than a ±2°C variance. In addition to the built-in oven temperature gauge, another gauge was used with the sensor located at the centre of the oven. Thermocouples were also placed in each of the specimen containers to monitor individual fluid temperatures and ensure that location in the oven or test fluid properties did not cause any large fluctuations from the required 80°C temperature.

All specimens were placed on thin copper piping to raise them off the bottom surface of the container and were completely submerged in their respective test fluids. This allowed the test fluids to surround the concrete prisms on all surfaces.

The first sets of measurements were taken after an initial 24 hour period of specimens in the test fluids. The containers were taken out of the oven, one at a time, for testing and were returned to the oven within 5 minutes of removal. Specimens were removed from the container, one at a time, for measurement testing, which was completed within 15 ± 5 seconds. Each specimen was gently patted to remove excess fluid before being placed in the length comparator for measurement readings. Subsequent measurements were taken at one-week intervals and stopped when results displayed satisfactory distinctions among test fluids, resulting in a 5 week testing period.

3.9 Copper and Steel Exposure Test

Objective:

This test was conducted as a result of observations noted from the Accelerated Expansion Test of Concrete Specimens [Section 3.8], which involved copper being in contact with the test fluids and the concrete. Gravimetry was used to determine the effects of de-icing fluids on copper and steel in a neutral environment, as well as in a high pH environment.

Specimens:

Test specimens used were 5/64" copper plates and 1/16" steel plates, approximately 25 mm x 25 mm in area. Three specimens of each metal were exposed to each of the four test fluids for a total of 12 specimens of each metal.

The ASTM G1-03 [ASTM G1-03] procedure of chemical cleaning procedures for removal of corrosion products was used to clean the copper and steel specimens before weighing and exposure as follows:

- A solution of 500 mL of hydrochloric acid (HCl, sp gr 1.19) plus reagent water to make 1000 mL was used to remove copper corrosion products. The copper plates were left in the solution for approximately 3 minutes.

- The steel plates were placed in a solution consisting of 1000 mL of hydrochloric acid (HCl, sp gr 1.19), 20 g antimony trioxide (Sb_2O_3), and 50 g stannous chloride ($SnCl_2$) for approximately 20 minutes to remove steel corrosion products.

- The solutions were stirred periodically during immersion of the specimens. Upon removal, the plates were rinsed in water, patted dry, and then left to air dry before being weighed.

Test Setup:

Four plastic containers were filled with each of the following fluids: ethylene glycol, de-icer, anti-icer, and water, as a control. Three copper plate specimens were then

completely submerged in the fluid in random positions. The same setup was used for the steel specimens.

The specimens remained submerged in fluid for the duration of the test period, which lasted 5 weeks. They were taken out after one week, two weeks, and five weeks for observations, including a visual inspection of surfaces and weight measurements to record any material weight loss. Upon removal from the fluid, they were rinsed in water and dried to remove any fluid films or debris before cleaning.

The subsequent test using the same steel and copper specimens used the same test setup as before, except with the addition of small cement paste pieces. Approximately 8 g of cement paste were placed into each container and scattered randomly. The same procedure for removal, inspection, and cleaning of surfaces was used.

3.10 Raman Spectroscopy

Objective:

The purpose of this analysis is to examine the compositions of de-icer and anti-icer used at the GTAA. In addition, comparisons of the two fluids will be made with respect to pure ethylene glycol, which is the primary constituent in both fluids.

Specimens:

No modification or sample preparation was used for testing as-received aircraft de-icer and anti-icer fluids. Pure ethylene glycol fluid was also tested in order to produce a relative baseline for the two aircraft fluids, upon which any variations in composition would produce additional peaks on the Raman spectra.

Analysis Technique:

Raman spectroscopy is an analysis tool that is useful in determining material composition. It is based on the Raman effect, which is the elastic and inelastic scattering of photons when a monochromatic laser irradiates a given material. Raman spectroscopy

is useful because sample preparation is easy and materials can be examined through glass or quartz cells if an inert environment is required [Skoog, 1998]. Moreover, the Raman effect occurs in gases, aqueous solutions, and crystals [Andrews, 1981], thus having an advantage over other techniques, such as SEM and XRD, which require much stricter conditions.

When a monochromatic laser irradiates a sample material, two different types of photon scattering can occur: Rayleigh or Raman. The majority of photons will scatter at the same wavelength as the incident photons, which is referred to as Rayleigh scattering, or elastic scattering. A small fraction of photons will scatter at wavelengths that are different than those of the incident photons, due to interactions with molecules of the given material, which is referred to as Raman scattering. Raman scattering can be further classified as Stokes or anti-Stokes scattering, in which the scattered photon leaves with less energy or more energy than the incident photon, respectively [Skoog, 1998].

The resulting Raman spectrum is shown as a plot of intensity versus wavelength difference. The wavelength difference is zero for Rayleigh scattering and, since the majority of scattering occurs in this manner, it is visible as the largest peak on any Raman spectrum. On the other hand, Raman scattering produces various shifted peaks on a spectrum and each molecule yields a distinctive set of peaks. The location of peaks remains the same, irrespective of the type of laser excitation employed [Skoog, 1998], because the wavelength shift is dependent on the thermal energy change required by the atoms of a molecule to change vibration modes [Andrews, 1981]. Substance identification is possible with the use of Raman spectral databases, which have been compiled by various universities and laboratories.

3.11 ESEM/EDS Analysis

Objective:

The purpose of performing ESEM was to obtain micrographs of precipitates and cement paste from the various tests, such as the submerged cement paste test (Section 3.4) and

the compression test (Section 3.7). EDS analysis was then performed to acquire elemental information of various points and areas on the specimens.

Specimens:

The particular specimens analysed under ESEM were cement paste specimens and precipitates from the submerged cement paste test, namely those in ethylene glycol, de-icer, and anti-icer containers. In addition, precipitate was collected from the de-icer container used in the accelerated expansion test of concrete prisms (Section 3.8). This particular precipitate was analysed due to formation of precipitate not previously observed in the submerged cement paste test.

Cement paste specimens and precipitates were placed in the chamber without any specimen preparation. However, the precipitates, which were in solution, were placed on a flat surface and experienced drying during de-pressurization within the chamber. The precipitates remained on the surface, allowing microscopy and elemental analysis to be carried out.

Analysis Technique:

An environmental scanning electron microscope (ESEM) is an electron beam-based imaging tool that is useful for situations in which a scanning electron microscope (SEM) would be impractical or unsuitable.

With an ESEM, there is greater flexibility for specimen testing because several requirements for an SEM limit the type of specimens that can be analysed. Instead of a high vacuum within the chamber, the specimen chamber can be at pressures as high as 10 torr while the electron gun chamber is maintained at a pressure of approximately 10^{-6} torr, made possible by a differential pumping system. The gaseous environment used in the sample chamber is water vapour, which eliminates sample preparation and greatly reduces the drying effects caused in a SEM chamber. This was noted by Mouret [Mouret, 1999], who analyzed the same cement paste specimen under SEM and ESEM. Microcracks were visible in images taken using SEM, but not present in images taken using ESEM. This indicates that the drying preparation employed, which involved

placement within an evaporator and a high vacuum chamber, created microcrack artifacts throughout the cement paste and gaps between aggregates and their surrounding paste [Mouret, 1999]. The gaseous environment also acts as a conductor and signal amplifier, thus eliminating the need to coat specimens. The water vapour is able to effectively neutralize the negative charge build-up of electrons because of positive ions provided by the gas [Danilatos, 1994].

The ESEM is able to detect the same main electrons and x-rays that a SEM is able to detect and a detector for Energy Dispersive Spectroscopy (EDS) can be installed, which performs semi-quantitative elemental analysis. X-rays are emitted when an outer shell electron moves to occupy a vacancy in an inner shell position as a result of an inner shell electron being knocked out of position by an incident electron. X-rays are characteristic to a particular atom and an electron's x-ray possesses an energy that is dependent on the distance that the electron traveled to fill a void. As a result, they can be used to identify elements and yield quantitative results. Each atom will have a several characteristic peaks corresponding to various electron shell transitions.

One limitation to element identification using EDS is its inability to accurately quantify low atomic number elements below Na, such as C, N and O, because they produce low energy peaks that are not reliable for analysis. At the low energy range, the peaks produced by these elements are likely to be concealed by the weaker x-ray peaks produced by higher atomic number elements, such as Fe, Cu, and Z. [Ramcholan, 2006; Gabriel, 1985]

3.12 Thermo-Gravimetric Analysis

Objective:

The purpose of thermo-gravimetric analysis (TGA) was to identify the compounds present in precipitates formed during the Submerged Cement Paste Test (Section 3.4).

Specimens:

There were four precipitates collected from the following solutions: 38% ethylene glycol mixed with water, 48% ethylene glycol mixed with water, 100% ethylene glycol, and anti-icer. The precipitates were placed in an oven at 80°C for drying. They were then crushed into a fine powder for placement within the TGA specimen holder.

Analysis Technique:

TGA is a technique that is used to identify material compositions by monitoring mass change with respect to increasing temperature. This is based on phase changes occurring at specific temperatures for certain compounds, which causes a mass change in the sample. As temperature increases, substances may either lose weight or gain weight due to several reasons. They may experience drying, decomposing, liberation of gases, and other physical or chemical reactions. In the majority of cases, processes will result in mass loss, rather than weight gain.

The equipment used to perform a TGA analysis should be stable and isolated from the external environment because the arm balance, which holds the specimen, is highly sensitive. Even the material to be tested should be ground into a fine powder in order to get a level distribution of material within the crucible. This is to avoid any sudden weight changes caused by physical movement of material shifting locations rather than phase changes.

Helium gas is used within the specimen chamber to provide an inert environment, which prevents any unwanted reactions from occurring. Different environmental factors can cause peak temperatures to vary between different samples, but TGA of cement components has been examined by many researchers [Castelotte, 2004; Perruchot, 2006; Williams, 2003; Ye, 2007] and the temperatures of major peaks have been roughly agreed upon and fall within the temperature ranges shown in Table 3.3.

Table 3.3 Thermogravimetric analysis of major cement components.

Temperature	Component	Reaction
80°C - 250°C	C-S-H	dehydration
120°C - 400°C	ettringite	dehydration
450°C - 500°C	$Ca(OH)_2$	dehydroxylation
600°C - 900°C	$CaCO_3$	decarbonation

Different environmental factors can cause peak temperatures to vary between different samples. In addition, analysis of the resulting TGA plots is also operator-dependent, which can introduce greater variation between peak temperatures found in different literature.

One major problem encountered in TGA analysis of cement is the carbonation of calcium hydroxide. This process occurs rapidly in air, thus, samples can be sealed in a CO_2-free environment to minimize air exposure. Otherwise, carbonation will cause calcium hydroxide to convert to calcium carbonate, affecting the resulting analysis plot. Consequently, it may be very difficult to determine the original calcium hydroxide content apart from the calcium carbonate content.

3.13 X-Ray Diffraction

Objective:

X-ray diffraction analysis was used to identify crystalline phases by examining the diffraction pattern that occurs when an x-ray beam interacts with a specimen. It was used to analyse precipitates collected from the Submerged Cement Paste Test (Section 3.4) and from the Accelerated Expansion Test of Concrete Prisms (Section 3.8).

Specimens:

Precipitate from cement paste submerged in ethylene glycol and precipitate from cement paste submerged in anti-icer were collected for analysis. Precipitate from the de-icer container in the accelerated expansion test was also collected. All specimens, which were initially collected from solution, were placed in an oven at 80°C for three days to

dry. They were then crushed into fine powder, which is required for XRD testing. They were each placed in a specimen holder, leveled, and patted down to ensure that the powder surface was level with the holder surface.

A Rigaku diffractometer was used at 50 kV, 40 mA, and 2 kW, with a Cu x-ray tube that emits a 0.3 mm Ø beam. The detector is phosphorus, with a crystal-to-detector distance of 120 mm. Three images were scanned, traveling through three different ranges of angles between 0° and 90°.

Analysis Technique:

When incident x-rays encounter a crystalline material, each x-ray may interact with parallel atomic planes, as shown in Figure 3.8.

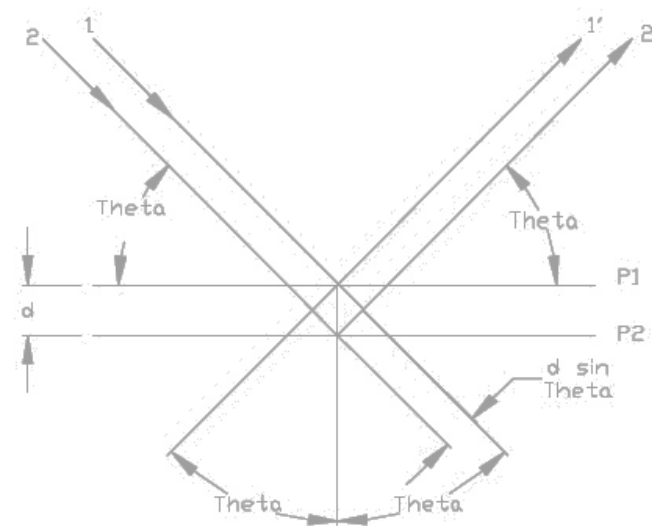Figure 3.8 Diffraction of two x-rays by parallel planes of a crystal [Scintag].

X-rays that are initially in phase before interacting with the material may stay in phase, producing constructive interference, or may become out of phase, producing destructive interference. Two x-rays produce constructive interference when Bragg's Law is satisfied:

$$n\lambda = 2d\sin\theta \qquad\qquad (3.5)$$

The order of reflection, n, represents the number of whole wavelengths between the two x-rays with wavelength, λ. The distance between two parallel atomic planes of the crystal is represented by d and the angle of incidence, also known as Bragg's angle, is represented by θ.

An XRD diffraction pattern displays intensity versus 2θ and constructive interference appears as vertical lines at the particular 2θ position. A greater line intensity represents stronger constructive interference. Each crystalline material produces a distinctive diffraction pattern and a mixture of crystalline materials will produce a pattern that is a superposition of each unique diffraction pattern. The patterns are compiled by the Joint Committee for Powder Diffraction Standards (JCPDS) [The International Centre for Diffraction Data]. A common means of identifying each particular substance by its three strongest lines is known as the Hanawalt method, named after J.D. Hanawalt, who first devised the system of compiling and classifying diffraction patterns to serve as a reference for identification [Hanawalt, 1938].

CHAPTER 4 - RESULTS & DISCUSSION

4.1 Steel Reinforcing Bar Corrosion Test

Corrosion testing was carried out over a 3-week time period, with measurements being taken immediately upon exposure and after 5, 7, and 28 days. The results are shown in Figure 4.1 below.
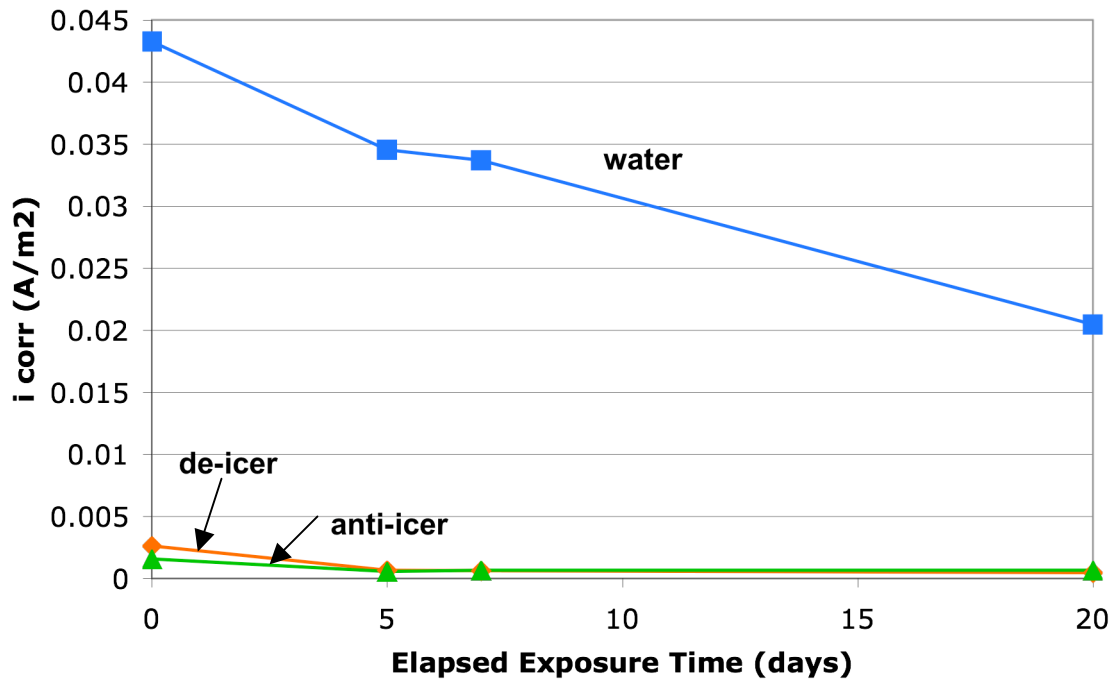
Figure 4.1 Corrosion results for steel reinforcement bars submerged in various fluids.

Initial measurements show that steel corrodes immediately upon submersion in water, with an initial corrosion current density of 0.043 A/m^2. Corrosion rate was then calculated using Faraday's Law:

$$CR = \frac{i_{corr} \cdot t \cdot A}{\rho \cdot n \cdot F} \qquad (4.1)$$

where i_{corr} is the corrosion current density in A/cm^2, t is time in seconds, A is the gram atomic weight, ρ is the material density in g/cm^3, n is the valency, and F is Faraday's constant (96, 500C/eq.). To convert this to a corrosion rate in μm/year, this value should

be multiplied by 3153.6. Using this equation, the corrosion rate of steel in water was found to be approximately 50 μm/year. As exposure time elapsed, the corrosion current density decreased, probably due to a combination of a lack of oxygen at the tested submerged steel region and a build-up of corrosion products at the surface.

The plots of corrosion current density for steel immersed in de-icer and anti-icer show that there was very little corrosion activity. This was expected because these fluids would have a corrosion inhibitor as a part of the Ad-Pack, though it is uncertain whether the corrosion inhibitors are added for steel protection, or as aluminum protection. Nevertheless, after only 5 days, measurements became steady at a negligible corrosion rate of approximately 0.6 μm/year, with a corrosion current density of approximately 5×10^{-4} A/m^2.

A plot for corrosion rates in ethylene glycol was not obtainable due to its low conductivity. Although there may have been corrosion activity, the rebar could not be polarized since the ethylene glycol does not allow easy electron flow within the system. However, corrosion of steel in ethylene glycol does not appear to be a problem based on visual inspection of the rebars in the ethylene glycol container.

4.2 Rapid Freeze-Thaw Test

Two concrete batches were required to produce the prisms for the freeze-thaw test, and, as described in Section 3.5, there was a difference in air content due to the doubling of air-entraining admixture for the second batch. Recalling that the air content was 3.2% for batch A and 5.0% for batch B, this led to a variance in 28-day compression strength tests. Batch A cylinders had compressive strengths of 49.2 MPa ± 0.3% and batch B cylinders had compressive strengths of 38.9 MPa ± 4%. The compression strengths of batch A cylinders were approximately 10 MPa greater than those of batch B, which was expected due to the lower air content. However, both batches met the GTAA concrete specifications of a 35 MPa average minimum compressive strength and all prisms were valid for use in the rapid freeze-thaw test.

Throughout the duration of the test, none of the specimens fell below the modulus limit, thus all prisms were put through 300 cycles. Weight measurements were taken with a scale that had a resolution of 0.1 g. Prisms from batch A weighed more than prisms from batch B. This is expected because batch B had a higher air content, which resulted in lower density concrete. There was one specimen in each batch that was noticeably outside their respective weight ranges, at initial weights of 7675 g for batch A and 7790 g for batch B. When these two specimens were removed from the average specimen weight calculations, batch A had an average weight of 7821 g ± 1.2%, while batch B had an average weight of 7693 g ± 1%. This shows a weight difference of 1.7% between batch A and batch B, which corresponds well with the air content measured during batching. Average percentage change in mass values for each set of prisms are shown in Figure 4.2.

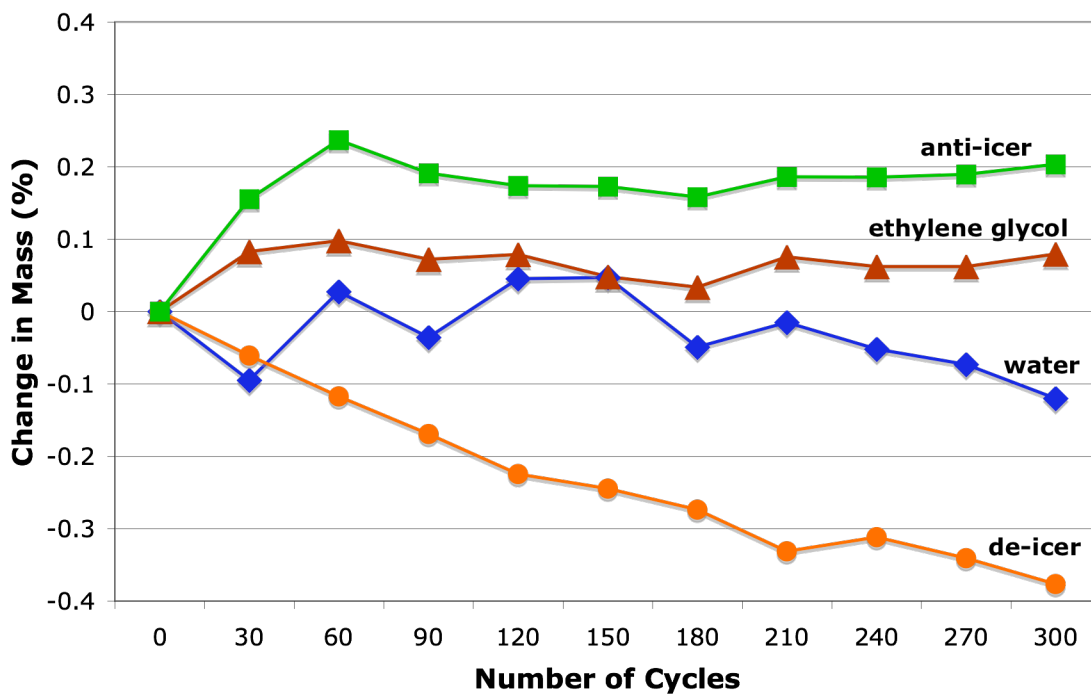Figure 4.2 Average change in mass versus number of freeze-thaw cycles.

The changes in weight after each 30-cycle interval were not significant for any of the prism sets. Prisms in ethylene glycol remained at consistent weights throughout most of the test period, with an overall 0.08% increase. Meanwhile, prisms in water and de-icer displayed noticeable decreases in weight. The prisms in de-icer steadily decreased from

7783 g to 7753 g over 300 cycles, which is a 0.38% drop, while prisms in water were not as great and as steady in their overall decline from 7717 g to 7707 g, which is a 0.12% drop in weight. Anti-icer prisms gained 0.20% in weight, going from 7711 g to 7726 g.

The measurements for the specimens in water were likely the least accurate of the four because of the temperature at which the measurements were taken. Ethylene glycol and aircraft fluids remain liquid for the majority, if not all, of the cycle temperature range due to their low freezing points, but the prisms in water actually experience freezing and thawing behaviour. The fluctuations in the first half of the entire test duration may have been due to opposing processes of a gradual filling of the air void system with water, causing an increase in weight, versus surface scaling, causing a decrease in weight. It was noted that at every 30-cycle interval, when the specimens were removed for testing, there was considerable concrete debris within the water containers. This was not observed in the containers filled with the other three test fluids. Although there was much debris, there were no visible signs of cracking on any of the prisms in water. From 210 cycles onward, however, they showed a steady decline in mass, suggesting that the mass loss due to scaling became the primary factor in weight change.

The steady weight decline of prisms in de-icer is surprising because there was no visible debris found within the housing containers. One explanation for this would be the leaching of cement paste components by the de-icing fluid, which would not be noticeable when removing the prisms from the container.

Overall, the weight gains and losses of the prisms were insignificant when considering the weight of the prisms, with a maximum change of 0.40%.

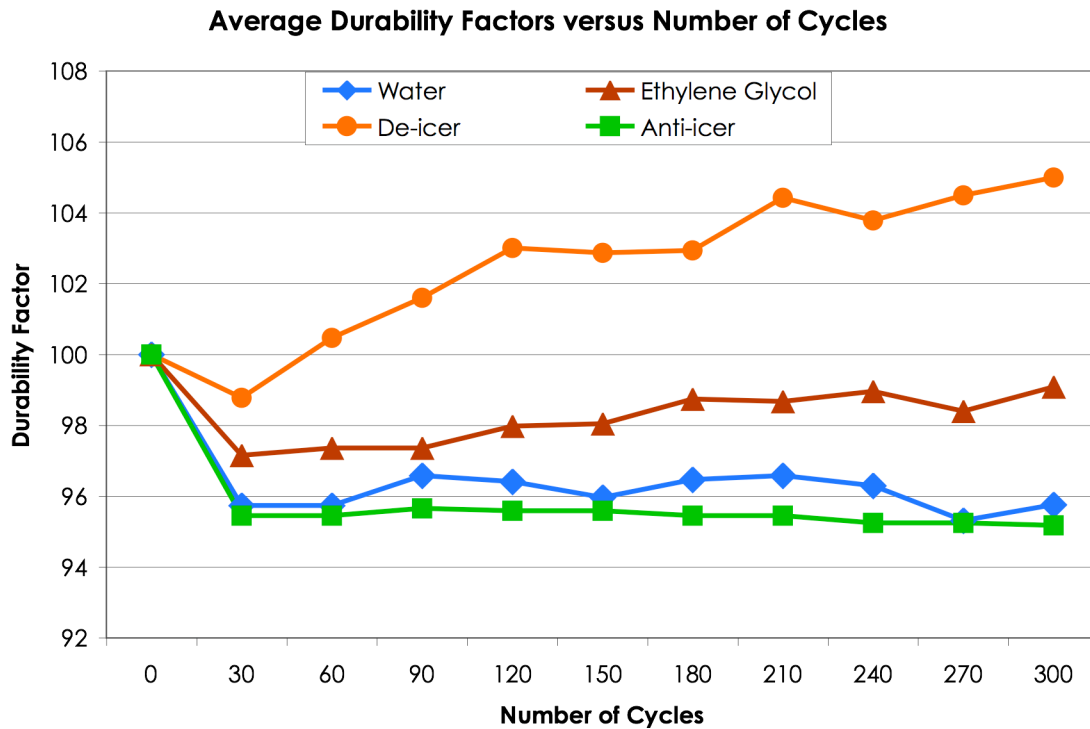The durability factors for all specimens are shown in Figure 4.3.

Figure 4.3 Freeze-thaw prism durability factors over 300 cycles.

Figure 4.3 shows that the prisms in water and anti-icer initially had a significant decrease in durability factor after the first 30-cycle interval and then both remained fairly constant throughout the rest of the test duration at approximately 96%. On the other hand, the prisms in ethylene glycol and de-icer slightly decreased in durability factor after the first 30 cycles, but had steadily increasing durability factors thereafter. The prisms in de-icer had the greatest increase in durability factor, jumping from 98.8% of the original value after 30 cycles to a final durability of 105%.

When the prisms are first submerged in their respective fluids, it takes time for permeation of the fluid into the concrete to occur because, up to the test commencement, all prisms were submerged in saturated calcium hydroxide solution. As a result, the pores within the prism would have been filled with solution already and required time for fluid exchange to occur.

After the very first interval, the drop in durability can be attributed to the formation of microcracks within the concrete due to the 30 freeze-thaw cycles. The very first freeze-thaw exposure interval would cause the most damage because all capillary and gel pores are likely filled and the trapped water, upon freezing conditions, would have nowhere to escape to. Subsequent freeze-thaw intervals did not cause a major change in the prisms submerged in water and anti-icer. After the creation of a microcrack network within the prisms by the first interval, subsequent microcracks caused by further freeze-thaw action may possibly be negligible, which may be the case for the water specimens. For the anti-icer specimens, however, another explanation for the steady durability behaviour after the initial drop may be the formation of reaction products within the prism. The durability factor is based on the disruption of ultrasonic waves, signifying cracks. If cracks are filled with reaction products, it may have offset the decrease in durability caused by the creation of microcracks within the anti-icer prisms. The formation of reaction products may have occurred with the specimens in ethylene glycol and de-icer, which displayed an increase in durability.

In order to check if the change in durability factor was due to mass loss or to mechanical properties, a theoretical resonant frequency was calculated as well, based on mass change alone. The resonant frequency of an object is a function of mass and stiffness, which is, in turn, a function of geometry and the object's mechanical properties. A prism's geometry consists of length, L, and moment of inertia, I, while its elastic mechanical properties consist of elastic modulus, E, and Poisson's ratio, ν. The geometry of the prism does not change significantly during freeze-thaw testing, thus the resonant frequency can be thought of as a function of mass and mechanical properties.

A change in resonant frequency due to mass change can be found with the following equation when the prism is set up in the arrangement used for the ASTM C 215 test for fundamental transverse resonant frequency [ASTM C 215]:

$$\frac{f_r}{(f_r)_o} = \sqrt{\frac{m_o}{m_r}} \qquad (4.2)$$

Where $(f_r)_o$ is initial resonant frequency, m_o is initial mass, m_r is current mass, and f_r is frequency after a mass change from m_o to m_r. This equation was used to calculate a theoretical resonant frequency for the prisms at each 30-cycle interval based on the measured weights, which was in turn used to calculate a durability factor for each prism. A comparison of the calculated versus measured values can be seen in Figure 4.4.
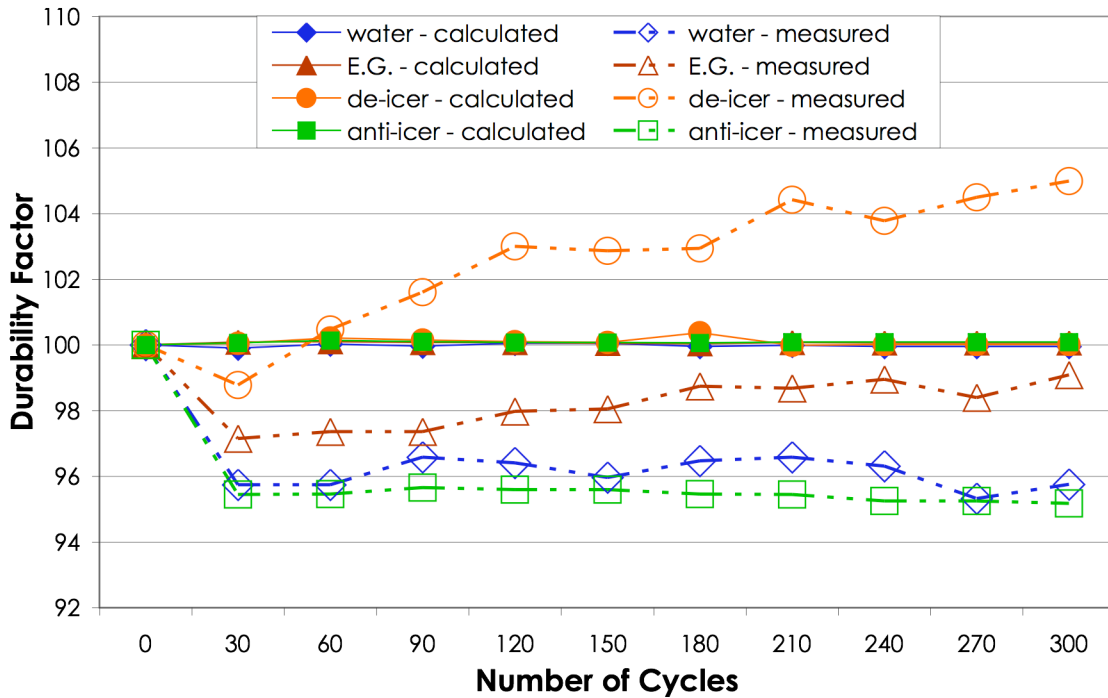

Figure 4.4   Average mass-based and average measured durability factors.

The solid lines, representing the theoretical mass-based durability factors, stay near the initial durability factor of 100. The measured durability factors, represented by the dashed lines, deviate from the initial value of 100, indicating that changes in concrete microstructure were likely the reason for the bulk change in durability factors. This confirms the explanation given earlier concerning the creation of microcracks and/or reaction products within the prisms.

Photographs of the test specimens surfaces after 300 cycles are shown in Figure 4.5.

(a)

(b)

(c)

(d)

(e)

(f)

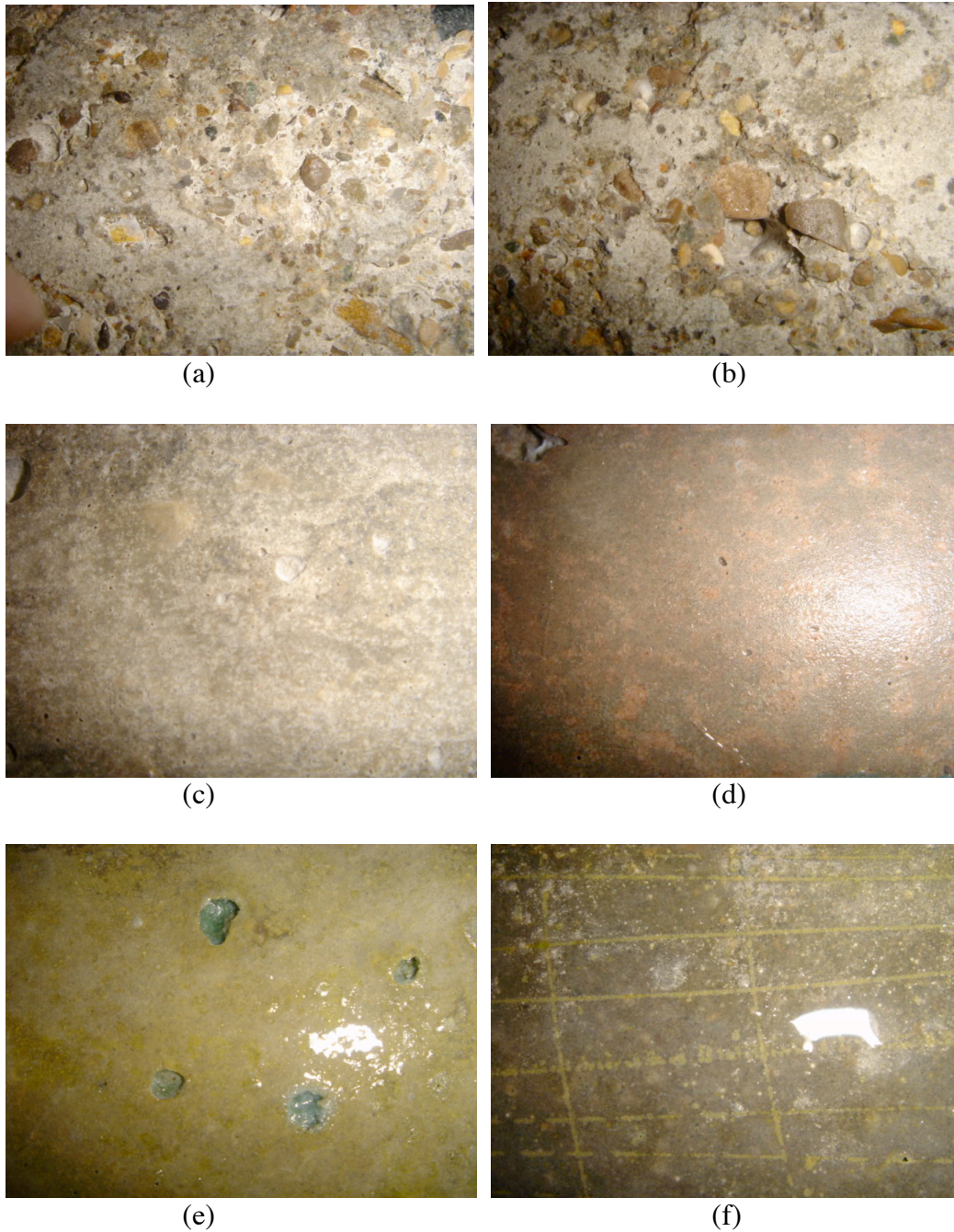Figure 4.5 Surface conditions of freeze-thaw prisms submerged in (a) & (b) water, (c) ethylene glycol, (d) de-icer, (e) and (f) anti-icer.

It is clearly seen in Figure 4.5(a) and (b) that freeze-thaw deterioration occurred for the prisms submerged in water. There was severe scaling of the prism surface, which resulted in the aforementioned debris found within the containers after every interval.

This was expected since the specimens in water experienced freezing and thawing over the temperature range of 4°C and -18°C. The absence of scaling on specimens placed in de-icer and anti-icer are due to the fact that these fluids did not undergo freezing within the range of 4°C and -18°C. Ethylene glycol, with a freezing temperature of -12.9°C, experienced freezing, however it did not affect the surface of the prisms submerged in it. Ethylene glycol and de-icer appeared to have no surface effects on the concrete prisms, as shown in Figure 4.5(c) and (d), other than a pinkish discolouration of the prism surfaces in de-icer. Anti-icer had the most interesting effect on the concrete prisms, as seen in Figure 4.5(e) and (f). A bluish gel precipitate formed on the prisms, which was washed away after each interval, but remained within voids on the surface. Further analysis of the gel was conducted, and is discussed in following sections. In addition to the gel formation, a grid-like pattern was found on the surfaces of two of the four specimens. No explanation could be found for this appearance.

Despite the differences, the most significant overall result from the freeze-thaw test is the fact that all specimens remained well above the 60% minimum durability factor limit. Overall, with a spread of only 10% between the worst and the best specimens, the deterioration caused by freeze-thaw cycling can be considered insignificant when comparing the effects of submerging the prisms in various fluids during testing. Further testing to determine the microscopic differences between sets was considered unnecessary in the scope of research.

4.3 Four-Point Bending Test of Freeze-Thaw Prisms

Two specimens of each set from the freeze-thaw test were subjected to a four-point bending test, illustrated in Figure 4.6. Prisms that were cast at the same time as the freeze- thaw prisms, but were not exposed to freeze-thaw conditions, were used as controls.

Figure 4.6 Prism after failure under four-point bending conditions.

The results for all rupture strengths calculated from Equation 3.4 (Section 3.6) are given below in Figure 4.7.
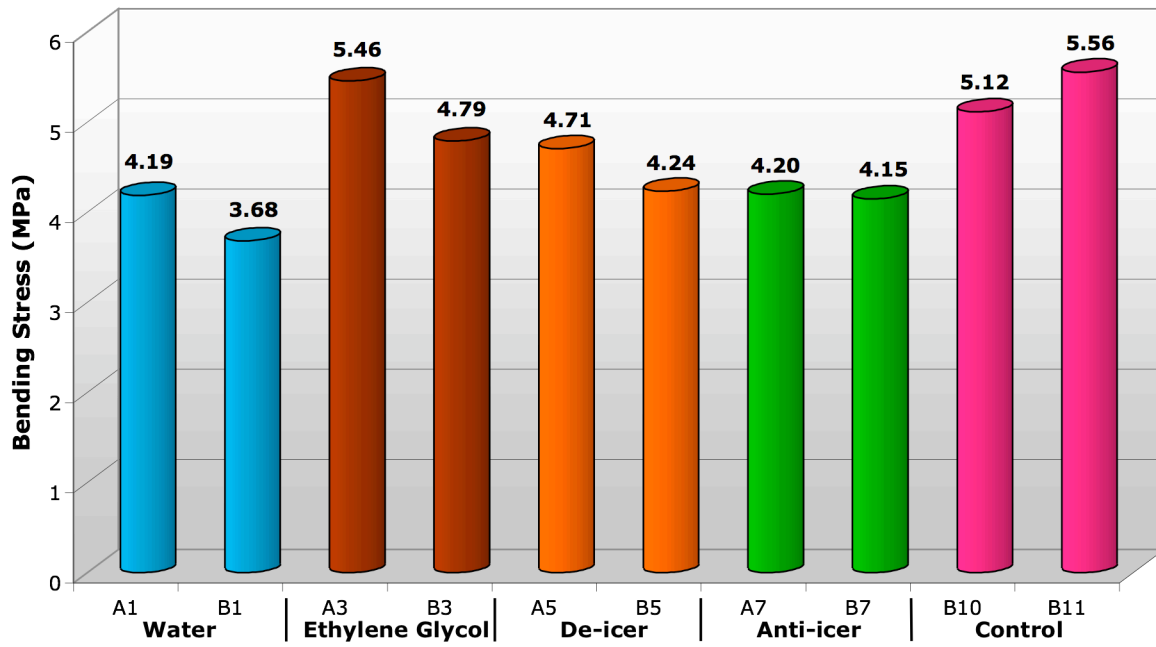

Figure 4.7 Four-point bending rupture strength results for the freeze-thaw specimens.

Note that, in all cases, type A specimens failed at higher bending stresses than their respective type B specimens. This was due to a lower air content of 3.5% for batch A

compared with 5% for batch B. These results clearly show that as air content increases, strength decreases, which is in agreement with 28-day compression strength results for freeze-thaw prisms without freeze-thaw exposure given previously in Section 4.2.

Predictably, the control prisms, which did not have any freeze-thaw exposure, withstood the highest bending stresses before failure. Even though both control prisms were from batch B, they had maximum bending stresses greater than 5 MPa. If control prisms from batch A had been available for rupture testing as well, it is likely that they would have displayed an even greater maximum bending stress than these from batch B.

Of the freeze-thaw prisms, those exposed to water were the weakest, failing at the lowest bending stresses, while prisms exposed to ethylene glycol were the best, failing at the highest bending stresses. Prisms in de-icer were second-best and then prisms in anti-icer performed almost as poorly as the prisms in water.

These results correlate very well with the results from the freeze-thaw test. Prisms in water were expected to fail at the lowest bending stresses because the surfaces showed many signs of deterioration and the prisms also had the lowest durability factors. The durability factors for prisms in the anti-icer were more or less equal to those in water, and the four-point bending test results showed very similar results again.

Although the prisms in de-icer had higher durability factors than prisms in ethylene glycol, the four-point bending test results showed that prisms in ethylene glycol withstood higher maximum bending stresses than those in de-icer. At first glance, this appears to be contradictory, but recalling that the prisms in de-icer displayed a steady weight decline throughout the course of the freeze-thaw test, these results may also correlate quite well. It would seem that a decrease in prism weight would result from removal of concrete components, thus decreasing the overall strength of the prism. In addition, it was noted that there may have been formation of de-icer precipitation within the prism microstructure. While that would affect the resonant frequency measurements used to calculate durability factors, it would have little effect on the strength of the prism under four-point bending because the de-icer precipitation is likely a filler within the

microstructure, but not bonded well with its surroundings. Thus, it may not be effective at increasing the maximum bending stress at which the prism would fracture.

Overall, the results show that ethylene glycol and de-icer had little effect on the strength of the prisms, even after 300 freeze-thaw cycles and constant exposure to the fluids. Exposure to anti-icing fluid was no worse than exposure to water, which produced concrete specimens with the lowest maximum bending stresses.

4.4 Compression Test

The measured maximum applied forces required to cause fracture were used to calculate cylinder compression strengths, given in Table 4.1.

Table 4.1 28-day compression strengths for the compression test.

Type	Compressive Strength (MPa)
Water	14.2 ± 1.0
Ethylene Glycol	17.6 ± 1.2
De-icer	16.0 ± 1.1
Anti-icer	14.8 ± 0.5

The values for all cylinders are low for 28-day compression strengths, with average values for each set ranging from 14.2 ± 1.0 MPa to 17.6 ± 1.2 MPa. This can be explained by the concrete air content, which was measured as 11% at time of casting. For every 1% increase in entrained air content, there is a reduction of 3% to 5% in compression strength [West, 2005]. By comparison, cylinders that were cast using the same mixture design during the freeze-thaw specimen batching had an air content of 3% for batch A and 5% for batch B. The mix design used during batching was chosen to match batch B, however, a change in air-entraining agent fluid resulted in the increased air content. Average values for each batch, A and B, were 49.2 ± 0.2 MPa and 38.9 ± 1.5 MPa, respectively. Batch A values are greater than batch B values because of the 1.5% air content difference. As stated previously, the air content of the compression test cylinders was 11%, which is 6% greater than those used in the freeze-thaw test concrete. It is estimated that, with a 5% decrease in strength for every 1% increase in air, the

compression strengths should be approximately 30% lower than batch B compression strengths, at approximately 21 MPa. It can be seen in Table 4.1 that the strengths are all well below 21 MPa, with specimens in ethylene glycol averaging 17.6±1.2 MPa and specimens in water averaging 14.2±1.0 MPa. Consequently, it appears that there are further decreases in strength that can be attributed to a combination of several other factors.

It was also noted that the data in Table 4.1 were obtained in April 2007, while those for batch A and batch B of the freeze-thaw cylinders were obtained in April 2006. Both tests were carried out on the same Fornay compression machine, but in July 2007, it was determined that the Fornay had not been calibrated properly, thus displaying applied force values that were much lower than the actual applied forces. Consequently, the extremely low 28-day compression strength results for the exposed cylinders can partially be explained by the equipment calibration error. However, compression testing was conducted to compare the effect of the various fluids on cylinder strengths, hence, absolute values are not as critical in this particular application.

Additional possible contributions to the low compression strengths are likely due to the curing regime and submergence in test fluids. The freeze-thaw cylinders were cured in saturated $Ca(OH)_2$ solution for two weeks and then cured in a humidity room for two weeks. The saturated $Ca(OH)_2$ solution prevents leaching of calcium hydroxide from the concrete and the additional two weeks in the humidity room reduces the probability of any drying shrinkage cracking occurring before compression testing. On the other hand, the 28 days before compression testing of cylinders for this compression test consisted of 1 day of wet-burlap curing, 5 days of humidity room wet curing after de-moulding, 12 days of air curing, and then 10 days of complete immersion in test fluids. The 12 days of air curing would allow the cylinders to dry to some extent, thus possibly allowing drying shrinkage to occur, but also to encourage the absorbance of fluid upon immersion in fluids [Cement Association of Canada, 2007]. The continuous exposure to test fluids up to the time of testing could affect compression strength performance because, under these conditions, components can easily leach out of the cement paste, as discussed in

Section 4.8 to 4.10 below. As shown in Figure 4.8, these results correlate very well with freeze-thaw durability results.
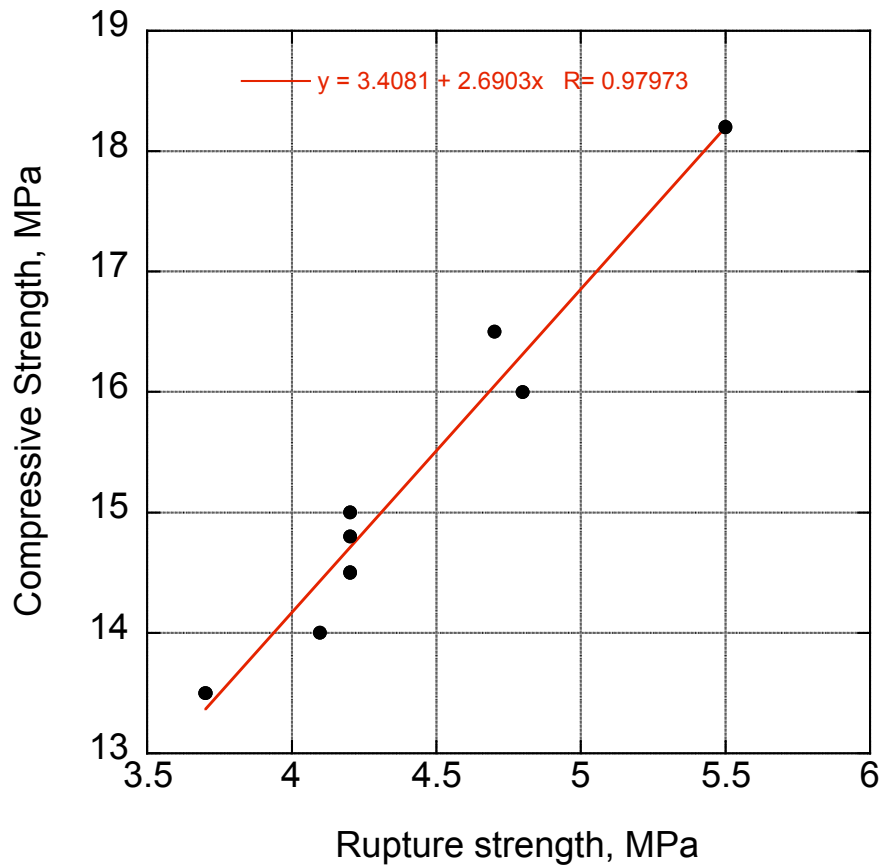

Figure 4.8 Plot of compressive strengths versus 4-point bending rupture strengths.

Water appears to encourage leaching of cement components from the concrete cylinders. The water in the containers was initially clear before the cylinders were placed inside, but was very cloudy by the time of cylinder removal. This was most likely caused by leaching of calcium hydroxide.

Results for specimens exposed to anti-icer in the freeze-thaw test, 4-point bending test, and compression test were very similar to those in water. This may be explained by the anti-icer component ratio of 64% ethylene glycol and 35% water. The amount of water in the anti-icer appears to be enough to cause similar behaviour in concrete specimens placed in water, such as leaching and freeze-thaw deterioration.

De-icer, on the other hand, contains 92% ethylene glycol and only 7.5% water. As a result, it yields concrete test results more similar to those placed in 100% ethylene glycol. The low percentage of water may still cause some leaching of calcium hydroxide, but not enough to affect its performance in mechanical tests.

The cylinders in ethylene glycol had the highest compression strengths, which is to be expected if the damage is proportional to water content. As ethylene glycol has zero water content and has a viscosity greater than that of water, it is likely that it does not leach out calcium hydroxide to the same extent. It is also hypothesized that there may be a solvent exchange occurring between ethylene glycol and water in the prisms. Ethylene glycol is highly miscible in water due to similar hydrogen bonding between like-molecules. As a result, it is possible that ethylene glycol molecules may be replacing water molecules within the prism, thus decreasing the water content and, consequently, the water to cement ratio. Since the prisms were only 18 days old when they were immersed in the fluids, hydration would not have been complete, especially with 12 days of air curing of the 18 days. If solvent exchange occurred, it would have effectively decreased the water-to-cement ratio for the prisms submerged in ethylene glycol, resulting in higher strength concrete. Since the ethylene glycol content of de-icer is 92% as well, the same theory may explain why the cylinders in de-icer had compression strengths that were similar to those in ethylene glycol.

4.5 Accelerated Expansion Test of Concrete Prisms

Test temperatures, which had to be tightly regulated at 80°C with a ±2°C variance, were measured using thermocouples placed within each of the four specimen containers, consisting of ethylene glycol, de-icer, anti-icer, and a 1 M NaOH solution as a control.
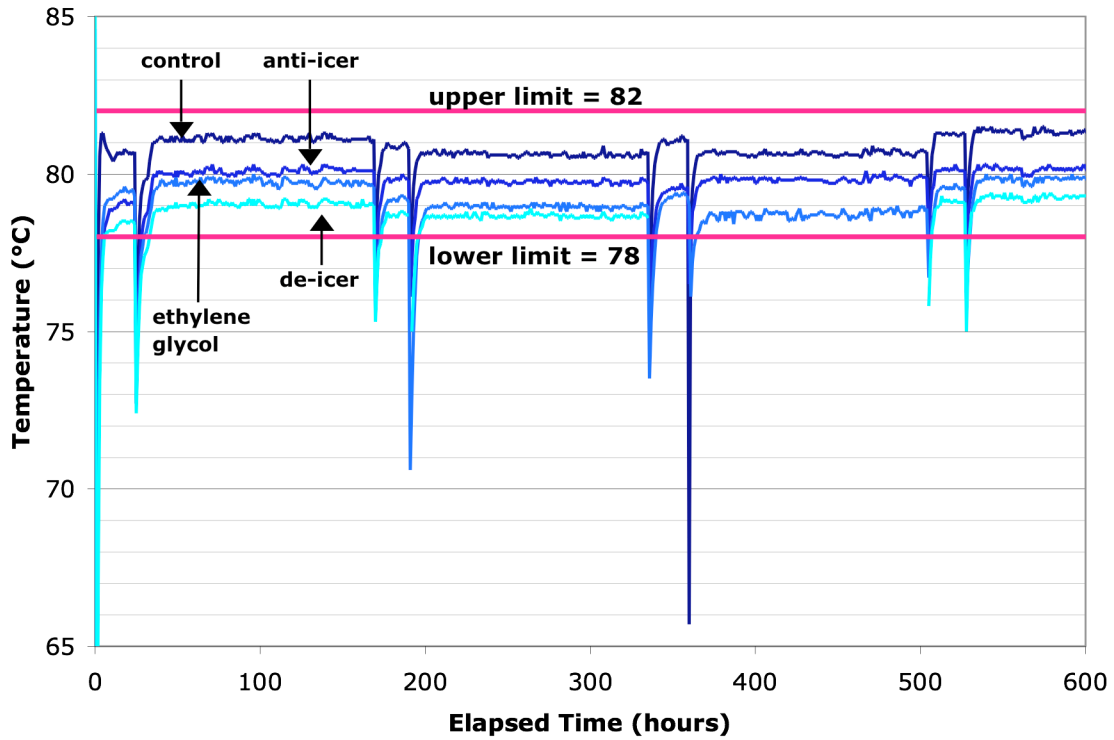
Figure 4.9 Thermocouple temperatures from each of the four test containers.

During steady state operation, all temperature values were well within the lower and upper limit of 78°C and 82°C, respectively, as denoted by the horizontal solid lines shown in Figure 4.9. The consistent dips in temperature for the specimen thermocouples occurred when the oven was opened for removal of concrete specimens for weekly expansion measurements. There are two dips per week because, as mentioned in Section 3.8, two batches of concrete prisms had to be cast a day apart, due to the availability of the moulds. One prism from each batch was placed in a test container for a total of two specimens per test fluid. Consequently, testing for batch A and batch B occurred one day apart as well, requiring the oven to be opened two days per week. If this had any effect on expansion behaviour, at least it was consistent for all the prisms and the effect can be considered insignificant when comparing the behaviour of the prisms in different media.

Expansion measurements were taken each week for a total of five weeks. The results are shown in Figure 4.10.
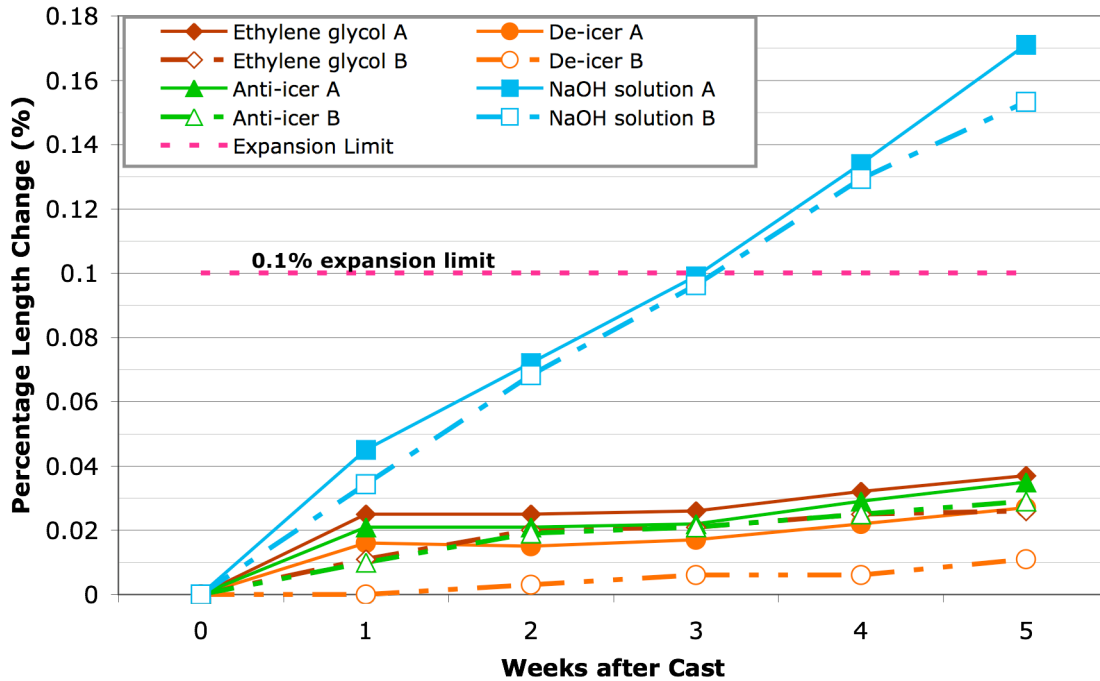
Figure 4.10 Accelerated expansion test results for concrete prisms in various media.

The horizontal dashed line in Figure 4.10 represents the expansion limit of 0.1%, set by the Standard for this test [Ministry of Transportation of Ontario]. It states that, for aggregates quarried from Gull River & Bobcaygeon Formations of South and East Ontario, in which the Pittsburg quarry lies, expansion must be less than 0.1% after 14 days of exposure in order to considered innocuous with respect to deleterious alkali-aggregate reactions.

After just one week, expansions of control prisms in the NaOH solution were greater than those in the other three test fluids. After 21 days, the control prisms hit the MTO expansion limit, indicating that the aggregates are indeed alkali-reactive. Although it surpassed the 14-day time limit for expansion, it quickly reached the expansion limit seven days later and continued to expand at a constant rate until test termination with a final average expansion of 0.162%. Both control prisms correlated well with each other.

Results for prisms in ethylene glycol, de-icer, and anti-icer show relatively innocuous expansive behaviour for the entire 5-week test duration, with average expansions of 0.032%, 0.019%, and 0.032%, respectively. Results for both batches were also quite

75

similar, except in the case of prisms in de-icer. This is insignificant, however, because both prisms experienced the smallest expansions of all test specimens.

Visual inspections of the prisms afterward show the harmful nature of alkali-aggregate reaction within concrete prisms exposed to NaOH solution. As shown in Figure 4.11, there are visible cracks at various places along the length of the control prisms. On the other hand, prisms in ethylene glycol, de-icer, and anti-icer did not have any visible deterioration on the surface, which is expected since overall expansions were very low.
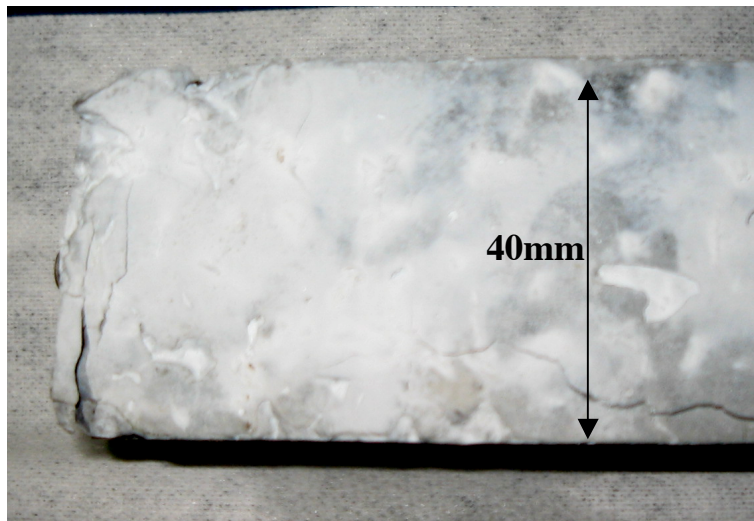

Figure 4.11 Expansion of alkali-reactive aggregates in concrete placed in NaOH solution causes visible cracking.

Other observations were noted regarding fluid appearance throughout the test period. After only one week, fluid consistencies and colours changed, as can be seen in Figure 4.12.
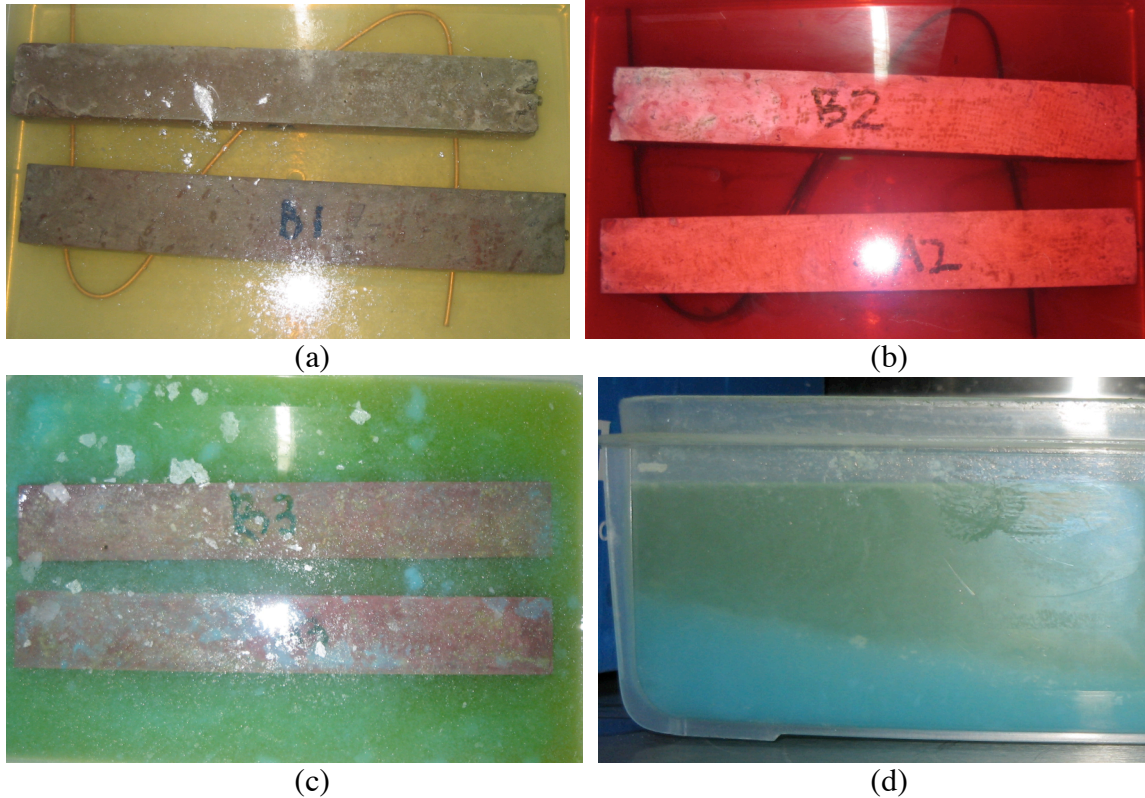
Figure 4.12 Various fluid changes were noted after one week exposure: (a) Ethylene glycol fluid became yellow-ish; (b) de-icer fluid turned a deep wine red colour; (c) and (d) anti-icer fluid appeared to separate into two layers.

The ethylene glycol changed slightly in appearance, from clear to yellow-tinged. After five weeks, a fine white precipitate could be seen at the bottom of the container. The de-icer changed drastically in colour from a bright orange to a deep red. Interestingly enough, a small amount of blue precipitate, similar to that found in anti-icer containers, was found in the de-icing fluid container. It was also found coating the copper wire. The anti-icer showed the most interesting change in appearance, separating into a less viscous liquid on top and a blue gel precipitate on the bottom.

Changes were also seen on the copper wires that were used to raise the concrete prisms off the bottom of the container. The most notable difference was the change in appearance of the copper placed in the de-icer container, which acquired a dark coating that appeared to be copper oxide.

4.6 Copper and Steel Exposure Test

As a result of the observations noted in the accelerated mortar bar expansion test, additional tests were performed concurrently to examine the effect of temperature of the fluids and of the fluids on copper corrosion. The effect of temperature on de-icer and anti-icer on copper was evaluated first. Figure 4.13 shows the fluids after being placed in the same test oven for one week.

The color and consistency of the fluids did not noticeably change from exposure to elevated temperatures. Recall also that de-icer is applied to aircraft at temperatures of up to 80°C, which implies that it should not undergo any ch.anges when brought up to elevated temperatures in that range.

Following these tests, a small copper plate was placed in containers with each of the fluids, as well as another container with ethylene glycol. After a one week period, they were removed and the fluids appeared as shown in Figure 4.14.

The ethylene glycol and anti-icer fluids do not appear to have changed a great deal from the addition of copper. The de-icer, however, appears to have darkened to a more reddish colour, although not to the same extent as the de-icer fluid in the accelerated mortar bar test container. This indicates that the precipitates and changes initially found in the mortar bar containers require the presence of concrete to occur and that they are likely due to an interaction between cement paste and the affected components. Precipitate samples were kept for further elemental analysis.

Gravimetric testing was conducted on new samples, in which copper and steel plate specimens were kept submerged in the four test fluids, ethylene glycol, de-icer, anti-icer, and water, for a period of 5 weeks. Weight measurements were taken before exposure and after 7 days , 14 days, and 35 days.
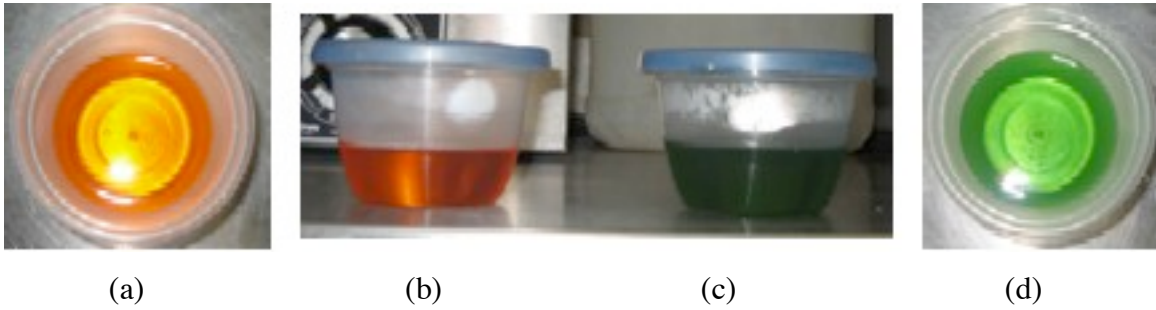
Figure 4.13 Appearance of fluids: (a) de-icer as-received, (b) de-icer after 80°C exposure, (c) anti-icer after 80°C exposure, (d) anti-icer as-received.
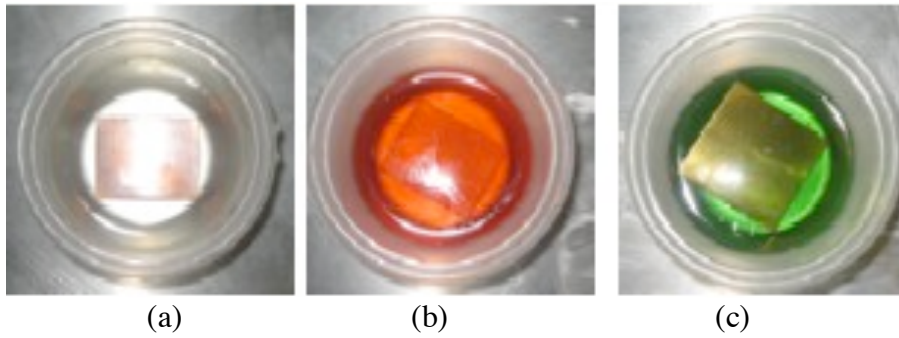

Figure 4.14 Appearance of fluids and copper after one week at 80°C: (a) ethylene glycol, (b) de-icer, and (c) anti-icer.

The specimens were visually inspected in solution before they were removed for corrosion cleaning and weighing. There did not appear to have been any reaction between the metals and their respective fluids, except in the case of steel in water. This was expected since steel shows corrosive behaviour almost immediately upon contact with water, as shown in the steel reinforcing bar corrosion test (Section 3.3). Gravimetric testing revealed minor weight losses for all copper and steel specimens after each 1-week interval. Respective steel and corrosion inhibitor solutions (Section 3.9) were used to clean the specimens before weighing and changes in weight due to exposure to the fluids are shown in Figure 4.15 for steel and Figure 4.16 for copper.

Corrosion was negligible for steel in ethylene glycol, de-icer, and anti-icer, but was significant for steel in water. The average corrosion rate of the steel specimens in water
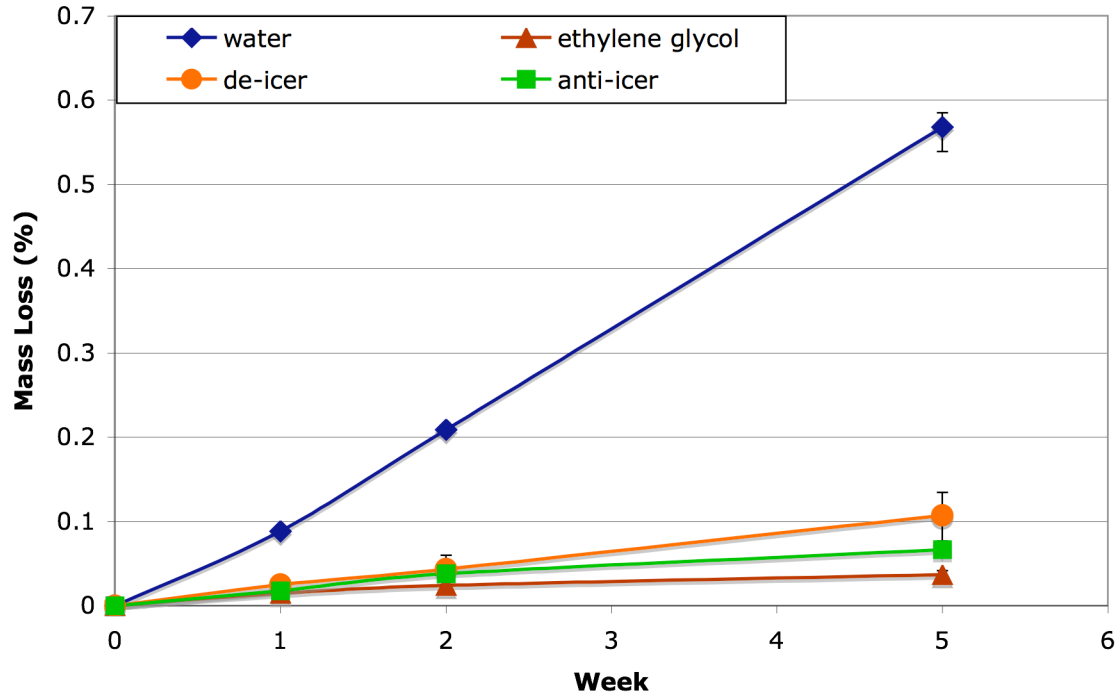
79
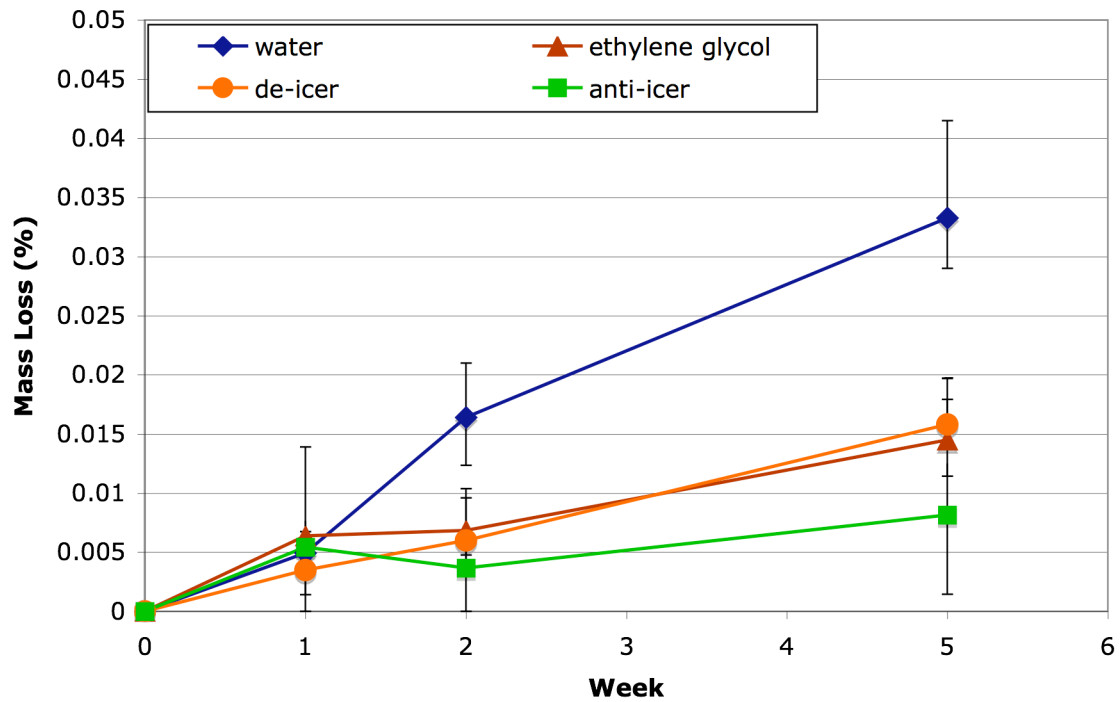
Figure 4.15 Accumulative mass loss of steel in test fluids.

Figure 4.16 Accumulative mass loss of copper in test fluids.

was 77 μm/year, while the lowest average corrosion rate occurred for steel in ethylene glycol at 5 μm/year. The average corrosion rates of steel in de-icer and anti-icer were 9 μm/year and 15 μm/year, respectively. These results are in accordance with visual indications of corrosion observed on the steel before cleaning.

It is clear from Figure 4.16 that negligible corrosion occurred to copper in any of the test fluids. Mass losses of copper specimens were less than their respective steel counterparts. The average corrosion rate of copper in water was 6 μm/year, which is double that of copper in ethylene glycol and de-icers, but still insignificant. The average corrosion rate of copper in anti-icer was 2 μm/year.

The next stage of testing the corrosivity of steel and copper in test fluids involved using the same setup as before, except with the addition of small pieces of concrete in the containers. The percentage mass loss for steel and copper placed in fluids with cement paste are shown in Figure 4.17 and Figure 4.18, respectively.

The behaviour of one of the steel specimens in water was peculiar, as it experienced a 0.20% mass loss after the first week, while the other two specimens only experienced a 0.015% mass loss. This was likely caused by the uncontrolled placements of specimens in the container, leading to different fluid exposure conditions for each specimen. Subsequently, the mass loss rates for the following weeks were consistent with those of the other two specimens. The average corrosion rate for steel in water was 86 μm/year, although omitting the outlier results in an average corrosion rate of 71 μm/year, which is approximately the same as without the cement paste. The average corrosion rates for steel in ethylene glycol, de-icer and anti-icer were negligible again, at 9 μm/year, 16 μm/year, and 11 μm/year, respectively.

The average corrosion rates were low for copper in all fluids with cement paste, with a rate of 15 μm/year for copper in water and 4 μm/year for copper in ethylene glycol, de-icer, and anti-icer. This is double the corrosion rate of copper in fluids without cement paste, but is still negligible. The slight increase in corrosion rate is likely due to a decreased stability of copper oxide in a higher pH environment provided by cement paste.
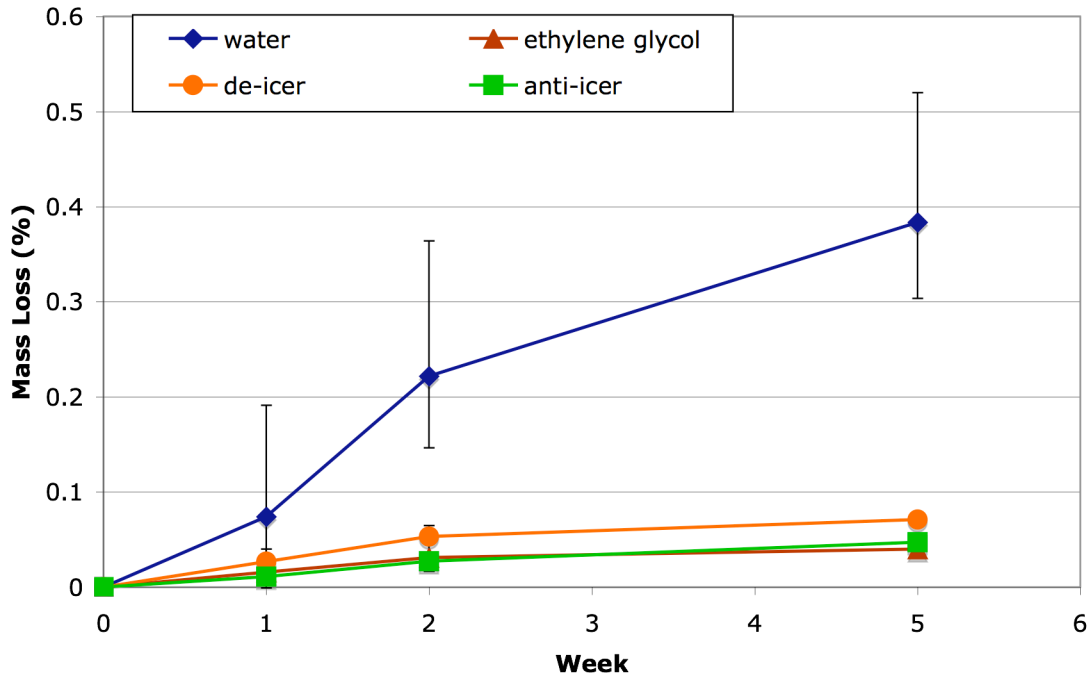
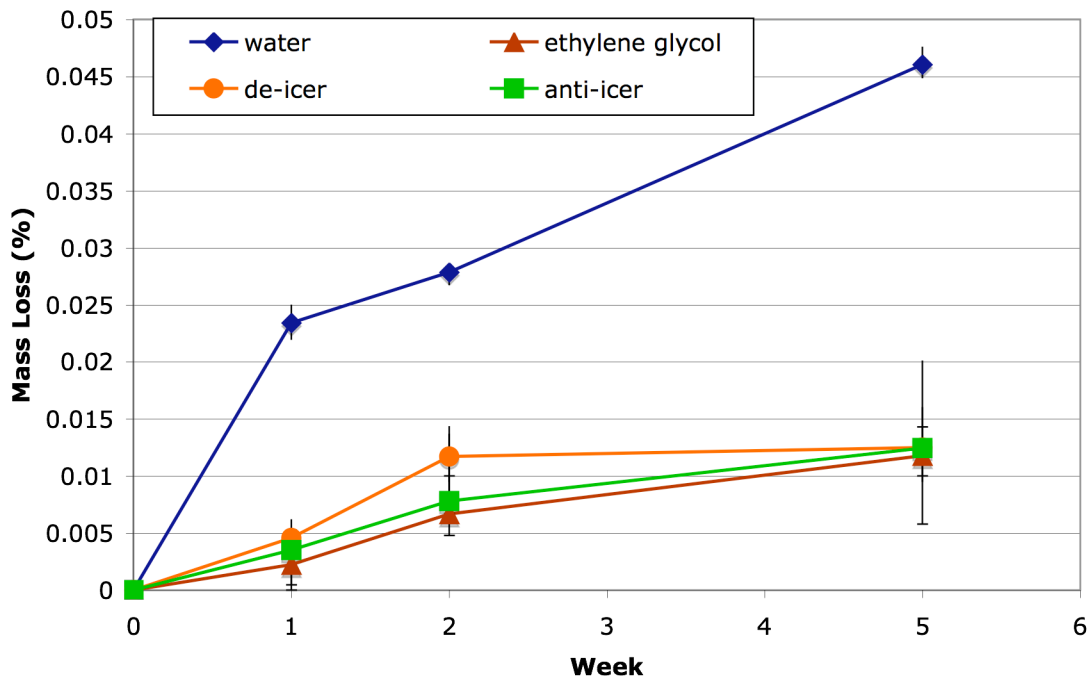Figure 4.17 Accumulative mass loss of steel in fluids with cement paste.

Figure 4.18 Accumulative mass loss of copper in fluids with cement paste.

4.7 Results & Discussion : Raman Spectroscopy

Raman spectroscopy was used to analyse de-icer and anti-icer fluid to obtain spectra that would be useful in comparing or identifying contrasting components between the two. Ethylene glycol was also analysed, in order to provide a baseline spectrum for the two fluids since it is the primary constituent in both fluids. The results for all three fluids are shown in Figure 4.19 below.
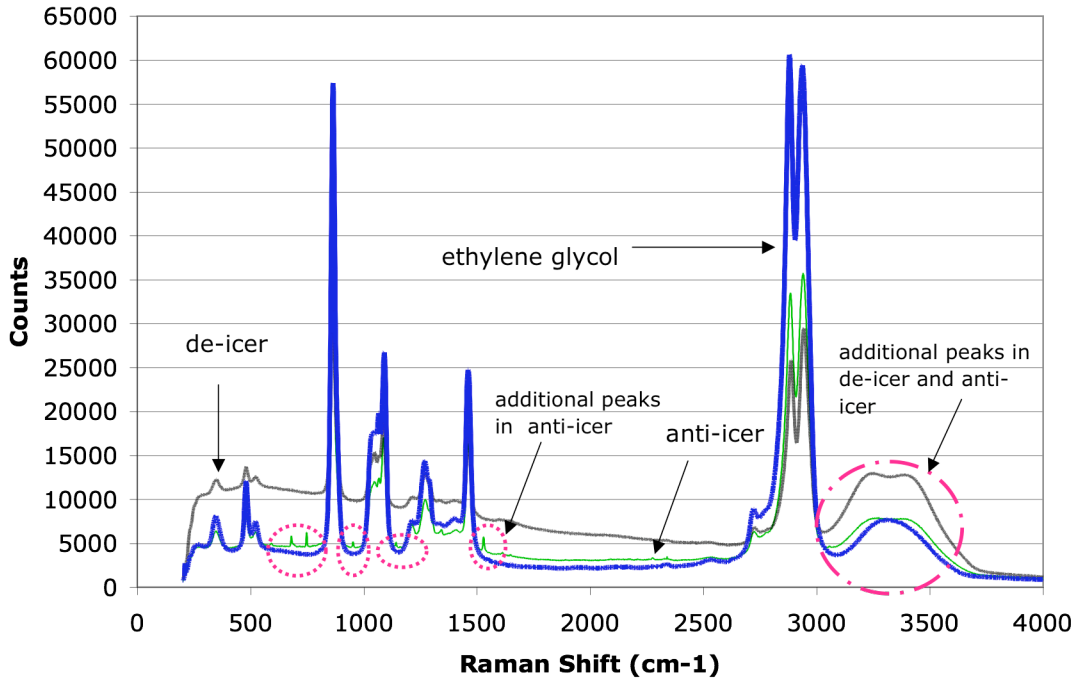
Figure 4.19 Raman spectra for ethylene glycol, de-icer, and anti-icer.

Ethylene glycol, represented by the darkest line, produced Raman peaks that are present in the de-icer and anti-icer. The peaks are shown at different intensities, which can be directly related to concentration [Skoog, 1998]. The de-icer spectrum shows consistently higher peaks than the anti-icer spectrum, which agrees well with the actual concentration of ethylene glycol in each of the fluids. The de-icer is composed of 92% ethylene glycol, while the anti-icer is composed of only 64%.

One common feature found in both de-icing fluids, indicated by the dash-dot circle in Figure 4.19 between approximately 3300 cm^{-1} and 3700 cm^{-1}. The ethylene glycol

spectrum has a single peak in that range, however, the de-icer and anti-icer spectra have two overlapping peaks. The spectrum for water has a double peak that starts at approximately 3000 cm^{-1} and ends at 3700 cm^{-1} [Chaplin], similar to the double peak seen in de-icing fluid spectra and corresponding well with the de-icer and anti-icer compositions since water is the secondary constituent at 7.5 % and 35 %, respectively.

Aside from the water peak and the different intensities, the de-icer spectrum does not differ greatly from the ethylene glycol spectrum. However, the anti-icer spectrum displays several small peaks, indicated by the dotted circles in Figure 4.19, that are not present in either the ethylene glycol or the de-icer spectra. These peaks have not been identified, but these results also correlate well with compositional information for the de-icer and anti-icer fluids. According to the DOW Chemical Company information sheets, the de-icer contains 0.5 % additives, while the anti-icer contains ≤ 1 % additives. The presence of a greater quantity of additional components in the anti-icer formulation is responsible for the extra compounds detected by Raman spectroscopy.

4.8 ESEM / EDS Analysis

ESEM and EDS analysis was performed on several specimens from the Submerged Cement Paste Test (Section 3.4) and Accelerated Expansion Test of Concrete Prisms (Section 3.8). Micrographs were obtained and elemental analysis was performed to identify the effects of exposure of cement paste and concrete to various environments.

4.8.1 Cement Paste in Ethylene Glycol

A fine white precipitate was observed inside the container housing cement paste submerged in ethylene glycol. EDS analysis was performed on the dried precipitate, shown in Figure 4.20.
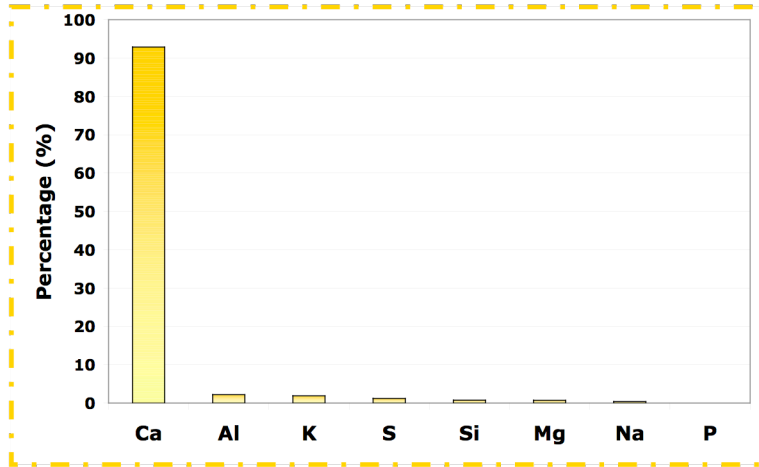
Figure 4.20 EDS analysis of precipitates formed from cement paste submerged in ethylene glycol.

It can clearly be seen that the major element present in the precipitate is calcium. This suggests that $Ca(OH)_2$ and/or $CaCO_3$, in which the C, H, and O would not be detectable by EDS, were likely leached out by ethylene glycol. There are only very small amounts of Al and Si, thus leaching of C_3A, C_2S, and C_3S may have also occurred, but to a lower extent.

4.8.2 Cement Paste in De-Icer

Because of the formation of adhered precipitate, the exposed surface of the cement paste was analyzed, as shown in Figure 4.21.
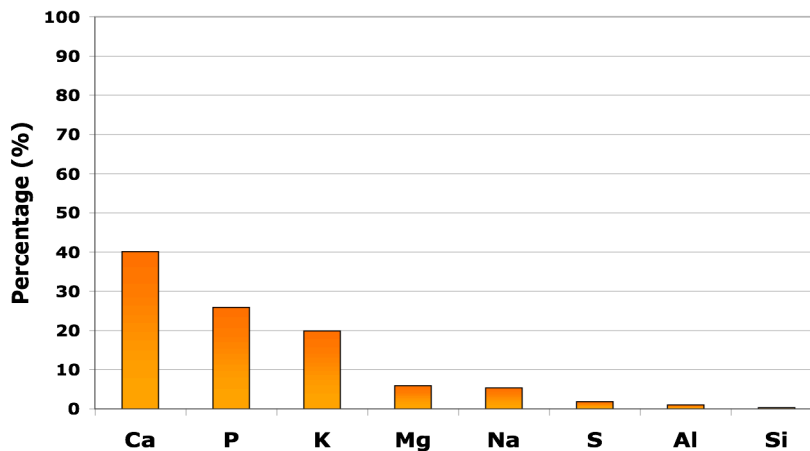

Figure 4.21 Micrograph and EDS analysis of exposed surface of cement paste in de-icer.

The EDS analysis shows the presence of Ca, P and K as the major constituents of the residue found on the exposed surface of cement paste in de-icer. The Ca content of 40% is likely due to leaching of $Ca(OH)_2$ and/or $CaCO_3$. The Na and K contents are high, at 5% and 20%, respectively. This may be due to leaching of the metal hydroxides, KOH and NaOH, which are present in the cement paste pore solution. The high P content cannot be explained by leaching of any cement paste constituent and, thus, likely exists as an element of a proprietary de-icer constituent.

The cement paste disk was removed from the de-icer and fractured in order to examine the interior paste, shown in Figure 4.22, away from the exposed surface. This was done to observe how the elemental analysis changed at a distance away from the exposed surface.
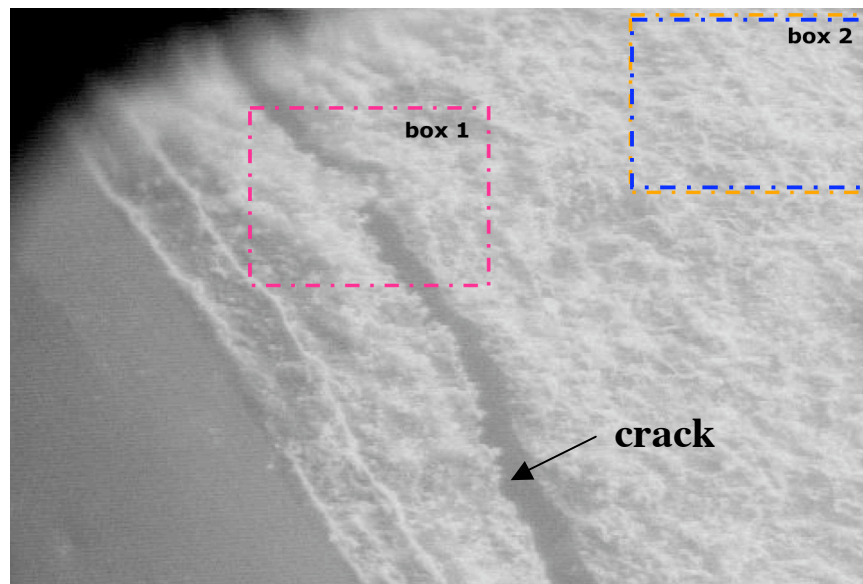

Figure 4.22 Micrograph of interior paste away from exposed surface of cement paste submerged in de-icer.
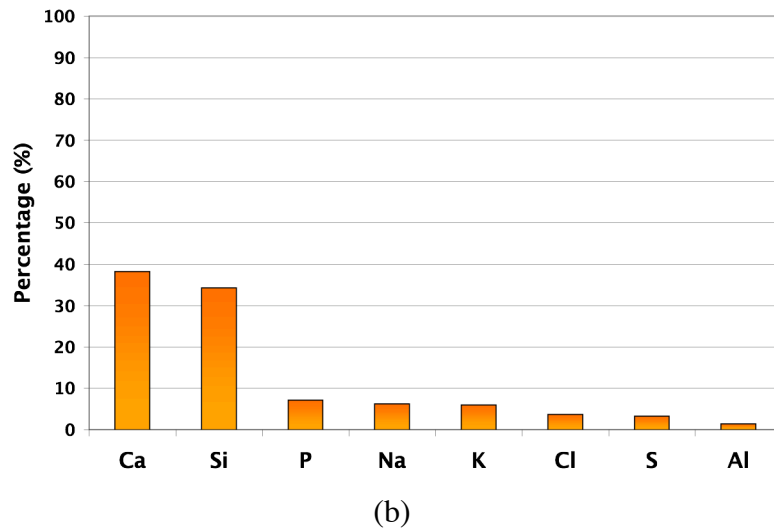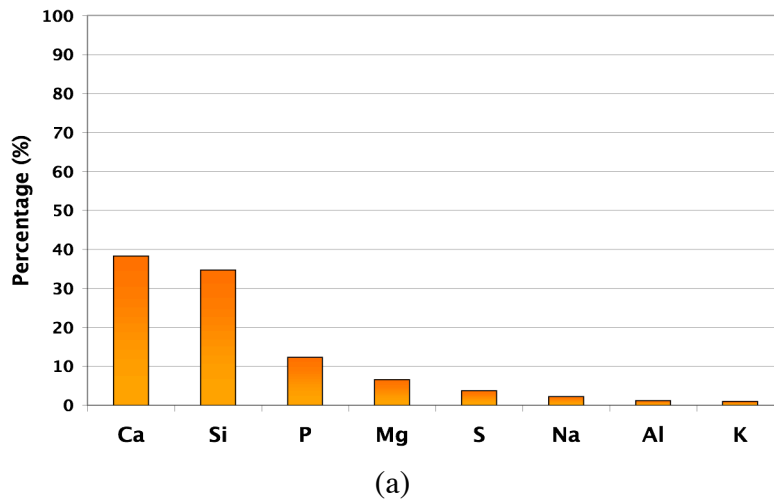
Figure 4.23 EDS analyses corresponding to Figure 4.22: (a) box 1 analysis at the crack and (b) box 2 analysis away from the crack.

It is interesting to note the differences in composition at two different locations from the same micrograph, as in Figure 4.23. A crack is visible, running along the left side of the micrograph. Box 1, corresponding to Figure 4.23(a), is located at the cracked section, while Box 2, corresponding to Figure 4.23(b), is located away from the cracked section. Figure 4.23(a) shows a higher P content, with a P value of 12%, than in Figure 4.23(b), with a P value of 7%. This suggests that the P may be present due to exterior conditions and is entering the cement paste through cracks, especially since there was a high P content of 26%, shown in Figure 4.21, in the adhered precipitates. Similar observations

can be made for K and Na, which were high in concentration in the precipitate adhered to the exposed surface. Figure 4.23(b) shows a higher Na and K content, with values of 6% each, than Figure 4.23(a), with values of 2% and 1%, respectively. This indicates that Na and K may be leaching out of the cement paste and corresponds with the high Na and K concentrations found in the precipitate analysis in Figure 4.21.

4.8.3 Cement Paste in Anti-Icer

Gel-like precipitates were collected from the containers holding cement paste in anti-icer. They were placed on a flat surface while still moist and allowed to dehydrate within the ESEM chamber, resulting in globular formations.   The EDS analysis is shown in Figure 4.24.
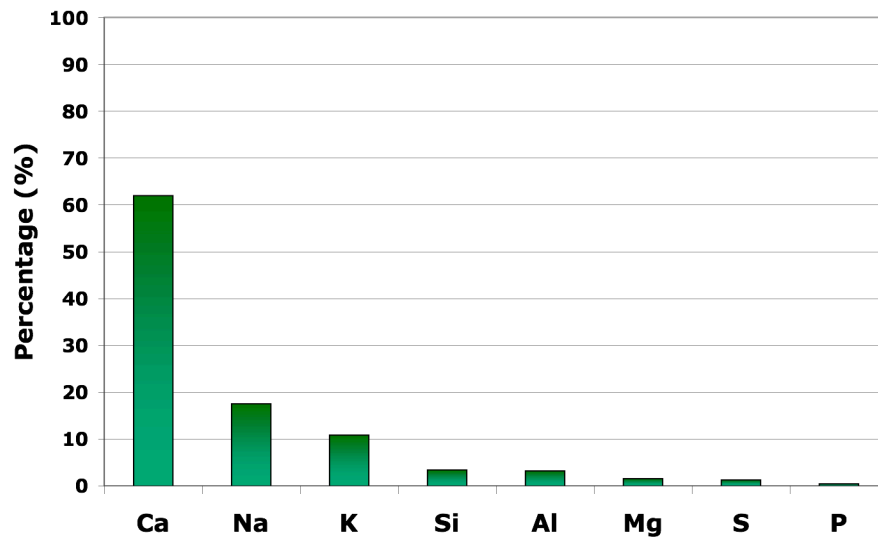
Figure 4.24 EDS analysis of precipitate from cement paste in anti-icer.

The major constituents consistently identified in the gel were Ca at 65%, Na at 20%, and K at 15%. This implies that Ca components, such as CaOH and $CaCO_3$, as well as Na and K components, NaOH and KOH, reacted with the anti-icer to form these precipitates. This is somewhat similar to results for the de-icer precipitate, however the Na content is approximately 15% higher and the P content is almost non-existent in the anti-icer precipitate.

4.8.4 Concrete in De-icer with Copper

A precipitate was found in the container holding concrete specimens in de-icer during the Accelerated Expansion Test of Concrete Prisms (Section 3.8). This precipitate was not observed in the submerged specimen test discussed above, therefore, EDS analysis was taken on collected samples and is shown in Figure 4.25.
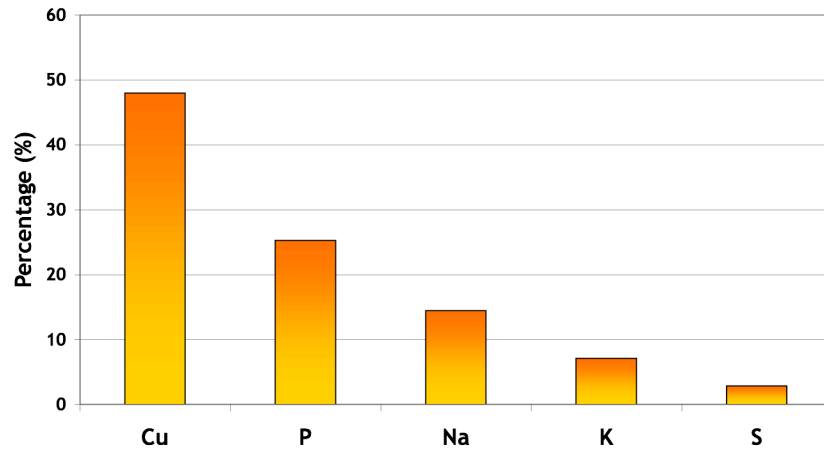
Figure 4.25 EDS analysis of precipitates collected from accelerated expansion test for concrete prisms in de-icer.

Copper was the major precipitate component, clearly indicating that there was a reaction between the copper tubing and the de-icer during the duration of the accelerated expansion test, which lasted 5 weeks at 80°C. The P content, at approximately 20%, was fairly high, which is consistent with the EDS analysis for the adhered precipitates formed on the submerged cement paste discussed earlier and reinforces the speculation of the existence of P as an element of a de-icer component. The Na and K contents were also high, at approximately 15% and 8%, respectively, indicating NaOH and KOH leaching from the cement paste.

4.9 Thermo-gravimetric Analysis

Precipitates were formed in all solutions with cement paste. The greatest amount of precipitate was produced by the cement paste in anti-icer fluid. Samples were collected after sixteen months each of fluid exposure and dried in an oven at 85°C to dry before

being crushed into a fine powder. Thermo-gravimetric analysis was conducted on dried samples of precipitates in order to determine the composition of the products.

Two samples were tested for each type of powder in order to check for consistency. A third sample would have been analysed if test results were not comparable between the first two analyses. Results for four different types of precipitates are shown in Figure 4.26.
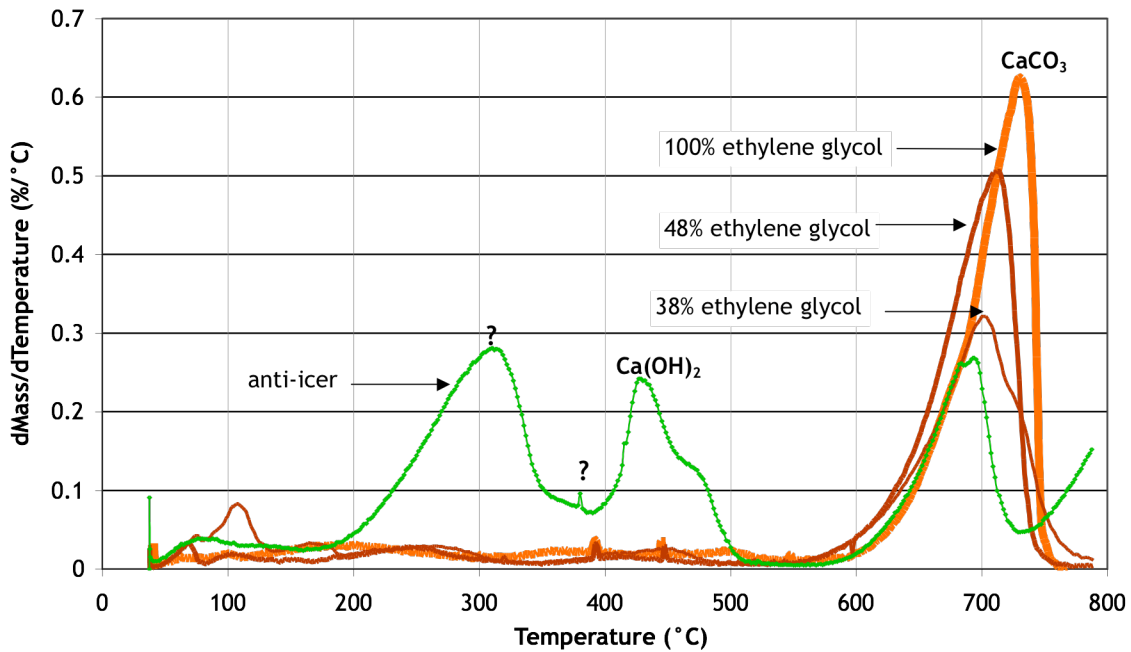
Figure 4.26 Thermogravimetric plots for four types of precipitates.

A major peak occurs at approximately 700°C in all four specimen plots and can be attributed to the decarbonation of calcium carbonate. Calcium carbonate is likely to be present in the powder samples because the specimens were exposed to ambient air at all times throughout the test period. In addition, immersion in solutions would provide a moist environment for carbonation of the cement paste surfaces to readily occur. The presence of calcium carbonate also indicates that calcium hydroxide may have been leached out of the cement paste by the fluids, which subsequently carbonated upon exposure to air.

The TGA plots for precipitates formed in ethylene glycol-based fluids show a few minor peaks and a slightly larger minor peak at approximately 100°C, which is most likely related to dehydration of various hydrates. The plot for precipitate from the anti-icer container, however, shows two additional major peaks at 310°C and 430°C. The broad peak starting at 430°C is likely related to dehydration of calcium hydroxide while the peak at 310°C does not correspond well to any cement paste components, indicating that it may be a component of the anti-icer solution.

4.10 X-Ray Diffraction

Two precipitates from the submerged cement paste test (Section 3.4), which were those from cement paste in ethylene glycol and anti-icer, were collected for XRD analysis. In addition, precipitate from the de-icer container of the accelerated expansion test of concrete prisms (Section 3.8) was collected. Prior to performing the XRD analysis, it was uncertain whether it was possible to obtain results for these precipitates since their structure was unknown, but all three specimens produced graphs with well-defined peaks, which are shown in Figure 4.27 to Figure 4.29.

The two compounds identified in the precipitate collected from cement paste submerged in ethylene glycol were calcium carbonate and vaterite, which is a polymorph of calcium carbonate. When vaterite is exposed to water, it converts to either calcite, at low temperatures, or aragonite, at temperatures above 60°C [WebMineral, 2007]. The XRD results are consistent with TGA results, in which calcium carbonate was the primary constituent found in the precipitate.
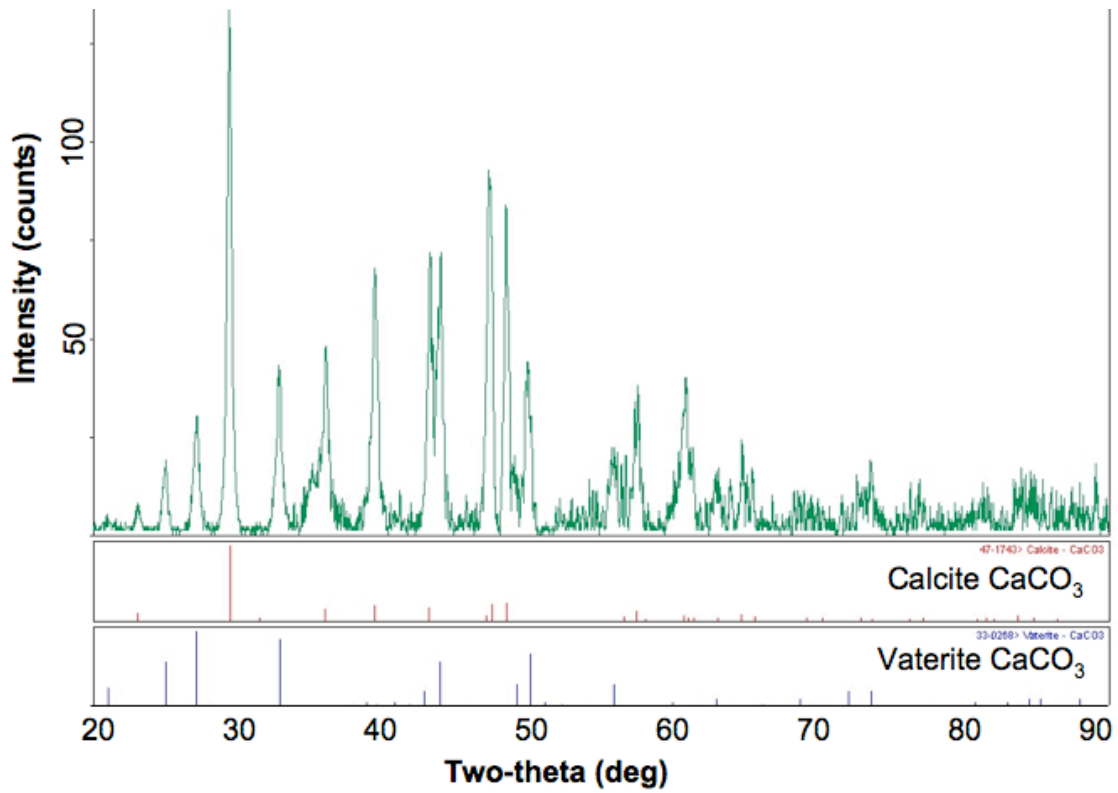
Figure 4.27 XRD analysis of precipitates from cement paste in ethylene glycol.
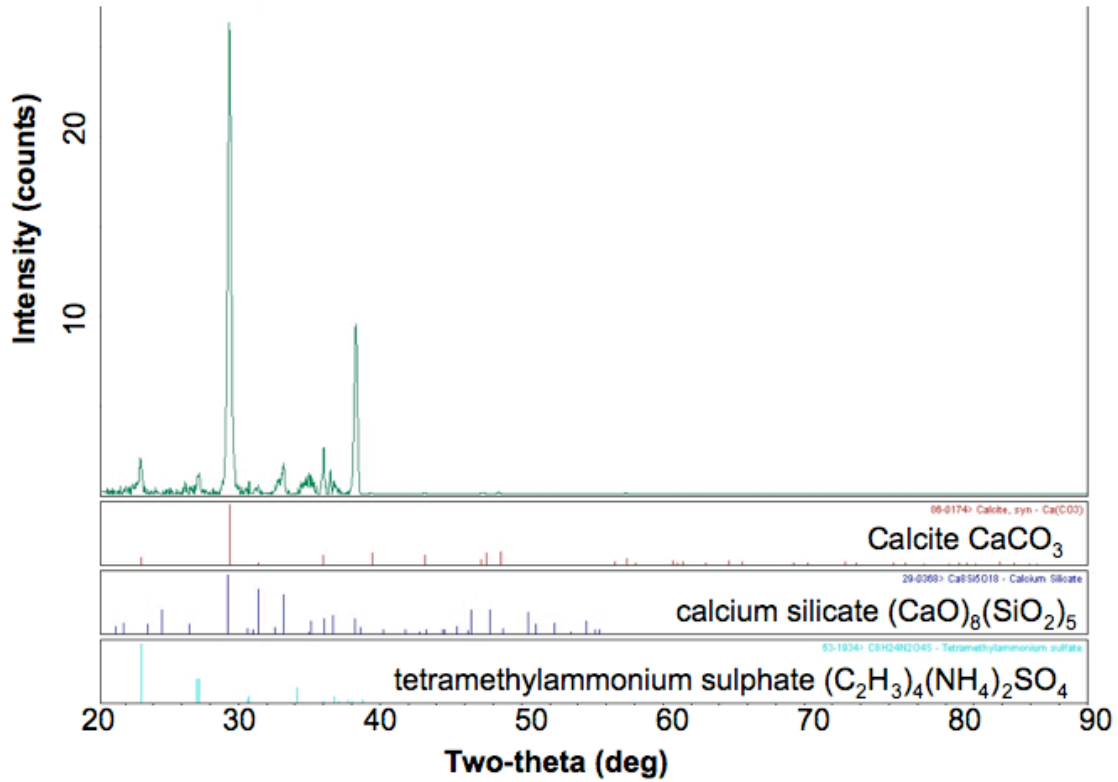
Figure 4.28 XRD analysis of precipitates from cement paste in anti-icer.

Three compounds were identified in the precipitate collected from cement paste submerged in anti-icer: calcium carbonate, calcium silicate, and tetramethyl ammonium sulphate. The occurrence of calcium carbonate is consistent with that found in the TGA results, as well. The TGA peak for C-S-H occurs between 80°C and 250°C, which is noticeable as a very gradual slope. The TGA peaks for tetramethyl ammonium sulphate occur at 263K and 462K [Malchus and Jansen, 1998], which represent the two, previously unknown, large peaks present on the TGA curve obtained for the same precipitates.
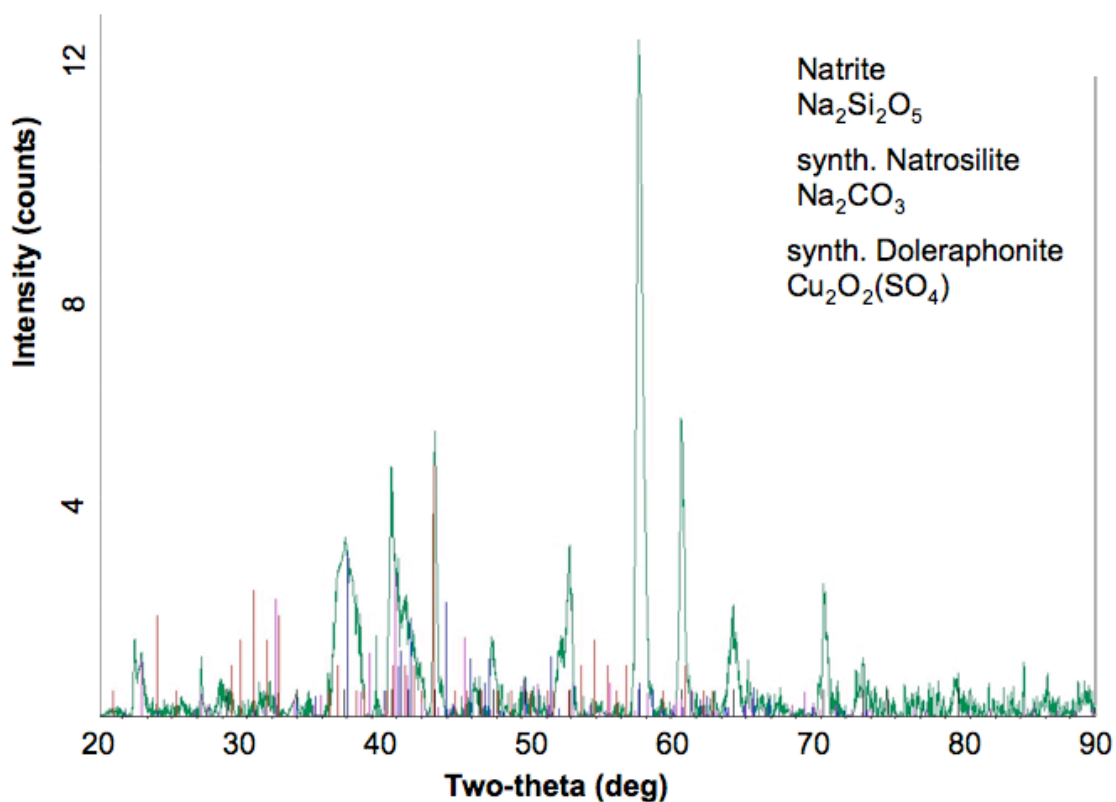
Figure 4.29 XRD analysis of precipitates from expansion test concrete in de-icer.

Three compounds were also identified in the precipitate collected from the de-icer container used in the accelerated expansion test: synthetic natrosilite, natrite, and synthetic dolerophanite. Natrite is an anhydrous sodium carbonate that is soluble in water. Natrosilite and natrite are associated with sodalite, which is a sodium aluminum silicate chloride. It can be light to dark blue, which corresponds to the color of the

collected precipitate. Sodalite, itself, is associated with calcium carbonate, which may explain its presence in the precipitate. It has been found to occur in great abundance at the Princess quarry in Bancroft, Ontario, which is near the Pittsburg quarry where the alkali-carbonate-reactive rocks for the expansion test were obtained [mindat.org]. Unlike the analyses for ethylene glycol precipitate and anti-icer precipitate, calcium carbonate was not detected. This seems to indicate that the de-icer may have reacted more strongly with the Pittsburg aggregate, rather than with the cement paste.

CHAPTER 5 - CONCLUSIONS

The following conclusions, pertaining to the effects of de-icing agents on a variety of issues, are based on the results obtained from mechanical, microscopic, and analytical tests.

1. De-icer and anti-icer did not instigate or accelerate corrosion of steel at high room temperature or at an elevated temperature of 80°C. In the presence of cement paste, which effectively changes the pH environment, there was still insignificant steel corrosion activity in both fluids. The same was found for copper in similar conditions, however, a precipitate formed during the accelerated mortar bar expansion test in the de-icer container. XRD analysis determined that reactions occurred between the copper, de-icer, and the alkali-carbonate-reactive aggregates.

2. It is well-known that freezing and thawing conditions can mechanically deteriorate concrete after repeated cycling. However, freezing and thawing of concrete in the presence of the de-icers appeared to cause insignificant concrete deterioration when the concrete is adequately air-entrained, which should be the case for concrete structures that are expected to be subject to freeze-thaw conditions. In addition, there was a great deal of surface scaling on prisms subject to freezing and thawing in the presence of water, while no surface scaling was observed on prisms in the presence of ethylene glycol, de-icer, and anti-icer. Subsequent mechanical testing, consisting of a four-point bending test of the freeze-thaw prisms and a compression test on cylinders submerged in de-icing fluids, showed that de-icing fluid exposure has minor effects on rupture strength and compression strength. The specimens exposed to de-icers performed the same, or better, than those exposed to water. The results from both mechanical tests correlated very well with each other. In all three tests, the results for ethylene glycol and de-icer were similar, while those for water and anti-icer were alike, which relates well with the compositions of each of the de-icing fluids.

95

3. Another major cause of concrete deterioration are alkali-aggregate reactions, which causes detrimental expansion and leads to surface microcracks, thus facilitating the ingress of harmful chemicals and water. Concrete prisms were subject to an accelerated expansion test, incorporating known reactive aggregates, and the results show that negligible expansion occurs in the presence of de-icing fluids.

4. Overall, the above test results showed that de-icer and anti-icer had very little impact on the mechanical behaviour of concrete and the electro-chemical behaviour of steel and copper. However, precipitates were formed in the tests involving cement paste and concrete exposure to de-icing fluids. The precipitates did not have a detrimental effect on concrete mechanical properties over the period of the tests.

5. Microscopic and elemental analyses conducted using ESEM, EDS, XRD, and TGA on the various precipitates from the submerged cement paste test and the accelerated expansion test on concrete prisms, determined that the main component leached out from cement paste in ethylene glycol and anti-icer was calcium carbonate. In the case of cement paste in de-icer, calcium carbonate was likely leached out, but there were also high concentrations of sodium and potassium in the precipitate. These could have been leached from the cement paste pore solution or present as a constituent of the de-icer itself. XRD analysis of precipitate from the de-icer container of the accelerated expansion test suggest that de-icer reacts with alkali-carbonate-reactive aggregates to a greater extent than with cement paste, as no calcium carbonate was detected by XRD.

6. It is concluded that de-icer and anti-icer do not have any significant unfavourable effects on concrete mechanical properties and durability. It should be noted that the tests performed in this study utilized de-icing fluids at undiluted concentrations and that specimens were under constant exposure. These do not realistically portray exposure conditions on the de-icing pad. During operations,

de-icer is applied at diluted concentrations and, while anti-icer is applied at full concentration, dilution naturally occurs upon application due to the snow and ice on the aircraft and on the pad. Moreover, trucks sweep the ground periodically to collect any fluids, which further reduces the exposure of concrete to de-icing fluids. At minimal exposure, the effect of de-icers on concrete durability should be much less than that observed during testing.   On the other hand, the existence of precipitates and subsequent elemental analyses performed on them indicate that reactions do occur between cement paste and the de-icers. In the short term, these reactions did not appear to have a significant effect on concrete stability, however, the long term effects of de-icer exposure are unknown.

CHAPTER 6 - RECOMMENDATIONS

Based on the experiments and analyses performed over the course of this study, it is concluded that de-icer and anti-icer do not appreciably cause premature concrete deterioration. Nevertheless, there are still many facets to be explored concerning the influence of de-icing fluids on concrete. Several areas that were investigated could be explored further and some issues were not investigated at all, but should be considered for future work.

The most conspicuous finding that requires further investigation is reactions that result in the formation of precipitates in all cases of cement paste exposure to de-icing fluids. Although several techniques were used to determine precipitate compositions, the reactions responsible for their appearance have not been determined. Even though they were not found to significantly cause damage to concrete, they should be considered. A better understanding of precipitate compositions would be useful in determining their possible long-term effects on concrete properties.

Cylinder compression testing could be very dependent on many factors, including concrete mixture design, curing time, de-icer exposure time, and drying time. The comparative results obtained during this particular study were only valid for the specific curing method used. It may be worthwhile to examine if similar trends can be observed at a variety of the above parameters.

De-icer was used as a concentrate during all experiments, but, in practice, it is diluted to 38% or 48% concentrations mixed with water. In view of the fact that water had the most negative impact in all mechanical tests, the effect of diluted de-icer solutions should be conducted. Presently, the results from de-icer exposure were similar to those from ethylene glycol exposure, which are sensible considering that the concentrated de-icer is composed of 92% ethylene glycol. The results of the same experiments tested using diluted solutions of de-icer may be significantly different than the results of the concentrate.

Concrete cores were removed from the GTAA CDF de-icing pad, but were not analysed during the course of the study. Petrographic analyses may be performed to examine the type of damage typically found on the de-icing pad. If concrete signs of distress can be identified, the mechanisms of concrete deterioration can be limited and identified, as well.

REFERENCES

Standards:

ASTM C 215 – Standard test method for fundamental transverse, longitudinal, and torsional resonant frequencies of concrete specimens. American Society for Testing and Materials International, West Conshohocken, PA.

ASTM C666 – Standard test method for resistance of concrete to rapid freezing and thawing. American Society for Testing and Materials International, West Conshohocken, PA.

ASTM C 305 – Standard practice for mechanical mixing of hydraulic cement pastes and mortars of plastic consistency. American Society for Testing and Materials International, West Conshohocken, PA.

ASTM C 78 – Standard test method for flexural strength of concrete (using simple beam with third-point loading). American Society for Testing and Materials International, West Conshohocken, PA.

ASTM C 490 – Standard practice for use of apparatus for the determination of length change of hardened cement paste, mortar, and concrete. American Society for Testing and Materials International, West Conshohocken, PA.

ASTM C 1260 – Standard test method for potential alkali reactivity of aggregates (mortar-bar method). American Society for Testing and Materials International, West Conshohocken, PA.

ASTM G1-03 – Chemical cleaning procedures. American Society for Testing and Materials International, West Conshohocken, PA.

MTO LS 626 – Method of test for the detection of alkali-reactive coarse aggregate by accelerated expansion of concrete prisms (Tang test). Ministry of Transportation of Ontario.

Journals and Web:

Andrade, C., Gonzalez, J.A. (1978). "Quantitative measurements of corrosion rate of reinforcing steels embedded in concrete using polarization resistance measurements." Materials and Corrosion **29**(8) pp. 515-519.

Andrews, D. H. (1981). "Raman Spectra." Industrial and Engineering Chemistry **23**(11)

Bazant, Z.P., Steffens, A. (2000). "Mathematic model for kinetics of alkali-silica reaction in concrete." Cement and Concrete Research **30** pp. 419-428.

Bogue, R.H., Lerch, W. (1934). "Hydration of Portland cement compounds." Industrial & Engineering Chemistry **26**(8) pp. 837-847.

Castellote, M., Alonso, C., Andrade, C., Turrillas, X., Campo, J. (2004). "Composition and microstructural changes of cement pastes upon heating, as studied by neutron diffraction." Cement and Concrete Research **34** pp. 1633-1644.

Chaplin, M. "Water Structure: Methods", Water Structure and Science. London South Bank University, London, UK. http://www.lsbu.ac.uk/water/methods. Accessed: July, 2007.

City of Toronto Staff Report (2002). "Management of de-icing activities at Toronto Lester B. Pearson International Airport." City of Toronto, Toronto, Ontario. CA.

Cordray, D.R., Kaplan, L.R., Woyciesjes, P.M., Kozak, T.F. (1996). "Solid-liquid phase diagram for ethylene glycol + water." Fluid Phase Equilibria **117**(1) pp. 146-152.

Corsi, S.R., Loyo-Rosales, J.E., Rice, C.P., Sheesley, R.J., Failey, G.G., Cancilla, D.A. (2006). "Characterization of aircraft deicer and anti-icer components and toxicity in airport snowbands and snowmelt runoff." Environmental Science and Technology **40** pp. 3195-3202.

Courtier, R.H. (1990). "The assessment of ASR-affected structures." Cement & Concrete Composites **12** pp. 191-201.

Danilatos, G.D. (1994). "Environmental scanning electron microscopy and microanalysis." Mikrochimica Acta **114/115** pp. 143-155.

Diamond, S., Kotwica, L., Olek, J., Rangaraju, P.R., Lovell, J. (2006). "Chemical aspects of severe ASR induced by potassium acetate airfield pavement de-icer solutions." Proceedings of 8th CANMET International Conference on Advances in Concrete Technology. Montreal, Canada pp. 261-278.

Duyou Lu, Laibau Mei, Zhongzi Xu, Mingshu Tang, Benoit Fournier. (2006). "Alteration of alkali reactive aggregates autoclaved in different alkali solutions and applications to alkali-aggregate reaction in concrete (I) Alteration of alkali reactive aggregates in alkali solutions." Cement and Concrete Research **36** pp. 1176-1190.

EPA (2000). "Preliminary data summary : airport deicing operations (revised)." Office of Water (4303) United States Environmental Protection Agency. Washington, D.C.

FODNews: www.fodnews.com. Accessed: Nov. 2005.

Forbes, J. GTAA CDF Manager (2006). Personal Communication.

Gabriel, B.L., (1985). "SEM: A user's manual for materials science." American Society for Metals. Metals Park, Ohio.

Gray, D.R. (2002). "Environmental impact of aircraft deicing." Greater Toronto Airports Authority, Toronto Pearson International Airport. Toronto, Ontario, Canada.

GTAA: http://www.gtaa.com. Accessed: Nov. 2005.

GTAA (2003). "Pearson Profile: An information guide to Toronto Pearson International Airport." Greater Toronto Airports Authority, Toronto, Ontario, CA.

GTAA Annual Report (2006): http://www.gtaa.com/en/gtaa_corporate/publications/annual_reports/. Accessed: June 2007.

GTAA Winter Operations (2007). "Fact Sheet – Winter operations at Toronto Pearson International Airport." Greater Toronto Airports Authority, Toronto, Ontario, CA.

Hadley, D.W. (1961). "Alkali Reactivity of Carbonate Rocks – Expansion and Dedolomitization." Highway Resarch Board Proceedings **40** pp. 462-474.

Health Canada. (2000). "Priority Substances List State of the Science Report for Ethylene Glycol." Canadian Environment Protection Act, 1999. Environment Canada.

Ho, E., Gough, W.A. (2005). "Freeze-thaw cycles in Toronto, Canada in a changing climate." Theoretical and Applied Climatology **83** pp. 203-210.

Jones, T.N. (1988). "A new interpretation of alkali-silica reaction and expansion mechanisms in concrete." Chemistry and Industry **2**(40).

Jordanovska, V., Siftar, J. (1991) Double sulfates of some rare earths with tetramethylammonium. Journal of Thermal Analysis 37 pp. 2361-2367.

Kao, M.J., Tien, D.C., Jwo, C.S., Tsung, T.T. (2005) The study of hydrophilic characteristics of ethylene glycol. Journal of Physics: Conference Series 13 pp. 442-445.

Korhonen, C. (2002). "Effects of High Doses of Chemical Admixtures on the Freeze-Thaw Durability of Portland Cement Concrete." US Army Corps of Engineers: Engineer Research and Development Center.

Kramarczyk, M., Kolodz, C., Matheny, A. (1999). "An introduction to lissajous patterns."   Department of Electrical & Computer Engineering, Michigan State University, MI, USA.

Lopez-Buendia, A.M., Climent, V.,Verdu P. (2006). "Lithological influence of aggregate in the alkali-carbonate reaction." Cement and Concrete Research **36** pp. 1490-1500.

Malchus, M., Jansen, M. (1998). "Structural investigation of the phase transitions of tetramethylammonium sulfate." Acta Crystallographica **B54** pp. 494-502.

MacKinnon, J. (2005). Personal Communication.

Mindat.org: http://www.mindat.org. Accessed: July, 2007.

Ministry of Transportation of Ontario (2007). "110S11 CDED Special Provisions." Ministry of Transportation of Ontario, Ontario, CA.

Moranville-Regourd, M. (1997). "Modelling of expansion induced by ASR – new approaches." Cement and Concrete Composites **19** pp. 415-425.

Mouret, M., Bascoul, A., Escadeillas, G., (1999). "Microstructural features of concrete in relation to initial temperature – SEM and ESEM characterization." Cement and Concrete Research **29** pp. 369-375.

Perruchot, C., Chehimi, M.M., Vaulay, M., Benzarti, K. (2006). "Characterisation of the surface thermodynamic properties of cement components by inverse gas chromatography at infinite dilution." Cement and Concrete Research **36** pp. 305-319.

Pigeon, M. (1994). "Frost resistance : a critical look." Mohan Malhotra Symposium on Concrete Technology, ACI Spring Convention, San Francisco.

Powers, T.C. (1955). "Basic considerations pertaining to freezing-and-thawing tests." American Society for Testing Materials. **55.**

Powers, T.C., Helmuth, R.A. (1953). "Theory of Volume Changes in Hardened Portland Cement Paste During Freezing." Materials and Construction pp. 285-297.

Ramlochan, T., (2006). "Analytical electron microscopy of cementitious materials." Instrumentation techniques in concrete technology course. University of Toronto, Toronto, Ontario, CA.

Rogers, A.D., Lee-Sullivan, P., Bremner, T.W. (1999). "Selecting concrete pavement joint sealants. II: case study." Journal of Materials in Civil Engineering pp. 309-316.

Rogers, C.A., Grattan-Bellew, P.E., Hooton, R.D., Ryell, J., Thomas, M.D.A. (2000). "Alkali Aggregate Reactions in Ontario." Canadian Journal of Civil Engineering **27** pp. 246-260.

Sarkar, S., Zollinger, D., Mukhopadhyay, A., Seungwook, L., Shon, C. (2004). "Handbook for indentification of alkali-silica reactivity in airfield pavement." Texas Transportation Institute for the U.S. Federal Aviation Administration DOT.

Skoog, D.A., Holler, F.J., Nieman, T.A. (1998). "Principles of Instrumental Analysis : fifth edition." Harcourt Brace College Publishers, Philadelphia, PA.

Suwito, A., Jin, W., Xi, Y., and Meyer, C. (2002). "A Mathematical Model for the Pessimum Effect of ASR in Concrete." Concrete Science and Engineering **4** pp. 23-34.

The Dow Chemical Company. (2002) DOW SAE AMS 1424 ethylene glycol-based type I fluids product information bulletin.

The Dow Chemical Company. (2002) DOW SAE AMS 1428 ethylene glycol-based type IV fluids product information bulletin.

The International Centre for Diffraction Data: http://www.icdd.com/. Accessed: June, 2007.

Tobin, R.E. (1995). "Reactive aggregates and popouts – causes and prevention." Concrete International **17**(1) pp. 52-54.

Transport Canada Civil Aviation: Structural defects found in Portland cement concrete pavements: http://www.tc.gc.ca/CivilAviation/International/Technical/Pavement/quality/structural/portlandcement.htm. Accessed: Nov. 2005.

Ulm, F., Coussy, O., Kefei, L., Larive, C. (2000). "Thermo-chemo-mechanics of ASR expansion in concrete structures." Journal of Engineering Mechanics **126** (3) pp. 233-242.

Unusual Aviation Pictures: www.aviationpics.de. Accessed: Nov. 2005.

Valenza II, J.J., Scherer, G.W. (2006). "Mechanism for Salt Scaling." Journal of the American Ceramic Society **89** pp. 1161-1179.

Van Dam, T.J. (2006). "Design and construction of concrete pavement for aircrat de-icing facilities." Innovative Pavement Research Foundation : Airport Concrete Pavement Technology Program, Skokie, IL, USA.

Verbeck, G.J., Klieger, P. (1957). "Studies of 'salt' scaling of concrete." Highway Research Board Bulletin. **150** pp. 1-17.

WebMineral: http://www.webmineral.com. Accessed: July, 2007.

West, J. (2005). "Durability design of new concrete infrastructure." University of Waterloo, Waterloo, Ontario, CA.

Williams, P.J., Biernacki, J.J., Bai, J., Rawn, C.J. (2003). "Assessment of a synchrotron X-ray method for quantitative analysis of calcium hydroxide." Cement and Concrete Research **33** pp. 1553-1559.

Ye. G., Liu, X., De Schutter, G., Poppe, A.-M., Taerwe, L. (2007). "Influence of limestone powder used as filler in SCC on hydration and microstructure of cement pastes." Cement and Concrete Composites **29** pp. 94-102.